Nano Research Energy

ISSN 2791-0091 (print); 2790-8119 (online)
https://doi.org/10.26599/NRE.2023.9120048

Review Article

Present and future of functionalized Cu current collectors for stabilizing lithium metal anodes

Yuhang Liu[1,§], Yifan Li[1,§], Jinmeng Sun[1], Zhuzhu Du[1], Xiaoqi Hu[1], Jingxuan Bi[1], Chuntai Liu[4], Wei Ai[1] (✉), and Qingyu Yan[2,3] (✉)

[1] *Frontiers Science Center for Flexible Electronics (FSCFE) & Shaanxi Institute of Flexible Electronics (SIFE), Northwestern Polytechnical University (NPU), 127 West Youyi Road, Xi'an 710072, China*
[2] *School of Materials Science and Engineering, Nanyang Technological University, 50 Nanyang Avenue, Singapore, 639798 Singapore*
[3] *Institute of Materials Research and Engineering, A*STAR, 138634 Singapore*
[4] *Key Laboratory of Materials Processing and Mold Ministry of Education, Zhengzhou University, Zhengzhou 450002, China*
[§] *Yuhang Liu and Yifan Li contributed equally to this work.*

Received: 28 October 2022 / **Revised:** 24 November 2022 / **Accepted:** 27 November 2022

ABSTRACT

Li metal has been recognized as the most promising anode materials for next-generation high-energy-density batteries, however, the inherent issues of dendrite growth and huge volume fluctuations upon Li plating/stripping normally result in fast capacity fading and safety concerns. Functionalized Cu current collectors have so far exhibited significant regulatory effects on stabilizing Li metal anodes (LMAs), and hold a great practical potential owing to their easy fabrication, low-cost and good compatibility with the existing battery technology. In this review, a comprehensive overview of Cu-based current collectors, including planar modified Cu foil, 3D architectured Cu foil and nanostructured 3D Cu substrates, for Li metal batteries is provided. Particularly, the design principles and strategies of functionalized Cu current collectors associated with their functionalities in optimizing Li plating/stripping behaviors are discussed. Finally, the critical issues where there is incomplete understanding and the future research directions of Cu current collectors in practical LMAs are also prospected. This review may shed light on the critical understanding of current collector engineering for high-energy-density Li metal batteries.

KEYWORDS

Cu current collectors, functionalization, Li metal batteries, lithiophilic modification, Li plating/stripping

1 Introduction

The burgeoning energy-consuming systems on modern society demand high-energy-density energy storage devices [1, 2]. Currently, the energy density of the state-of-the-art Li-ion batteries (LIBs) have reached the bottleneck due to the constraints of the graphite anode [3−6]. In pursuit of next-generation high-energy batteries, Li metal has been revived as an exciting anode in view of its high theoretical capacity (3,860 $mAh \cdot g^{-1}$) and the lowest electrochemical reduction potential (−3.04 V vs. standard hydrogen electrode) [7, 8]. Impressively, when coupling with a high-voltage or high-capacity cathode, the resulting Li metal batteries (LMBs) could deliver high energy densities, for example, >350 $Wh \cdot kg^{-1}$ in Li-$LiNi_{0.8}Co_{0.1}Mn_{0.1}O_2$ (NCM811) batteries and ~2,600 $Wh \cdot kg^{-1}$ in Li-S batteries [9–12].

The first-generation LMBs composed of metallic Li anode and TiS_2 cathode commence in the 1970s, however, quickly fell into a trough due to their poor cyclability and safety concerns [13, 14]. The cause of battery failure has been proved to be the uneven Li deposition and dissolution on Li metal anodes (LMAs) during cycling, where many troublesome issues in terms of dendrite growth, unstable solid electrolyte interphase (SEI) formation, infinite volume expansion and electrolyte depletion are involved [15–17]. Thus far, great efforts including the introduction of functionalized current collector, 3D lithiophilic hosts, artificial SEI, solid-state electrolyte, etc., have been devoted to solving these problems [18–20]. As the indispensable part of battery, Cu current collectors are not only responsible for electron conduction but also for Li metal deposition, making them attractive in guiding the plating/stripping behaviors of Li [21, 22]. Although much progress for stabilizing LMAs has been made, the durable cycling stability under high rate (>3 $mA \cdot cm^{-2}$) and large capacity (>3 $mAh \cdot cm^{-2}$) is still held back by the lithiophobic nature of Cu [23, 24]. To this end, functionalized Cu current collectors with reconstructed lattice plane, anchored lithiophilic sites, well-defined 3D architectures, etc., have been proposed to fabricate high-performance LMAs toward practical applications.

Address correspondence to Wei Ai, iamwai@nwpu.edu.cn; Qingyu Yan, AlexYan@ntu.edu.sg

In this review, we present the recent advances in functionalized Cu current collectors for dendrite-free LMAs. First, the design principles of Cu current collectors and the associated mechanistic insights of smooth Li deposition are elaborated. Second, strategies regarding the functionalization of Cu current collectors are presented, which are divided into three categories according to their structural design concepts (Fig. 1): 1) Planar modified Cu foils. Atom-scale modification and surface patterning of Cu foil, and the construction of lithiophilic sites and protective layers on Cu foil are discussed in this section. 2) 3D architectured Cu foils. Integrated Cu-based scaffolds and composited Cu-based skeletons based on Cu foil are contained in this part. 3) Nanostructured 3D Cu substrates. Lithiophilic designs of Cu meshes, Cu foams and self-built Cu skeletons are summarized in the chapter. Finally, summary and perspectives are outlined for highlighting the challenges and future development of high-performance LMAs based on functionalized Cu current collectors.

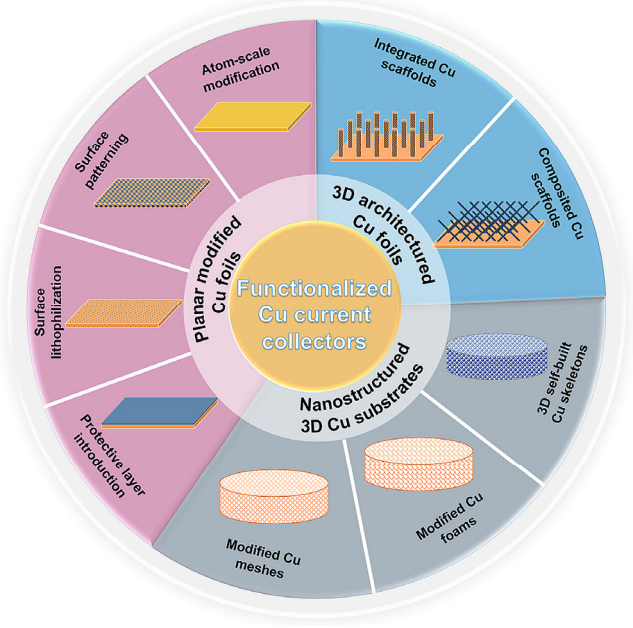

Figure 1 Schematic illustrations of the structural designs of functionalized Cu current collectors for LMAs.

2 Challenges and mechanism of LMBs

Li with an atomic number of 3 shows ultrahigh reactivity and the most negative potential, making it an ideal anode for high-energy-density batteries. Nevertheless, metallic Li is thermodynamically unstable, which can easily provoke serious side reactions with electrolyte as well as cause uncontrolled Li nucleation and deposition [25]. From the thermodynamical and kinetic viewpoints, Li nucleation in each cycle is the beginning of subsequent Li deposition, which plays a vital role in determining the eventual morphology of Li. Accordingly, several models have been established to elucidate the initial nucleation and the early growth of Li metal. On one hand, the surface diffusion model indicates that Li metal is preferable to form 1D dendritic whiskers due to its low surface energy and high migration energy [16, 26]. On the other hand, the space-charge model proposed by Chazalviel and Brissot et al. demonstrates that the electrode effective current density also strongly affects the cation concentration gradient (Eq. (1)):

$$\frac{\partial C}{\partial t}(x=0)=\frac{-J}{eD\left(1+\frac{\mu_c}{\mu_a}\right)} \tag{1}$$

once the current density is higher than the critical current density, the ionic concentration at the anode surface will go to zero. Meanwhile, Li dendrite growth occurs at a called Sand's time τ_s (Eq. (2)):

$$\tau_s=\pi D\left(\frac{C_0 e z_c}{2J}\right)^2\left(\frac{\mu_a+\mu_c}{\mu_a}\right)^2 \tag{2}$$

where μ_c and μ_a represent the cationic and anionic mobilities, respectively. e is the elementary charge, J is the current density, z_c is the cationic charge numbers, C_0 is the initial concentration, and D is the diffusion coefficient.

In the case of Li deposition on heterogeneous substrates, another heterogeneous nucleation model was proposed as well. Both space-charge model and heterogeneous nucleation model suggest that the size, shape, and areal density of Li nucleation are subjected to the influence of Li-ion distribution in bulk electrolyte and the surface state of substrate [27–29]. For instance, the initial Li nucleation needs to overcome a certain nucleation barrier when there is a lattice mismatch between the substrate (e.g., Cu) and Li [30]. With nonuniformly distributed Li-ion flux and concentration gradient in the bulk electrolyte, the anions in some areas of electrode surface will be rapidly exhausted. The as-generated large space charge region would consequently trigger the random nucleation and growth of Li dendrites [31, 32].

Given that the hyperactivity of Li metal will induce the formation of SEI during the initial Li nucleation, a SEI-induced nucleating model was suggested. The SEI with a heterogeneous mosaic or dual-layer structure can give rise to nonuniform Li-ion transport and Li dendrite growth easily [33, 34]. Moreover, SEI is fragile, which can be broken due to the huge electrode volume swings during Li plating/stripping processes. The continuous destruction and regeneration of SEI produce massive "hot spots" for dendrite nucleation, and hence rampant Li dendrite growth [35, 36]. Upon cycling, the dendritic Li grown from the uneven tips or pits could simply break off from the root to form "dead Li", resulting in the severe corrosion of Li anode and fast electrolyte depletion [37–40]. The resultant inactive components also lead to permanent volume expansion of the electrode and increased interface resistance, both of which are detrimental to the electrochemical performance [41, 42]. It is even worse that the Li dendrites with tree/whisker-like morphologies may pierce the separator, initiating short circuit and unexpected thermal runaway of the battery [43, 44].

To sum up, Li nucleation and SEI formation are related to a number of factors in bulk electrolyte and at the substrate surface, which determine the subsequent Li deposition/dissolution processes, as illustrated in Fig. 2. In case of uneven Li nucleation and SEI formation, the deposition/dissolution of Li is arbitrary and uncontrollable. Accordingly, many troublesome issues, such as Li dendrites growth, SEI fracture, uncontrolled volume expansion, "dead Li" accumulation, Li electrode corrosion, electrolyte depletion, etc., will be agitated, causing LMBs failure. These issues are not independent but interconnected among each other. Therefore, a uniform Li nucleation together with a stable SEI layer are absolutely necessary to afford a reliable LMAs.

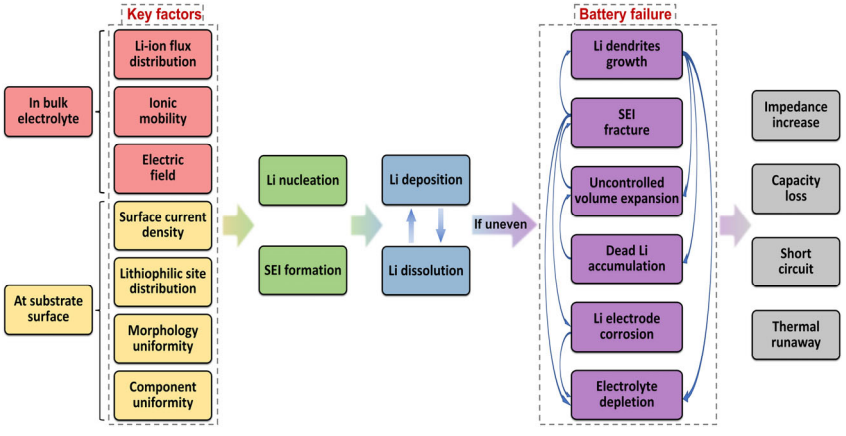

Figure 2 Key influencing factors and challenges of LMBs.

3 Planar modified Cu foils

3.1 Atom-scale modification

Cu foil, the current collector of commercial LIBs, plays a critical role in collecting current and supporting active materials. Because of its high density (8.96 g·cm^{-3}), Cu foil normally accounts for over 10% of the total battery weight [45, 46]. Accordingly, the thickness of Cu foil is suggested to be no more than 10 μm so that to achieve high-energy-density batteries [47]. Different from LIBs, the stability of LMAs during cycling is closely related to the surface structure of Cu substrate, which is capable of influencing the Li nucleation and deposition processes. However, the crystal mismatch between the commercial planar Cu foil and Li leads to a large heterogeneous nucleation barrier, which inhibits the full coverage of deposited Li metal on the substrate. Therefore, lithiophilic modification and the understanding of the surface properties of Cu foil are strongly desired.

From an atomic perspective, heterogeneous nucleation has to overcome the energy barrier of the crystalline mismatch between adsorbent and substrate [16]. Using cryo-transmission electron microscopy (cryo-TEM), Cui's group revealed that Li dendrites prefer to grow along the <111> direction (49% by number), but are not inclined to form along the <110> direction (19%) (Figs. 3(a)−3(d)) [48]. Normally, Li metal has a body-centered cubic crystal structure, where (110) plane surface with dense atomic arrangement exhibits the lowest energy. Therefore, inducing preferential Li deposition with (110) lattice structure is beneficial for suppressing dendrite

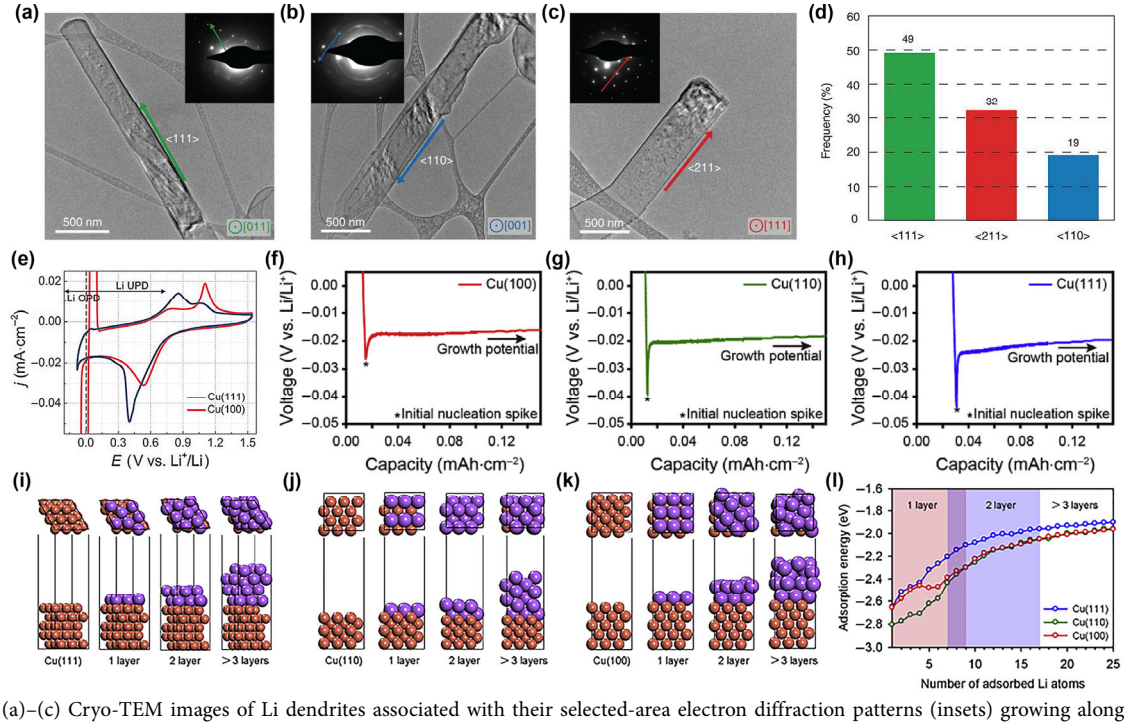

Figure 3 (a)–(c) Cryo-TEM images of Li dendrites associated with their selected-area electron diffraction patterns (insets) growing along (a) <111>, (b) <110>, and (c) <211> directions. (d) Statistics showing the frequencies of Li dendrites growth along the <111>, <110> and <211> directions. Reproduced with permission from Ref. [48], © Li, Y. Z. et al. some rights reserved; exclusive licensee American Association for the Advancement of Science 2017. (e) Cyclic voltammograms of Cu (111) and Cu (100) electrodes at a scan rate of 20 mV·s^{-1}. Reproduced with permission from Ref. [49], © Wiley-VCH Verlag GmbH & Co. KGaA, Weinheim 2019. (f)–(h) Voltage profiles successively showing Li nucleation overpotential on the (100), (110) and (111) planes of single Cu crystals at 0.2 mA·cm^{-2}. Top and side view of Li adsorptions on the (i) (111), (j) (110) and (k) (100) planes of Cu, and (l) the associated adsorption energies. Reproduced with permission from Ref. [50], © Elsevier B.V. 2019.

growth and minimizing the surface energy. It is well-known that (111) is the predominant plane of Cu foil, which is unfavorable for Li deposition because of its lithiophobic feature [51]. In this respect, numerous efforts have been focused on evaluating the impacts of Cu facets on Li deposition behaviors in the substrate [52]. Mao et al. discovered that the deposition of Li on Cu substrates undergoes under-potential deposition to form a Li metal monolayer. As shown in Fig. 3(e), the higher initial potential for Li deposition on Cu (100) than that on Cu (111) suggests its higher affinity with Li, which could guide more uniform Li nucleation and deposition [49]. Similarly, Kim et al. also demonstrated the Cu single crystal with (100) plane has the lowest Li nucleation overpotential with respect to the (110) and (111) planes (Figs. 3(f)−3(h)). Based on density functional theory (DFT) calculations, they found that Cu (111) shows the lowest Li adsorption energy, thus is unfavorable for Li adsorption (Figs. 3(i)–3(l)). While Cu (110) with the highest adsorption energy has a larger propensity for Li deposition in the initial stage, however, the presence of the highest degree of surface passivation layer is disadvantageous for subsequent Li growth. By contrast, the (100) plane-majored Cu showing decent surface energy and stable passivation layer would guarantee Li nucleation with good uniformity and high density [50]. Along this line, they further developed a Cu current collector with sharp wrinkles and highly uniform (100) facet, which promotes homogeneous Li-ion flux distribution and homogenizes Li adsorption energy at the Cu surface. Consequently, a smooth Li deposition morphology without dendrites growth was obtained, contributing to stable cycling performance [53].

Note that, the commercial Cu foil is polycrystalline consisting of plentiful small grains with randomly oriented planes. Therefore, the Li deposition behavior on the Cu substrate can be influenced by the grains, grain boundaries, defects, and impurities as well [54, 55]. As a typical defect in crystalline materials, dislocation can significantly affect the physicochemical properties of Cu and change its Li adsorption energy. Qin et al. introduced different dislocation densities into Cu foil by stretching with different strains ranging from 0% to 10%. They discovered that the Li nucleation barrier on Cu gradually decreases with the increase of dislocation density. At an optimized strain of 5%, the Cu substrate shows smooth and compact Li deposition morphology with good reversibility [55]. Therefore, it is not proper to conclude that Cu substrate is lithiophobic. The Li affinity of Cu substrate can be improved through the reconstruction of its crystal orientation

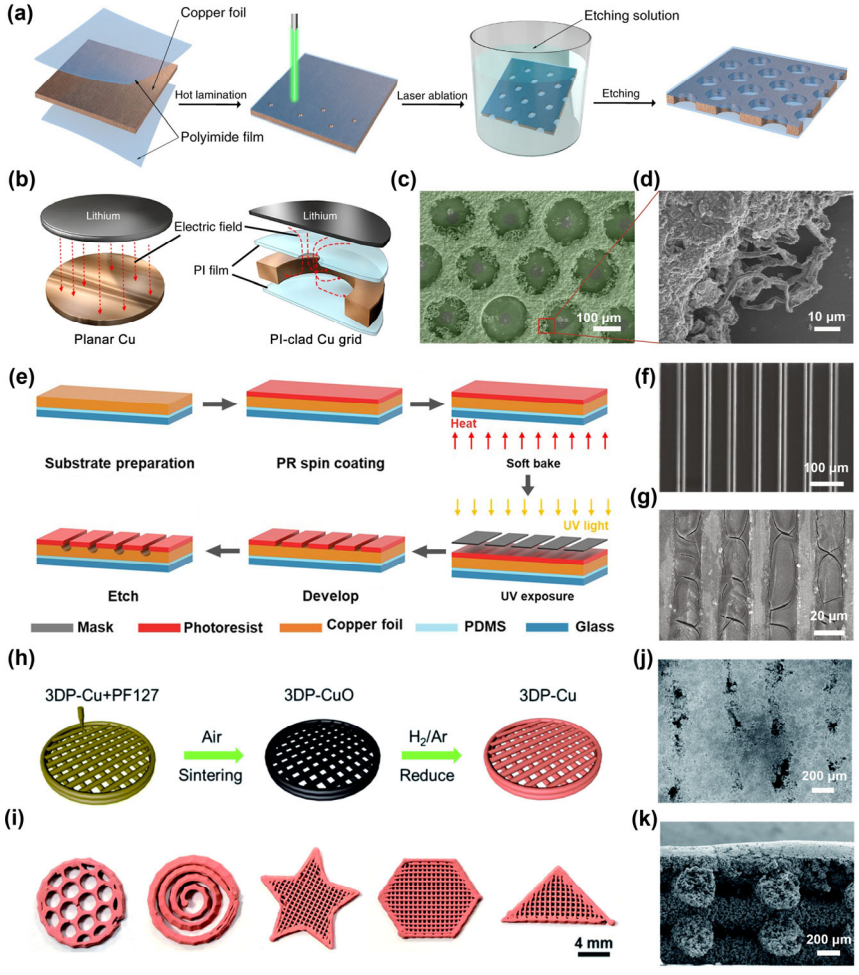

Figure 4 Schematic illustrations of (a) the fabrication of E-Cu and (b) the electric field distributions in planar Cu and E-Cu. (c) Low-resolution and (d) high-resolution SEM images of E-Cu after Li plating 0.5 mAh·cm^{-2} at 0.5 mA·cm^{-2}. Reproduced with permission from Ref. [56], © Zou, P. C. et al. 2018. (e) Schematic illustration of the fabrication of I-Cu foil. SEM images of I-Cu foil (f) after focused ion beam milling and (g) 1 mAh·cm^{-2} Li plating. Reproduced with permission from Ref. [57], © Elsevier B.V. 2021. (h) Schematic illustration of the fabrication of 3DP-Cu. (i) Schematics of 3DP-Cu with various shapes and sizes. (j) Surface and (k) cross-section SEM images of 3DP-Cu with a Li plating capacity of 20 mAh·cm^{-2}. Reproduced with permission from Ref. [58], © The Royal Society of Chemistry 2020.

or the rational arrangement of its surface defects. Given that the influencing aspects of Cu surface chemistry on Li plating/stripping behaviors are multitudinous and complex, a clear structure-performance relationship needs to be further studied to better guide the development of advanced Cu current collectors.

3.2 Surface patterning

Apart from the surface properties of Cu substrate, the external parameters, including electric field, ion concentration and distribution of ion flux, etc., also affect Li migration behaviors [16, 40]. Typically, the structural features of current collectors and separators have profound effects on the interfacial Li chemistry. On one hand, the planar Cu current collectors usually exhibit rough surface associated with "tips effects" to induce the buildup of electric charges [31]. On the other hand, the commercial separators with uneven pore structure are not conducive to uniform Li-ion flux. Therefore, pre-forming regular and ordered patterns on Cu foil surface has been considered to be a proven method to dissipate current density and uniformize Li-ion flux at the electrode surface.

Laser processing is a kind of micro/nano-machining technique that is frequently used for patterning Cu foils. As early as 2017, Guo and co-workers prepared vertically aligned Cu microchannels by laser micro-processing [59]. COMSOL simulations indicate that the current density within the Cu microchannels is larger than that on the upper surface, hence more preferential Li nucleation and deposition inside the channels. Such an unusual geometrical structure not only significantly homogenizes the distributions of electric field and Li-ion flux, but also provides appropriate pore volume for Li accommodation without dendrites growth. Likewise, Zou et al. developed a polyimide (PI)-clad Cu grid current collector (E-Cu) through the joint strategies of hot lamination, laser ablation and alkaline etching (Fig. 4(a)). In this case, the electric field of the E-Cu firstly goes through the pinhole of the insulative PI layer, and then extends laterally to the Cu scaffold surface (Fig. 4(b)). As demonstrated by the scanning electron microscopy (SEM) observations (Figs. 4(c) and 4(d)), the lateral growth of Li dendrites significantly improves the cycling stability and safety of LMBs [56]. Further, John Wang and co-workers proposed an *in-situ* polymerization of Li-affinity polydopamine (PDA) on the surface of laser-processed 3D porous Cu (PDA@3D Cu). The resultant PDA@3D Cu with holey structure shows dramatically reduced local current density and nucleation overpotential during Li cycling. Consequently, the electrode maintains a Coulombic efficiency (CE) of 96.4% (2 $mA{\cdot}cm^{-2}$, 1 $mAh{\cdot}cm^{-2}$) after 150 cycles and superior cycling for 1,000 h in symmetric batteries [60]. Following that, other surface-patterned Cu foils with tangent and lithiophilic hemispherical structure [61], fish-scale pattern [62], and hierarchically porous feature [63] have been explored. The as-constructed Cu current collectors with well-designed 3D patterns are beneficial for homogenizing Li-ion distribution, and inducing uniform Li metal deposition, as well as alleviating electrode volume expansion.

Photolithography is another approach for the scalable and controllable fabrication of surface-patterned Cu current collectors. As illustrated in Fig. 4(e), Park et al. combined the photoresist process and chemical treatments to construct an intagliated Cu foil (I-Cu). The I-Cu foil has a well-defined pattern of micrometer-scale line accompanied with nanopores-enriched trenches (Fig. 4(f)). After the introduction of oxygen functional groups by immersing I-Cu foil into hydrogen peroxide, Li metal will selectively nucleate and deposit into the trenches with a flat surface morphology (Fig. 4(g)) [57]. Similarly, Jang et al. prepared a 3D patterned Cu substrate containing a receding region with a depth of ~10 μm and a surface height of <10 nm [64]. The unique structure drastically lowers the local current density and promotes even Li nucleation/deposition within the electrode. Using a nano-micro-imprinting method, Li et al. synthesized a highly regular micro-hole-grid (MHG) Cu foil current collector [65]. Specifically, CuCl-coated pores were introduced into the MHG Cu foil, resulting in an *in-situ* formed SEI layer and high-specific-area Cu nanoparticles by subsequent CuCl reduction. Cryo-TEM and X-ray photoelectron spectroscopy results revealed that the as-made SEI is comprised of an elastic organic top layer and a lithiophilic LiCl-rich bottom layer, which not only withstands electrode volume fluctuation but also ensures rapid Li-ion supply. The as-assembled anode-free full cells using $LiFePO_4$ (LFP) as the cathode exhibit a discharge capacity of 95 $mAh{\cdot}g^{-1}$ with a high CE of up to 99.5% after 100 cycles.

3D printing is an emerging approach to produce self-supporting metallic substrate with specific structures. Figure 4(h) shows the fabrication of a porous Cu skeleton (3DP-Cu) by extrusion 3D printing technique [58]. Intriguingly, the 3DP-Cu can be engineered into a series of shapes with precise, replicable and complex structures (Fig. 4(i)). The as-obtained patterns well maintain their micro-channels between each filament even under a high pressure of 1.4 MPa, which consistently prevents Li dendrite growth and reduces electrode volume changes during Li plating/stripping processes. Therefore, the 3D skeletons still display stable Li plating/stripping behaviors at an ultrahigh capacity of 20 $mAh{\cdot}cm^{-2}$ and a rate of 10 $mA{\cdot}cm^{-2}$ (Figs. 4(j) and 4(k)). Cipollone et al. also reported a hierarchal 3D-printing Cu grid, which was patterned directly onto the solid-state $Li_{1+x}Al_xM_{2-x}(PO_4)_3$ electrolyte. The integrated structure facilitates the infiltration of molten Li into the pores of the Cu grid, and makes better physical contact between the anode and electrolyte. For these reasons, remarkable cycling stabilities in symmetric cells and full cells were obtained [66].

3.3 Surface lithophilization

Considering that Li nucleation and SEI formation collaboratively determine the subsequent Li plating/stripping processes, the Li nucleation barrier and surface geometry of Cu current collector are critical for stabilizing LMAs. Although atom-scale engineering and the pattern design of Cu foil improve Li-ion migration and facilitate uniform Li deposition, the formidable nucleation barrier of Li on Cu is unfavorable for durable LMAs [67]. To this end, surface lithophilization of Cu foil by anchoring lithiophilic sites was proposed and has achieved inspiring progress to date.

3.3.1 Metals

Among a multitude of lithiophilic species, Li metal itself is the ideal one due to its intrinsic ability of absorbing the surrounding Li ions for uniform deposition. The initial attempt found that Cu foil coated with powdery Li could afford high surface area and homogenous local current density for Li deposition [68]. As such, a patterned structure was constructed based on the pre-formation of Li metal on Cu foil [69]. The as-fabricated Li-Cu substrate presents vertically oriented

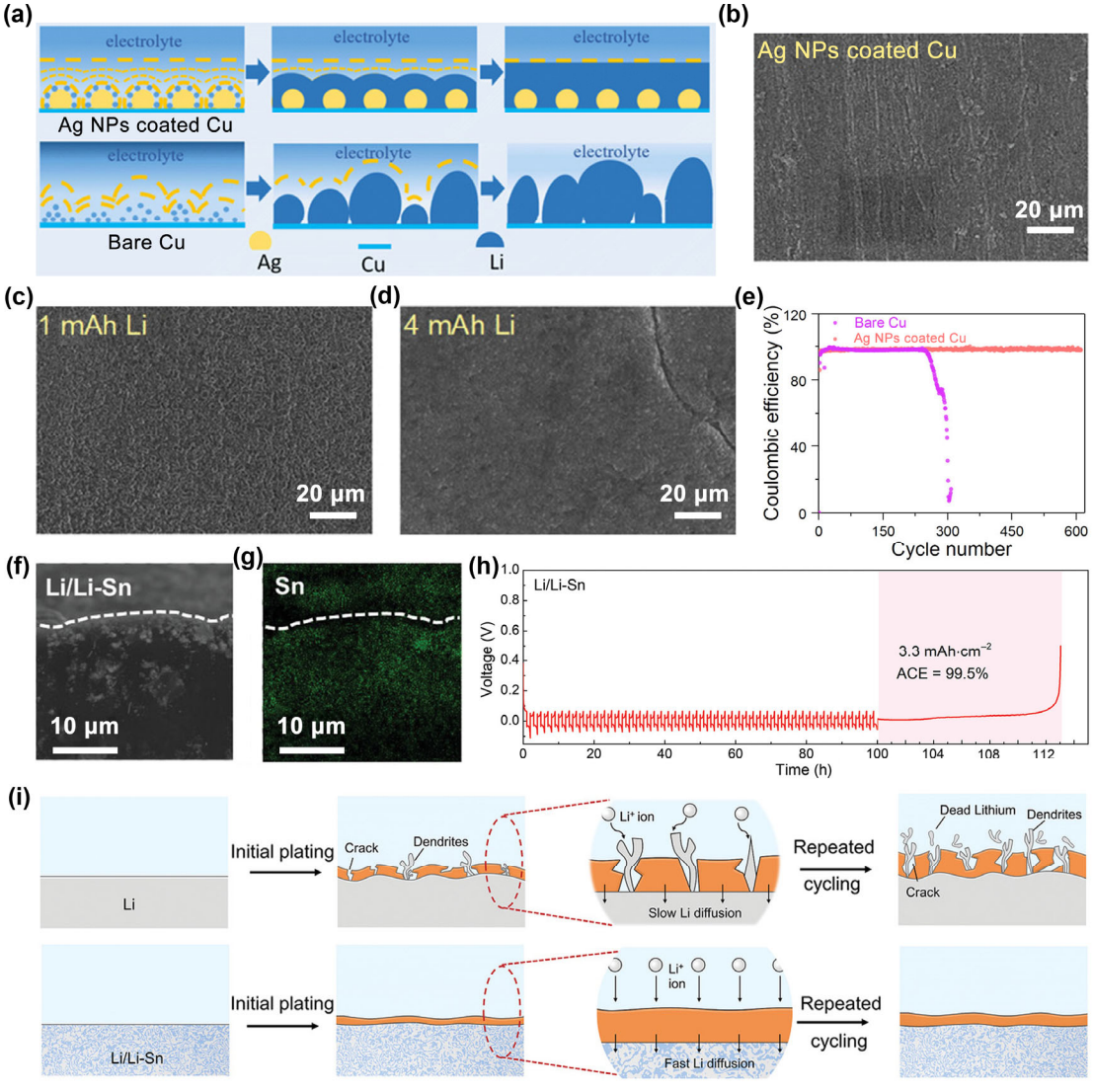

Figure 5 (a) Schematic illustrations of Li deposition on Ag nanoparticles coated Cu and bare Cu substrates. SEM images of (b) bare Ag nanoparticles coated Cu, (c) 1 mAh and (d) 4 mAh Li plating on Ag nanoparticles coated Cu. (e) CE of Ag nanoparticles coated Cu and bare Cu substrates at 0.5 mA·cm^{-2}. Reproduced with permission from Ref. [70], © American Chemical Society 2020. (f) Cross-section SEM image and (g) the corresponding Sn elemental mapping image of Li/Li-Sn electrode. (h) Aurbach CE test of Li/Li-Sn || Li/Li-Sn cell for 50 cycles at 1 mA·cm^{-2} and 1 mAh·cm^{-2}. (i) Schematics of the Li plating/stripping behaviors of bare Li and Li/Li-Sn electrodes. Reproduced with permission from Ref. [71], © Wiley-VCH GmbH 2021.

Li-Cu-Li arrays with ordered geometry, which could regulate both Li-ion flux and electric field distribution. Therefore, the anode exhibits a high charging and discharging capacity of up to 50 mAh·cm^{-2}, and meanwhile excellent cycling stability in full cells.

Regarding other lithiophilic metals for LMAs, Cui and co-workers [24] demonstrated that Au, Ag, Zn, and Mg could display almost zero overpotential for Li nucleation. Jung et al. prepared a periodic Au nanopattern dots coated Cu foil by nanolithography, which was used as the model substrate to investigate the structural influence of lithiophilic sites on Li deposition [72]. It is revealed that uniform Li nucleation and growth are attained on the substrate coated with 300 nm diameter and 50 nm height of Au dots. Otherwise, severe agglomeration of Li metal or even dendrite growth would take place, leading to the early failure of LMAs. Besides Au, Ag also shows a great potential for modifying Cu foil because of its facile fabrication and good electrical conductivity [70, 73]. Zhu et al. fabricated Ag coated Cu foil by a simple replacement reaction between Cu and $AgNO_3$, in which the spherical Ag nanoparticles were uniformly distributed on the substrate [70]. Compared with bare Cu current collector, the electrode with Ag is supposed to present more uniform Li-ion flux distribution, hence even Li nucleation and deposition (Figs. 5(a) and 5(b)). With the increase of Li plating capacity from 1 to 4 mAh, the electrode consistently shows a flat and smooth depositing morphology (Figs. 5(c) and 5(d)). In addition, a high CE of 99% can be attained over 600 cycles at 0.5 mA·cm^{-2} (Fig. 5(e)). Thanks to the uniform and dense Ag nanoparticles distribution, the nuclei density of Li and surface diffusion of Li ions on the electrode are substantially increased [74, 75]. Importantly, the preferential nucleation of Li metal on Ag sites guarantees a smaller Li nucleus size and a lower nucleation overpotential. Recently, Fan et al. prepared a flexible and free-standing network composed of porous 3D Ag nanowires coated Cu foil through a simple evaporation assembly [76]. The compact Ag nanowires layer increases the porosity and inner space of the framework, which promote electrolyte accessibility and uniform

Li deposition. In addition to Ag modification, Zhang et al. prepared a thin Zn layer covered Cu foil by electrodeposition, where the formation of Li-Zn alloy layer during Li nucleation gives rise to a smooth Li deposition without any dendrites [77]. Similarly, a superficial lithophilic Sn layer coated on Cu foil was fabricated through a facile blade-casting process (Figs. 5(f) and 5(g)) [71]. The Li/Li-Sn electrode delivers a stable cycling for over 900 h in symmetric cells and attains a high CE of 99.5% (1 mA·cm^{-2}, 1 mAh·cm^{-2}) after 100 h in half cells (Fig. 5(h)). The appealing performance is attributed to the uniform Li-Sn alloy layer that decreases the Li nucleation barrier and facilitates Li diffusion over the entire electrode, thus inhibiting the generation of large dendritic protrusions (Fig. 5(i)).

Despite remarkably improved Li deposition, the long-term durability may become uncontrollable when excessive Li metal or SEI passivates the lithiophilic interface. Aiming to explore durable lithiophilic metals, He et al. investigated the electronic localization and surface work function of the Cu foil coated with different metals (e.g., Bi, Al, and Au) [78]. It is demonstrated that Li-Au alloy exhibits the lowest electron localization function at the initial state of nucleation, indicative of its incompetency in regulating Li ions. While Li-Al alloy would attract free electrons to form undesired segregation associated with uneven localized electrons distribution, which trigger fast Li dendrite growth. By contrast, Li-Bi alloy presents a uniform distribution of localized electrons, which facilitates the absorption of Li ions and the decomposition of Li cluster. As a result, Bi is more suitable for the lithiophilic modification of Cu foil, where the formed Li-Bi alloy ensures a flat and compact Li deposition morphology. Alternatively, Zhang et al. studied the Li plating/stripping behaviors and phase transition of different lithiophilic metals modified Cu foil, such as Ag, Mg, Au, Al, Zn, Si, and Sn [79]. These metals are classified into two categories according to the way that they interact with Li. Ag and Mg form solid solutions with Li metal, thus delivering a slight structural variation during Li plating and stripping. Other metals including Au, Al, Zn, Si, and Sn generate Li-based intermetallic compounds, which could be easily passivated by the newly formed Li metal. Beyond that, the generated Li-based intermetallic compounds are likely to be pulverized during continuous Li plating/stripping, ultimately leading to fast capacity fading of the electrode.

3.3.2 *Metal compounds*

Apart from elemental metals, metal compounds are also ideal candidates to modify Cu foil by virtue of their excellent lithiophilicity, structural stability, and facile fabrication. It has been widely demonstrated that metal compounds can react with the deposited Li through the conversion reaction of Li + MX → M + LiX (X = O, N, S, F, P, Cl, etc., M = Au, Ag,

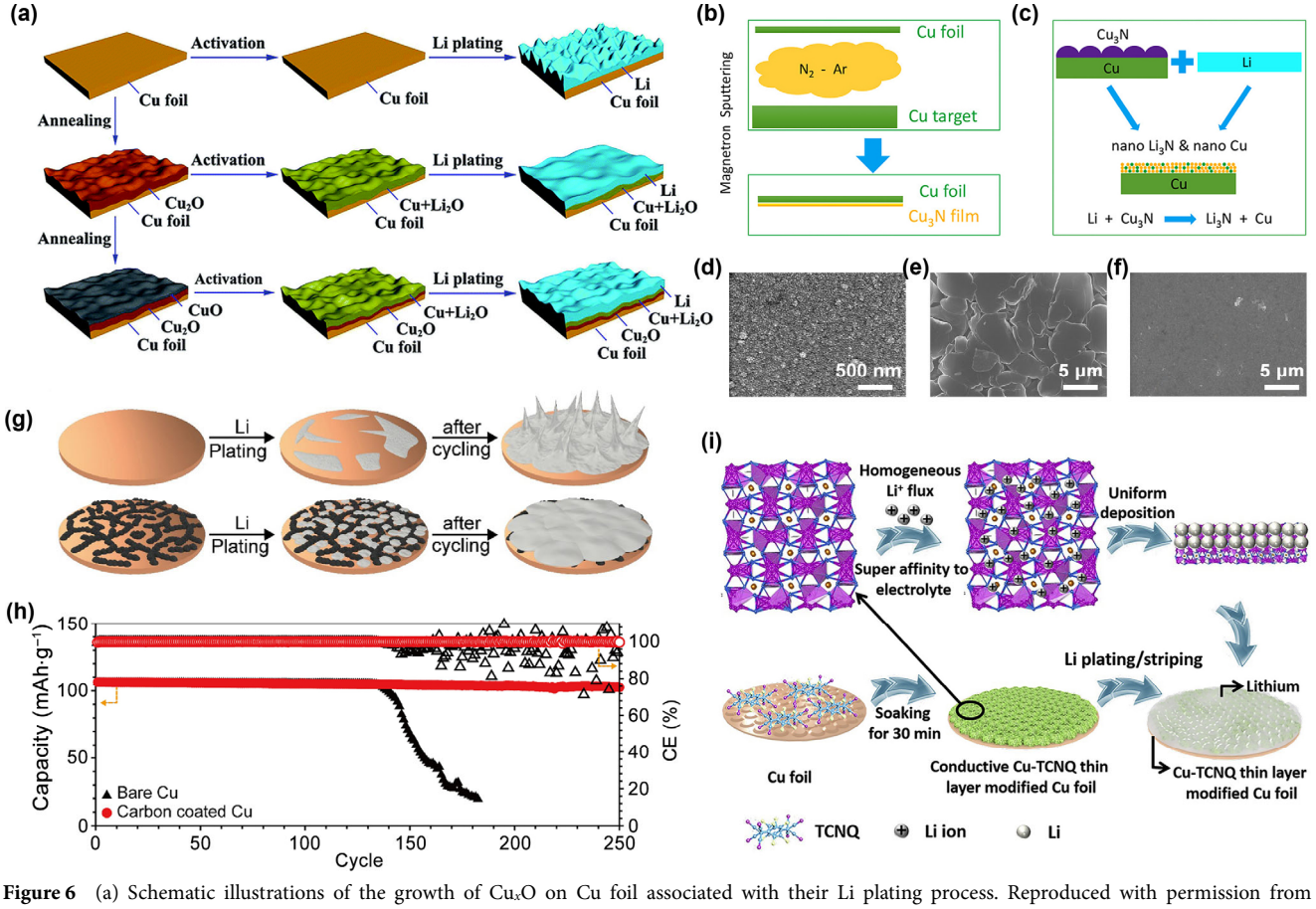

Figure 6 (a) Schematic illustrations of the growth of Cu$_x$O on Cu foil associated with their Li plating process. Reproduced with permission from Ref. [80], © The Royal Society of Chemistry 2018. Schematic illustrations of (b) the preparation of Cu$_3$N film coated Cu foil and (c) *in-situ* formation of Cu/Li$_3$N composite film. SEM images of Cu$_3$N/Cu foil (d) in the pristine state, (e) after first Li plating, and (f) Li stripping. Reproduced with permission from Ref. [81], ©American Chemical Society 2018. (g) Schematic illustrations of Li/Cu cells with and without carbon interlayer during repeated cycling. (h) Cycling performance of the full cells assembled with $LiMn_2O_4$ cathode and composite Li anode. Reproduced with permission from Ref. [82], © Elsevier B.V. 2020. (i) Schematic illustration for the growth of Cu-MOF thin layer on Cu foil and the corresponding Li deposition process. Reproduced with permission from Ref. [83], © Yin, D. M. et al. 2020.

Zn, Sn, Mg, Cu, In, etc.) [84–87]. The generated metals could form solid solution or intermetallic compounds when further alloying with Li (xLi + M → Li$_x$M), which not only provides abundant active sites for Li nucleation and deposition, but also accelerates the ionic transport at the interface. In this regard, Cu current collector can be directly engineered to bear a lithiophilic surface with copper oxides, sulfides, nitrides, or phosphides, which is beneficial for regulating Li deposition. As illustrated in Fig. 6(a), a facile air annealing of Cu foil could induce a Cu$_x$O (Cu_2O or CuO) layer on the substrate, namely Cu$_x$O@Cu, which delivers a lower nucleation overpotential of 28.8 mV compared to bare Cu foil (59.8 mV) [80]. Specifically, the initially deposited Li metal reacts with the superficial Cu$_x$O, forming a lithiophilic Li_2O layer that benefits Li deposition. Zhuang et al. further introduced boric acid as the electrolyte additive to construct a protective SEI layer on the Cu$_x$O@Cu substrate. The cross-linked borates endow the SEI layer with high mechanical strength and elasticity, which inhibit Li dendrite growth and uniformize Li plating/stripping effectively [88]. Given that the thickness and density of the oxidized Cu layer can be readily controlled by mediating the annealing parameters (e.g., temperature and time), this methodology is expected to achieve ultrathin LMAs. Very recently, Kay et al. fabricated Li-Cu composite anodes with adjustable thickness between 1−30 μm through a roll-to-roll dip coating of liquid Li metal on Cu_2O@Cu substrate [89]. At a thin Li layer of 5 μm, the electrode exhibits a high Li utilization in half cells, and moreover, contributes to significantly improved energy density in all-solid-state full cells. Beyond direct engineering, decorating lithiophilic metal compounds on Cu current collector is another efficient approach to modify its surface properties [90–92]. In order to construct a robust interlayer for LMAs, Chen and co-workers pre-coated a thin Cu_3N film on Cu foil by a reactive sputtering method, where Li_3N is generated through the reaction between Cu_3N and deposited Li (Figs. 6(b) and 6(c)). The formed Li_3N interlayer not only maintains high structural stability of Li metal, but also guarantees smooth Li plating/stripping processes (Figs. 6(d)–6(f)) [81]. Likewise, other metals nitrides, such as AlN and InN, also show high efficiency in constructing Li_3N-containing layer on Cu foils [93, 94].

3.3.3 *Carbon materials*

Carbonaceous materials, such as graphene, carbon nanotubes (CNTs), carbon nanofibers (CNFs) and porous carbon, have been intensively studied as the functional layer of Cu foils [95–97]. For instance, Jin et al. reported a submicron-thickness carbon interlayer coated Cu foil by blade casting process (Fig. 6(g)) [82]. Serving as a conducting bridge between the plated Li and Cu foil, the carbon layer affords compact Li deposition. After coupling with $LiMn_2O_4$ cathode, the full cells exhibit stable cycling with CE reaches up to of 99.9% after 250 cycles (Fig. 6(h)). It is noted that pristine carbon generally displays poor lithiophilicity due to the mismatched lattice structure between carbon and Li. To this end, a composite layer comprising reduced graphene oxide and lithiophilic Cu_2O was *in-situ* constructed onto the Cu foil, which remarkably decreases the overpotential of Li nucleation [98]. Recently, Luan et al. prepared a g-C_3N_4 modified Cu foil substrate by means of mechanical pressing. The g-C_3N_4 with plentiful O and N sites promises fast Li-ion transport and strong affinity to Li ions, thus smoothing Li plating/stripping significantly [99]. In addition, Wang et al. demonstrated that graphdiyne nanosheet with uniformly distributed acetylene bonds realizes a highly stable Li plating/stripping for 1,000 cycles at 2 mA·cm^{-2} [100].

3.3.4 *Organic species*

Organic compounds have attracted considerable attention as the coating materials of Cu foil by virtue of their abundant lithiophilic functional groups. For example, Fan et al. plated a uniform polythiophene derivatives (PTs) layer on Cu foil. The PTs with oxygen functional groups provide higher absorption energy of Li ions, which is advantageous to induce the directional deposition of Li ions in a dendrite-free manner [101]. Alternatively, Wen et al. reported a self-assembled hydrolyzed 3-mercaptopropyl trimethoxysilane layer coated Cu current collector. Owing to the flexible and lithiophilic Si-O-Si backbones, the surface energy of Cu foil was remarkably decreased, which promotes the lateral growth of Li nuclei [102]. Covalent organic frameworks (COFs) and metal-organic frameworks (MOFs) with periodic units were also found to provide well-defined channels for accommodating Li metal and accelerating Li-ion transport when coated on Cu substrates [103, 104]. The rich lithiophilic functional groups remarkably enhance the absorption of Li ions, resulting in even Li deposition and dissolution processes. Yin et al. prepared a thin-layer Cu-based MOFs on Cu foil by the coordination between Cu metal nodes and 7,7,8,8-tetracyanoquinodimethane (TCNQ) [83]. As shown in Fig. 6(i), the polar functional groups of TCNQ increase the wettability of electrolyte toward electrode, and simultaneously enhance the adsorption of Li ions. Therefore, Cu-TCNQ layer ensures uniform Li-ion flux and smooth Li plating/stripping behaviors, resulting in superior rate capability and cyclability of the electrode in both half and full cells.

3.4 Protective layer introduction

Although surface structuralization and lithophilization of Cu substrates have exhibited remarkable regulation for Li nucleation and deposition, too thick Li metal or excessive SEI accumulation would shield the lithiophilic surface, especially under high current density or cycling capacity [105, 106]. Constructing a protective layer on Cu foil is a valid route to induce Li deposition in their interlayer spaces, which not only avoids the direct contact between Li metal and the electrolyte, but also homogenizes Li-ion flux of the electrode [107]. An ideal protective layer generally holds good permeability of Li ions and electrolyte, excellent physical/chemical stability, and high mechanical strength [108, 109]. To date, inorganic, polymeric, and their composite protective layers have been widely evaluated.

3.4.1 *Inorganic coatings*

As a representative example of inorganics, carbon is deemed as one of the most promising protective layer candidates for Cu foil. Cui's group pioneeringly reported a flexible hollow monolayered carbon nanosphere on Cu foil for durable LMAs (Fig. 7(a)) [110]. The carbon layer exhibits a highly monodisperse structure with long-range order and a high

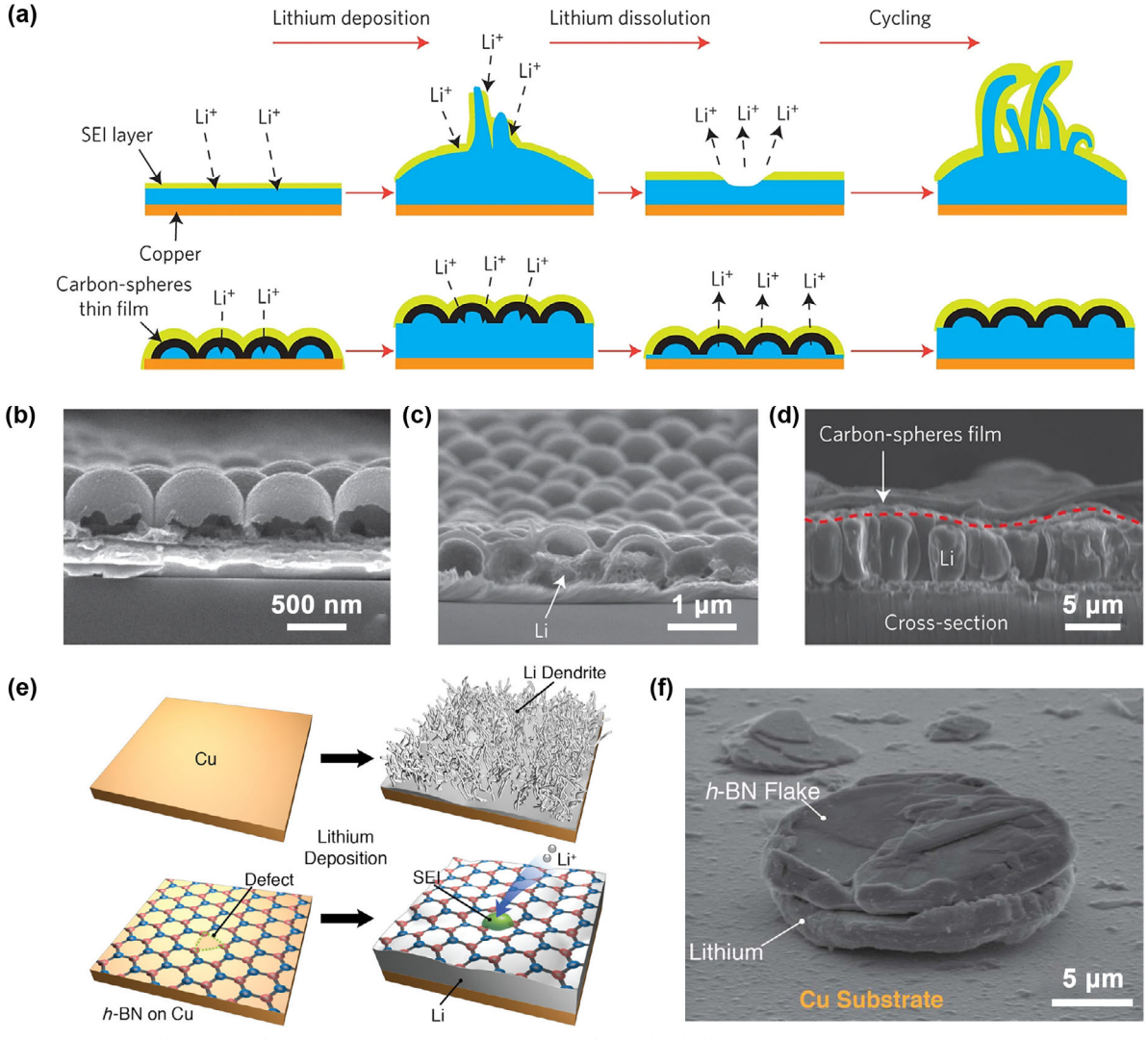

Figure 7 (a) Schematic illustration of Li deposition on bare Cu and the Cu foil with a hollow carbon nanosphere layer. Cross-section SEM images of (b) bare hollow carbon nanospheres, (c) initial Li deposition and (d) continues Li deposition underneath carbon nanosphere layer. Reproduced with permission from Ref. [110], © Macmillan Publishers Limited 2014. (e) Schematic illustration of Li deposition on bare Cu and h-BN coated Cu foil. (f) SEM image of Li deposition on Cu foil with exfoliated h-BN flakes. Reproduced with permission from Ref. [111], © American Chemical Society 2014.

Young's modulus of ~200 GPa, in which Li metal deposits into the hollow carbon nanospheres during the initial nucleation (Figs. 7(b) and 7(c)). With the increase of Li plating capacity, granular Li starts to grow below the hollow carbon nanosphere layer due to the weak binding force between the protective layer and substrate (Fig. 7(d)). As a result, the Cu foil with carbon layer achieves a CE of ~99% (1 mA·cm^{-2}, 1 mAh·cm^{-2}) for more than 150 cycles. Furthermore, they also reported a spectrum of 2D atomic crystals as the protective layers for modifying Cu foil. For example, hexagonal boron nitride (h-BN) was grown on Cu foil via a chemical vapor deposition (CVD) method (Fig. 7(e)) [111]. In this case, Li ions can penetrate the point or line defects of h-BN layer and deposit below, thus regulating the conduction and dispersity of Li ions (Fig. 7(f)). The ultrathin h-BN atomic layer displaying excellent chemical stability, flexibility, and close to 1 TPa Young's modulus provides good interface protection for LMAs. Based on DFT calculations, Liu et al. further revealed that h-BN can reduce the adsorption energy and strengthen the transport of Li ions, thereby inducing Li deposition beneath the protective layer [112]. Besides, the insulating and lithiophobic h-BN layer not only inhibits excessive interface reaction between Li metal and electrolyte, but also increases the surface tension for Li nucleation and growth to realize dendrite-free deposition. Considering that CVD-grown h-BN layer is polycrystalline with numerous defects, the growth of Li dendrites from these "hot spots" might be unavoidable. To this end, LiF was anchored on the h-BN by atomic layer deposition (ALD) [113]. The defects of h-BN provide distinct anchoring sites for LiF, which in turn repairs the defects for better Li deposition. As a result, the improved cycling stability of LiF/h-BN hybrid films lead to a long cyclic life of the LMBs.

3.4.2 *Polymeric coatings*

Compared with inorganic counterparts, polymeric protective layers have superior flexibility and adhesion, thus better

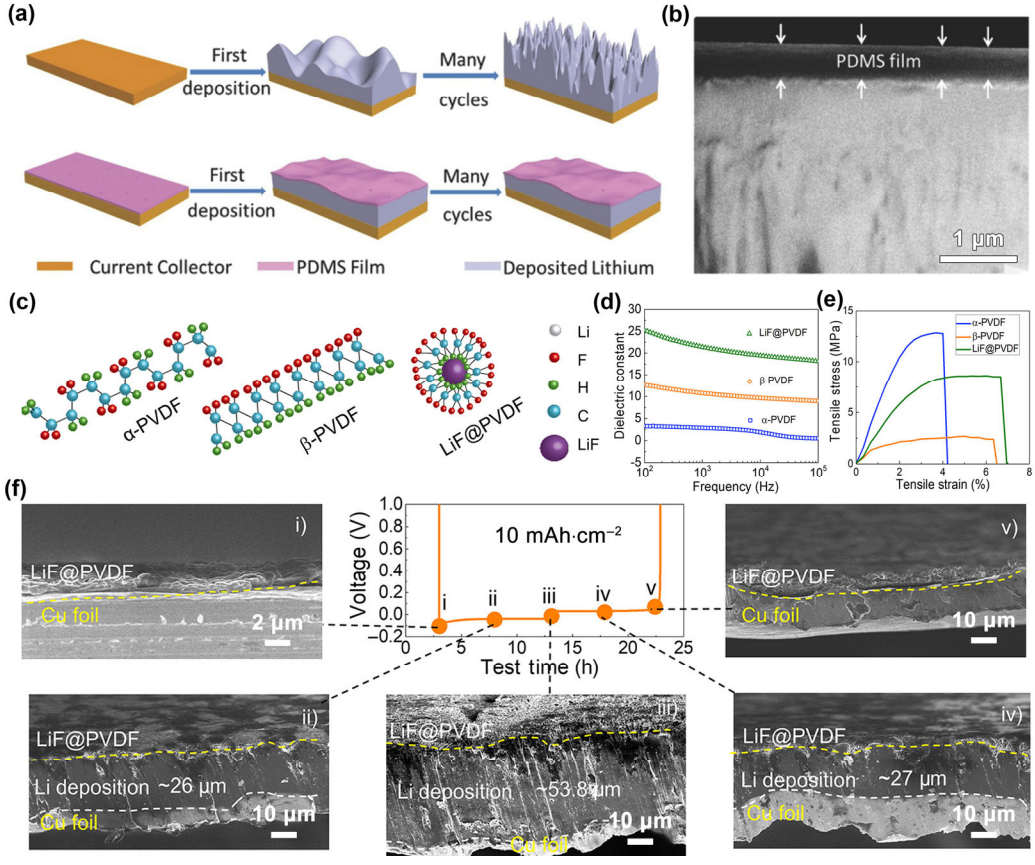

Figure 8 (a) Schematic illustration of Li deposition on bare Cu and PDMS coated Cu foil. (b) Cross-section SEM image of PDMS coated Cu foil after HF treatment. Reproduced with permission from Ref. [114], © WILEY-VCH Verlag GmbH & Co. KGaA, Weinheim 2016. (c) Molecular structures of *α*-PVDF, *β*-PVDF, and LiF@PVDF. (d) The dielectric constants and (e) stress-strain curves of different PVDF-based films. (f) Voltage profiles and the corresponding cross-section SEM images of Li plating and stripping on LiF@PVDF at a capacity of 10 mAh·cm^{-2}. Reproduced with permission from Ref. [115], © American Chemical Society 2021.

interfacial contact for alleviating the local stress of Li metal [116]. In addition, the structural diversity of organics enables the easy introduction of lithiophilic functional groups into the polymeric layers, which is capable of reducing the Li nucleation barrier and affording a Li-ion buffering area [117]. To date, a series of polymers, including MOFs, COFs, biopolymers, and polymeric composites have been extensively evaluated as the coating layers of Cu substrates. Zhu et al. fabricated a porous poly(dimethyl siloxane) (PDMS) film on Cu foil through the combination of spin-coating and HF etching (Fig. 8(a)) [114]. Beyond efficient protection of LMAs, the generated nanopores significantly increase the Li-ion conductivity and uniformize the distribution of Li-ion flux (Fig. 8(b)). Moreover, the robust chemical stability of PDMS protective layer renders good compatibility of the electrode in both carbonate and ether-based electrolytes. Polyvinylidene difluoride (PVDF) is another appealing candidate for modifying Cu foil toward LMAs application [118]. For *α*-PVDF, F atoms take alternating trans-gauche conformation with antiparallel dipole moments, which displays low polarity and thus is barely used in LMAs [119]. By contrast, the F atoms in *β*-PVDF exhibit all-trans conformation with parallel dipole moments, meaning a higher polarity for adsorbing Li ions (Fig. 8(c)) [115]. Luo et al. coated PVDF solution onto Cu foil, which was then slowly evaporated at 65 °C to get *β*-phase PVDF [119]. The numerous electronegative C-F functional groups in *β*-PVDF absorb Li ions and F-atom alignment, which facilitate Li-ion transport by a hopping model and hence decrease the interfacial resistance. It is noted that the interactions between Li ions and fluorine functional groups result in the *in-situ* formation of a LiF layer during cycling. This LiF layer exhibits good stability in the electrolyte and provides high surface energy and low diffusion energy barrier to induce lateral Li deposition. Unfortunately, the fluoride content in PVDF is insufficient to afford a uniform and compact LiF layer on the electrode. Accordingly, the construction of PVDF/fluorides (e.g., LiF) composites and the development of highly fluorinated polymers (e.g., poly(vinylidene fluoride-co-hexafluoropropylene (PVDF-HFP)) have been proposed [120]. For example, Tamwattana et al. introduced LiF nanoparticles into PVDF (LiF@PVDF) and then coated on Cu foil by slurry coating, which shows a higher dielectric constant and tensile strain compared to the pure *α*-PVDF and *β*-PVDF (Figs. 8(d) and 8(e)) [115]. Consequently, the LiF@PVDF protective layer significantly promotes the surface distribution of Li ions on Cu foil, resulting in uniform Li plating and stripping at a high capacity of 10 mAh·cm^{-2} (Fig. 8(f)).

Yu et al. discovered that PVDF could serve as the medium of lithiophilic amino phosphonic acid resin (APAR), where the polar functional groups of APAR enhance the Li-ion affinity of the cross-linked matrix and accelerate ion transfer at the electrode/electrolyte interphase [121]. With this design, the

electrode achieves conformal Li plating morphology and high cycling stability for over 120 cycles in Li-O_2 full cells. Chen et al. further prepared a composite nanofibers layer consisted by PVDF and polymethyl methacrylate (PMMA), in which PVDF acts as a highly porous carrier of PMMA for modifying Cu foil [122]. During Li nucleation, PMMA is gradually released from the PVDF skeleton and forms numerous C-O-Li bonds, forming a lithiophilic PMMA-Li SEI layer on the Cu foil. As a result, a smooth and dendrite-free Li deposition morphology with long-term cycling performance (500 h at 5 mA·cm^{-2} for 5 mAh·cm^{-2}) were achieved. To improve the mechanical property of PVDF, inorganic compounds with high mechanical stiffness and ionic conductivity were extensively applied as the additives. The as-designed rigid/flexible composites not only reinforce the structural stability of PVDF matrix, but also suppress its crystallinity to elevate the Li-ion conductivity. Typically, a conformal layer comprising g-C_3N_4 and PVDF was developed to decorate Cu foil [123]. The pyridinic nitrogen sites in g-C_3N_4 layer show strong coordination with Li ions, facilitating the migration of Li ions by site-to-site hopping. Therefore, the Li-ion conductivity and uniformity of Li nucleation were significantly improved as compared to the pristine PVDF layer. Xiong et al. prepared a thin $Li_4Ti_5O_{12}$/PVDF layer coated Cu foil. During the initial Li plating, a Li-rich region is built through Li-ion insertion into $Li_4Ti_5O_{12}$, namely, inverse concentration gradient, which affords an ionic conductivity of 2.32 × 10^{-3} S·cm^{-1} at room temperature and ensures smooth Li plating/stripping processes [124]. Recently, Yang et al. utilized PVDF-HFP and Al_2O_3/$LiNO_3$ additives to construct a rigid/flexible composite protective layer with one-side surface pits (PVDF-HFP@Al_2O_3/$LiNO_3$) [125]. Benefiting from the high-strength inorganic particles, the Young's modulus of the composite protective layer reaches up to 7 GPa that is high enough to inhibit dendrite growth. Also, a good ionic conductivity of 7.75 × 10^{-4} S·cm^{-1} and a high Li-ion transference number of 0.78 are obtained. When coupling with either LFP cathode or S cathode, the full cells exhibit remarkable cycling stability and rate capability.

He et al. modified Cu foil using a biopolymer of PDA layer, which is prepared by the oxidation polymerization of dopamine. In the initial stage of Li deposition, Li metal reacts with the hydroxyl groups of PDA to form Li complexing carbonyl

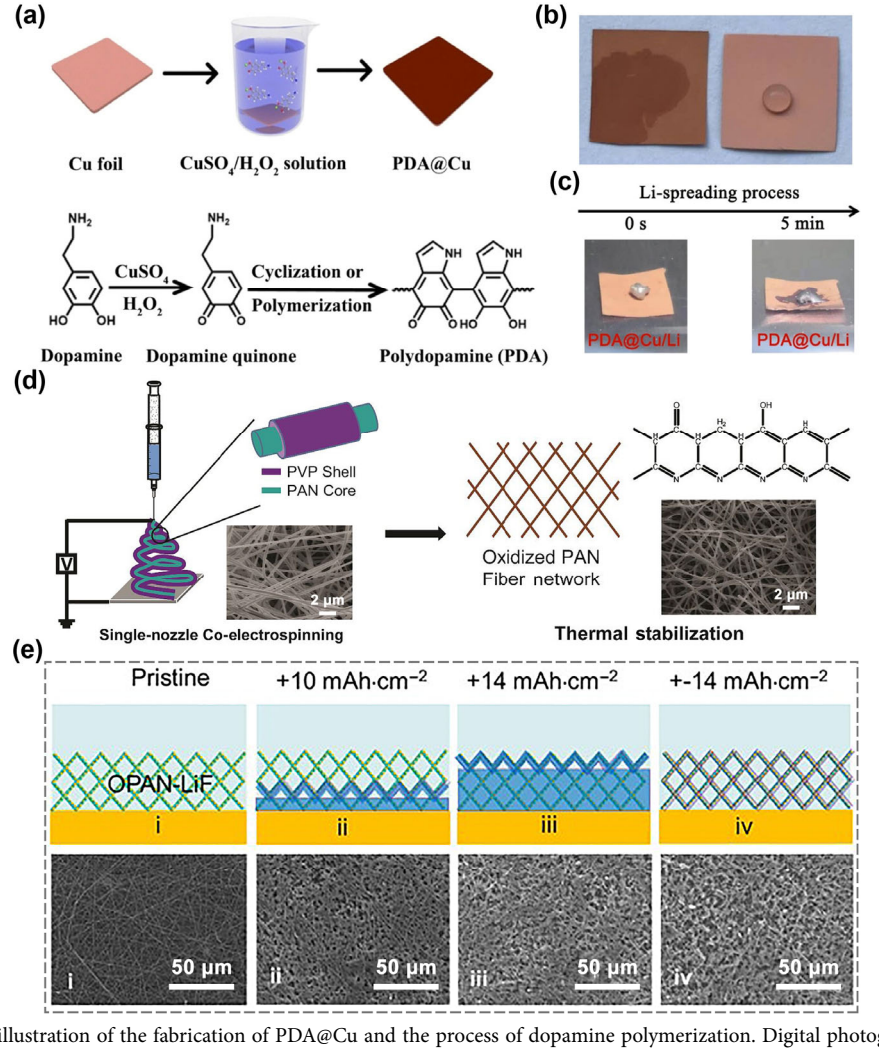

Figure 9 (a) Schematic illustration of the fabrication of PDA@Cu and the process of dopamine polymerization. Digital photographs of (b) hydrophilic tests of Cu foils with (left) and without (right) PDA coating, and (c) the associated molten Li spreading process on the PDA@Cu foil. Reproduced with permission from Ref. [126]. © American Chemical Society 2020. (d) Schematic of the preparation of OPAN nanofiber layer on Cu foil and corresponding SEM images. Reproduced with permission from Ref. [127]. © American Chemical Society 2015. (e) Schematic illustration and SEM images of Li plating/stripping on OPAN-LiF-Cu: i) bare substrate; ii) 10 mAh·cm^{-2} Li plating; iii) 14 mAh·cm^{-2} Li plating; iv) 14 mAh·cm^{-2} Li plating and re-stripping. Reproduced with permission from Ref. [128]. © Elsevier B.V. 2020.

groups [129]. These lithiophilic sites would induce flat Li deposition without dendrite growth in the electrode. Huang et al. optimized the modification procedure by using $CuSO_4/H_2O_2$ as the oxidation reagent, which achieves a faster polymerization of PDA on Cu foil (PDA@Cu) (Fig. 9(a)) [126]. The rapid-polymerized PDA layer shows higher uniformity and stability for promoting the homogeneous distribution of Li-ion flux (Figs. 9(b) and 9(c)). Recently, the incorporation of inorganic SiO_2 nanoparticles into PDA (SiO_2@PDA) was also reported, which not only enhances the mechanical property of PDA, but also improves the dielectric permittivity of the hybrid overlayer [130]. In addition, the SiO_2@PDA layer effectively homogenizes the local current distribution and Li-ion flux within SEI, resulting in uniform Li deposition. Accordingly, the anode protected by SiO_2@PDA exhibits a stable cycling performance for 2,800 and 800 h at a high current density of 5 and 10 mA·cm^{-2}, respectively.

Polyacrylonitrile (PAN) possessing abundant polar functional groups shows strong absorption of Li ions, making it competent to induce even Li nucleation and deposition. Since PAN can be easily electrospun into non-woven and ordered nanofiber films, it has been considerably explored to modify Cu current collectors [131]. With micro-sized space and 3D interconnected structure, electrospun PAN nanofiber films are capable of improving electrolyte accessibility, smoothing Li-ion flux distribution, and buffering electrode volume variations during Li plating/stripping. In 2015, Cui's group constructed 3D oxidized PAN (OPAN) nanofiber layer on Cu foil through the pre-oxidation of PAN at 300 °C in air (Fig. 9(d)) [127]. During this process, PAN transforms into a ladder-like structure with polar functional groups (i.e., C=N, C–N, C=O, O–H), rendering excellent chemical and mechanical stability. To further improve the mechanical and chemical properties of OPAN, Zhou et al. embedded LiF nanoparticles into the nanofiber [128]. The resultant OPAN-LiF-Cu framework could induce gradient growth of Li from bottom to top, resulting in uniform Li plating and stripping at a high capacity of 14 mAh·cm^{-2} (Fig. 9(e)). Impressively, a high capacity of 14 mAh·cm^{-2} at 1 mA·cm^{-2} for 60 cycles (1,680 h), and 1 mAh·cm^{-2} at 5 mA·cm^{-2} for 120 cycles were obtained. The full cells based on LFP cathode and Li/OPAN-LiF anode deliver a prolonged cycling of 1,600 cycles at 850 mA·g^{-1}. In addition to serving as the protective layer of LMAs directly, the electrospun PAN films can be utilized as a buffer layer to protect PI sphere coated Cu substrate [132]. The delicate double-layer structure (PAN/PI@Cu) displays ultralight mass, good mechanical/thermal stability, and high flexibility, which enable the homogeneous deposition of Li metal without dendrite growth. Furthermore, Sahalie et al. proposed a Al_2O_3/PAN layer coated Cu foil, where the composite protective layer enhances the mechanical strength of SEI to inhibit Li dendrite growth. In addition, the excellent wettability of Al_2O_3/PAN@Cu promotes the fast diffusion of electrolyte and uniformizes the distribution of Li-ion flux [133].

Given that polymeric layers showing low Li-ion conductivity would trigger high interfacial resistance and distinct Li-ion concentration polarization, Weng et al. developed an ultrathin Li-ion ionomer membrane (≤100 nm) to modify Cu foil. This coating layer consists of Li-exchanged sulfonated polyether ether ketone embedded with polyhedral oligosilsesquioxane [134]. After sulfonation and Li-ion exchange using titration, the protective layer presents an ionic conductivity of 1.6×10^{-4} S·cm^{-1} and Li-ion transference number of 0.73. In addition, Nan et al. developed an interlamellar ion conductor reformed artificial SEI based on 2D stratified lithium-montmorillonite (Li-MMT) coated Cu foil [135]. The Li-MMT shows superhigh ionic conductivity (4.78×10^{-4} S·cm^{-1}) by allowing fast Li-ion transfer in interlaminations and sheet-to-sheet. Subsequently, Dong et al. found that a suitable degree of Li ions substitution in carboxymethylcellulose (CMC) could improve its Li-ion conductivity and afford a Li-ion transference number of 0.66 [136]. As a coating layer of Cu foil, the CMC-Li with a large number of hydrogen bonds enables uniform Li-ion distribution, and hence a flat and dense Li deposition.

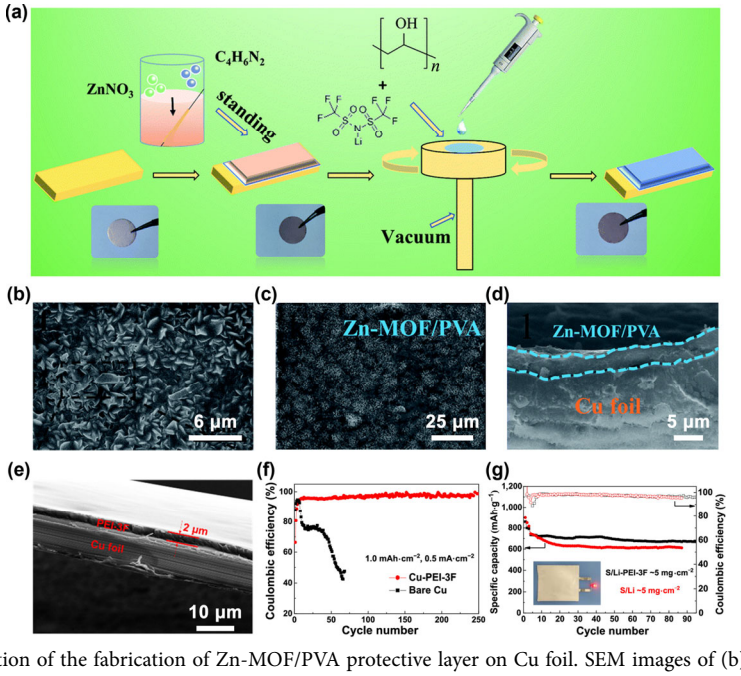

Figure 10 (a) Schematic illustration of the fabrication of Zn-MOF/PVA protective layer on Cu foil. SEM images of (b) bare Zn-MOF/PVA, (c) surface view and (d) cross-section view of Li deposition on Zn-MOF/PVA-Cu substrate after 50 cycles. Reproduced with permission from Ref. [137]. © The Royal Society of Chemistry 2020. (e) Cross-section SEM image of Cu-PEI-3F foil. (f) CE of Cu-PEI-3F and bare Cu substrates at 0.5 mA·cm^{-2}. (g) Cycling performance of the full cells assembled with S cathode and Cu-PEI-3F-Li or bare Li anode; the inset shows the battery lighting a LED bulb. Reproduced with permission from Ref. [138]. © American Chemical Society 2021.

COFs with intrinsic porosity, well-dispersed nanochannels, and robust organic skeletons are expected to achieve uniform Li-ion distribution and diffusion when applied as the protective layer of Cu foil [139]. For example, Li et al. designed a lithiophilic COFs protective layer containing preorganized triazine rings and carbonyl groups by solvothermal process [140]. The periodic structure exhibits long-range open nanochannels in the vertical direction, which remarkably facilitates Li-ion transport. Besides, the triazine rings of COFs hold abundant lone pair electrons to strongly absorb Li ions, whereas the electroactive carbonyl groups with high dielectric constant coordinate with the Li ions. Therefore, the COFs protective layer ensures smooth Li-ion flux to induce dendrite-free Li deposition. Distinct from COFs, MOFs are a class of coordination polymers that consist of metal ions and organic ligands, which is anticipated to show more lithiophilic sites and higher Li-ion conductivity [141]. Fan et al. used the polyvinyl alcohol (PVA) with lithium bis(trifluoromethane sulfonyl) imide (LiTFSI) as a "glue" to cement the Zn-based MOFs sheet onto Cu foil (Zn-MOF/PVA) (Figs. 10(a) and 10(b)) [137]. The Zn-MOF/PVA layer possessing high ionic conductivity (1.47×10^{-4} S·cm^{-1}) and plentiful polar bonds (O-H, Zn-N) to adsorb Li ions, leading to a uniform SEI and a flat Li deposition morphology (Figs. 10(c) and 10(d)). Following this line, great efforts have been made to design high-performance MOFs protective layer on Cu current collectors, such as ZIF-8@PVDF-HFP [142], ZIF-8@PVDF [143], MOF-199/PVDF [143], and ZIF-67/PVDF [144].

Other functional polymeric layers have also been developed to modify Cu foil toward high-efficiency LMAs application [145]. Zhang et al. reported a solution-processable conjugated microporous thermosetting polymer (CMP) by the concomitant polymerization of 3,6,12,15-tetrabromotetrabenzo[a,c,h,j]phenazine [146]. The novel CMP layer presents rich nanofluidic channels (5–6 Å) for Li-ion transport and diffusion, thereby delivering an ultralong cycling stability of over 3,200 h at 1 mA·cm^{-2} and 2,550 h at 20 mA·cm^{-2}. Zwitterionic polymeric interphase composed of cationic and anionic charges immobilized on the same molecule has been proposed to further enhance the Li-ion conductivity and Li-ion transference number [147]. Jin et al. prepared a polymer zwitterion-based interlayer coated Cu foil by a reversible addition-fragmentation chain transfer polymerization, which results in high ionic conductivity (0.75×10^{-4} S·cm^{-1}) and Li-ion transference number (0.81) [148]. In addition, Cui et al. reported a self-healable polymer interlayer that consists of a trifluorophenyl-modified poly(ethylene imine) network cross-linked by dynamic imine bonding on Cu foil (Cu-PEI-3F) (Fig. 10(e)) [138]. Owing to the uniform distribution of Li-ion and autonomous repair of SEI, Cu-PEI-3F exhibits impressive electrochemical performances in terms of a high CE of 99.7% (1 mA·cm^{-2}, 0.5 mAh·cm^{-2}) for 250 cycles in Li || Cu-PEI-3F half cells and 91% capacity retention after 100 cycles in Li-S full cells (Figs. 10(f) and 10(g)).

4 3D architectured Cu foils

In an attempt to effectively release the huge stress concentration of LMAs, 3D architectured Cu foils are developed in view of their large surface area with more sufficient diffusion channels [149, 150]. In addition, 3D architectured Cu foils are more beneficial for improving the uniformity of Li plating/stripping due to their intrinsic properties of homogenizing electric field and Li-ion flux distribution. According to the hybridization patterns, 3D architectured Cu foils can be divided into two categories, that is, integrated Cu scaffolds and composited Cu scaffolds. In this section, the synthesis process and structural design of 3D architectured Cu foils will be discussed in detail.

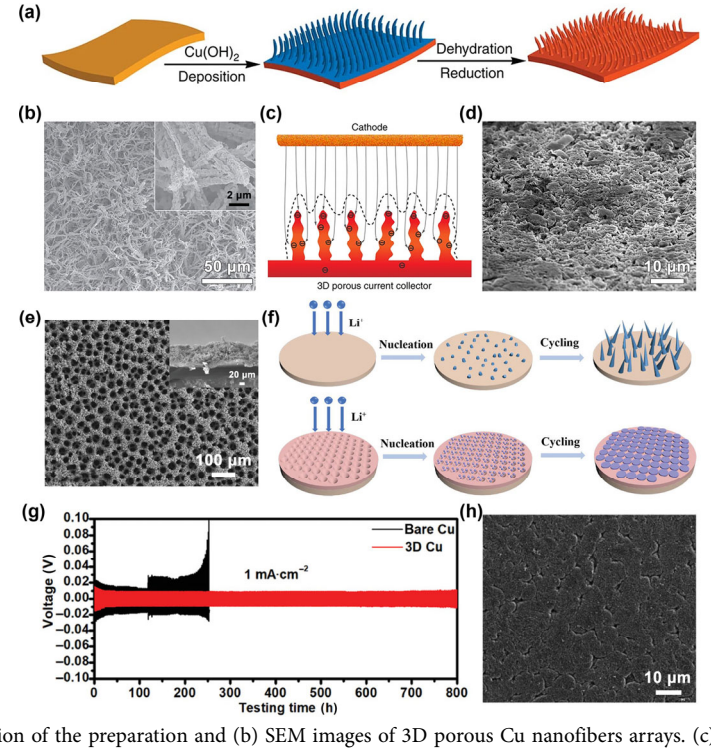

Figure 11 (a) Schematic illustration of the preparation and (b) SEM images of 3D porous Cu nanofibers arrays. (c) Schematic illustration of electrons and electrical field distribution in 3D Cu nanofibers arrays. (d) SEM image of 3D porous Cu nanofibers arrays after 2 mAh·cm^{-2} Li plating. Reproduced with permission from Ref. [151]. © Yang, C. P. et al. 2015. (e) SEM images of 3D porous Cu foil. (f) Schematic illustrations of Li deposition on bare Cu foil and 3D porous Cu foil. Cycling performance of the symmetrical cells based on 3D porous Cu foil at (g) 1 mA·cm^{-2} and (h) 2 mA·cm^{-2}. Reproduced with permission from Ref. [152]. © WILEY-VCH Verlag GmbH & Co. KGaA, Weinheim 2019.

4.1 Integrated Cu scaffolds

Cu foils can be directly engineered into 3D nanoarrays through chemical oxidation by alkaline solution (i.e., NaOH or ammonium hydroxide) and subsequent reduction [151, 153]. When immersing into alkaline solution, the Cu foils will be oxidized to Cu^{2+} and immediately coordinate with the OH^- to form $Cu(OH)_2$. Typically, Guo's group utilized the ammonia solution to prepare $Cu(OH)_2$ according to Eqs. (3) and (4):

$$Cu^{2+} + 4NH_3 \rightarrow Cu(NH_3)_4^{2+} \quad (3)$$

$$Cu(NH_3)_4^{2+} + 2OH^- \rightarrow Cu(OH)_2 + 4NH_3 \uparrow \quad (4)$$

The $Cu(OH)_2$ presenting bundles of nanofibers arrays could be converted to CuO after dehydration (Fig. 11(a)). Subsequently, the CuO nanofibers bundles were reduced to Cu by calcining under a reducing atmosphere (e.g., H_2/Ar mixed gas) [151] or by chemical reduction (e.g., nitroaniline and ammonia borane in ethanol) [154]. The resultant Cu nanofibers with submicron in diameter show a nanosized protuberant secondary structure, which greatly increases the specific surface area for distributing the local current density of the electrode (Fig. 11(b)) [151]. Notably, the integrated skeletons provide smooth electronic connection and structural robustness for electrochemical reactions. While the protruding tips on each fiber are recognized as the charge centers and nucleation sites, enabling homogenous electric field distribution (Fig. 11(c)). Therefore, Li metal would be uniformly deposited into the skeleton without dendrite growth (Fig. 11(d)). Electrochemical tests suggest that the as-designed 3D Cu nanofibers arrays display a stable cycling of over 600 h [151]. In addition, the electrochemical performances of the 3D Cu nanofibers arrays can be further boosted by decorating lithiophilic species, such as Sn layer [155]. Yin et al. employed an acetonitrile solution of 7,7,8,8-tetracyanoquinodimethane (TCNQ) to oxidize the Cu foil, which generates a layer of Cu-MOF nanorod arrays [156]. After heating under H_2/Ar mixed flow, nitrogen-doped carbon anchored with Cu nanorod arrays (NC/Cu) was obtained. The NC/Cu with integrated electronic and ionic transport network is beneficial to improve the electrochemical kinetics of the electrode. Moreover, the 3D framework enhances the structural stability of the scaffolds, rendering a CE of over 97% (2 $mA \cdot cm^{-2}$, 1 $mAh \cdot cm^{-2}$) and a long-term cycling stability over 1,000 h.

Electrodeposition is a facile, controllable and low-cost approach to construct 3D Cu scaffolds, which is usually conducted in a two-electrode system using a potentiostatic mode. This process involves the following reactions of Eqs. (5) and (6) [157]:

$$Cu^{2+} + 2e^- \rightarrow Cu \quad (5)$$

$$2H_2O \rightarrow O_2 + 4e^- + 4H^+ \quad (6)$$

The porosity and thickness of the Cu skeletons can be well adjusted by tuning the solution concentration, operating time, additives, etc. While the generated hydrogen bubbles during electrodeposition function as the templates to induce porous Cu deposition [158, 159]. As shown in Fig. 11(e), Qiu et al. utilized hydrogen bubbles and acetic acid as the templates and bubble stabilizer, respectively, to regulate the layer thickness and pore number/size of the Cu scaffold [152]. Thanks to the interconnected porous architecture, the electrode shows reduced local current density and homogenized electric field distribution (Fig. 11(f)). As a consequence, the well-designed 3D porous Cu skeleton exhibits stable cycling in symmetrical cells (Figs. 11(g) and 11(h)), accompanying with a smooth Li deposition morphology after 50 cycles. Following that, Wang et al. adopted a two-step electrodeposition to introduce an additional Sn layer to the 3D Cu scaffold [160]. During the initial Li nucleation, the Cu@Sn nanocones preferentially form Li-Sn alloy with fast-ion conductivity, which brings about uniform Li deposition and hence excellent cycling performance of the solid-state full cells.

Combining electrodeposition and template techniques, 3D Cu scaffolds with highly periodic and uniform pattern can be obtained. For example, Tang et al. synthesized a 3D ordered macroporous (3DOM) Cu using PMMA microspheres-assisted colloidal template and electrodeposition [161]. The 3DOM Cu presents an arc area with high curvature radius, which induces preferential Li nucleation and deposition in the pores. Also, the high specific surface area contributes to greatly improved electrochemical reaction kinetics of the 3DOM Cu. Chen et al. used a porous polycarbonate track-etched template and electrodeposition to fabricate vertically aligned Cu pillar arrays on Cu foil [162]. The highly ordered Cu pillar provides

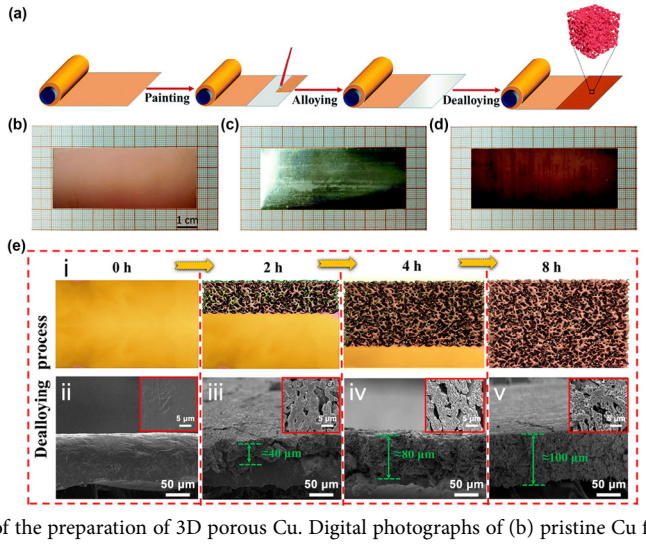

Figure 12 (a) Schematic illustration of the preparation of 3D porous Cu. Digital photographs of (b) pristine Cu foil, (c) $CuGa_2$ alloy and (d) porous 3D Cu after dealloying. Reproduced with permission from Ref. [163], © The Royal Society of Chemistry 2019. (e) Dealloying process of Cu-Zn alloy to synthesize 3D porous Cu: i) schematics of the preparation of 3D porous Cu; ii)–v) cross-section and upper surface (inset) SEM images of Cu-Zn sheets after dealloying for 0, 2, 4, and 8 h, respectively. Reproduced with permission from Ref. [164], © American Chemical Society 2019.

a uniform current density and electric field distribution at the electrode surface. Notably, the optimal Cu pillar arrays with a diameter of 2 μm and an average pore spacing of 5 μm enable vertical diffusion channels for Li ions. Therefore, Li metal was preferentially deposited at the bottom of the pillar arrays, resulting in a compact and uniform structure. To reduce Li nucleation barrier and facilitate deposition, a conformal ZnO thin film (50 nm in thickness) was further coated on the Cu pillar arrays. The as-assembled half cells exhibit good reversibility for Li plating/stripping in terms of a high CE of 99.5% and 99.4% at 0.5 and 1 $mA \cdot cm^{-2}$, respectively.

Dealloying of metal coated Cu foil by selective etching is a typical method to fabricate 3D interconnected Cu with nano-porous channels [165]. Shi et al. proposed a painting-alloying-dealloying strategy using liquid Ga metal to prepare self-supporting porous Cu scaffolds (Fig. 12(a)) [163]. At 80 °C, liquid Ga can be evenly coated on Cu foil to form $CuGa_2$ intermetallic phase (Figs. 12(b) and 12(c)). After dealloying in the mixed-acid solution of HNO_3 and HF, both Ga and $CuGa_2$ alloys were selectively etched (Fig. 12(d)). In this process, the Cu atoms were rearranged to form a 3D Cu skeleton with rich porosity, which effectively reduces the polarization overpotential and improves the overall electrochemical performances. Zhang et al. prepared metal X slurry-covered Cu foils (X = Sn, Zn, Al), which was then subjected to dealloying procedure based on the Kirkendall effect [166]. Since the diffusion rate of Cu into metal X is much higher than that to the reverse direction, abundant voids will be formed inside and on the surface of the Cu foil, attaining a highly porous nanostructure. The obtained 3D integrated porous structure not only reduces the local current density of the electrode but also provides numerous "cages" for suppressing dendrite growth, consequently delivering a long-term cycling of 2,000 h. In pursuit of more facile and cost-effective strategies to obtain 3D porous Cu skeletons, the direct dealloying of commercial Cu alloy foils, such as Cu-Sn (bronze) and Cu-Zn (brass) was developed. In general, chemical dealloying of Cu-Zn alloy can be conducted in a mixed solution containing HCl and NH_4Cl (i in Fig. 12(e)). After the complete dissolution of metallic Zn, an integrated 3D porous Cu skeleton with interconnected structure was obtained (ii-v in Fig. 12(e)) [164]. The porous structure enables the well accommodation of deposited Li metal and alleviates the volume changes during Li plating/stripping. Note that, the as-produced 3D porous Cu skeleton still maintains a large amount of lithiophilic Zn sites, which not only reduce the Li nucleation barrier, but also facilitate molten Li metal infusion [167, 168]. In view of the boiling point differences (Zn: 907 °C, Cu: 2,562 °C), the Zn atoms of brass could be sublimed and diffused into the 3D porous structure after annealing [169, 170]. Accordingly, the homogeneous distribution of nanopores leads to uniform nucleation and flat deposition of Li metal with an overpotential of ~40 mV.

Zhao et al. completely removed the Zn species of Cu-Zn alloy through a linear sweep voltammetry between –1 and 0.2 V, forming 3D porous Cu foils with uniform pore size distributions [171]. Compared with the chemical dealloying obtained one, the 3D porous Cu skeleton shows higher tensile strength (13.5 MPa) and electrical conductivity (1.12×10^5 $S \cdot cm^{-1}$). After decorating with lithiophilic sites of ZnO or polar fluorine-based functional groups, the Li migration in the skeleton could be further improved [172]. CuO is also an ideal lithiophilic species, which can be grown on Cu foil easily. The negative Gibbs free energy of the replacement reaction between CuO and Li metal would trigger the spontaneous generation of a Li-enriched SEI, which is of high effectiveness for regulating the Li plating/stripping behaviors. The as-formed Li_2O-rich SEI layer not only suppresses the undesired side reaction between Li metal and electrolyte, but also promotes uniform Li nucleation and deposition. Accordingly, a series of CuO nanostructures including nanowires, nanorods, nanosheets, etc., were applied to integrate with Cu foil [173–177]. As a notable example, Yang's group reported vertically aligned CuO nanosheets decorated Cu skeletons (VA-CuO-Cu) [176]. The CuO nanosheets arrays enhance the Li affinity of the electrode, thus lowering the Li nucleation barrier and uniformizing the Li-ion flux distribution [178]. Intriguingly, when bronze foils were immersed into the ammonia solution, a spongy 3D Cu skeleton covered by CuO and SnO_2 was fabricated [179]. The lithiophilic CuO and SnO_2 in the substrate remarkably improve the adsorption of Li and induce the generations of Li_2O and Li-Sn alloy during the initial Li deposition, contributing to a stable SEI and fast Li-ion transport for reliable LMAs. Recently, the self-assembly of copper 7,7,8,8-tetracyanoquinodimethane MOFs combined with a subsequent annealing has been proposed to fabricate self-supporting CuO nanorod arrays with lithiophilic N-containing functional groups (CuO NAs/CF) [180]. In the electrolyte with LiTFSI, a Li_2O- and LiF-enriched SEI layer was obtained, which significantly improves the CE and cycling stability of the electrode. It is worth noting that although Li_2O with high lithiophilicity shows outstanding ability in regulating Li deposition, its low ionic conductivity would increase the interfacial resistance and may cause poor rate capability. Considering that Li_2S, Li_3N, and Li_3P show higher ionic conductivity than Li_2O, 3D architectured Cu-based sulfides, nitrides and phosphides have been utilized to modify the Cu foils [181–184]. Benefiting from the robust SEI with high Li-ion conductivity, the 3D integrated Cu_xM@Cu scaffolds (M = S, N, P, etc.) normally display lower Li-ion diffusion barrier and more efficient regulatory ability in homogenizing the electric field and Li-ion flux as compared to their CuO@Cu counterpart.

4.2 Composited Cu scaffolds

Given that the insufficient lithiophilicity of the 3D integrated Cu scaffolds may still induce heterogeneous Li nucleation and growth during long-term cycling, many other 3D frameworks, such as metal-based skeletons, carbon-based skeletons, and polymeric skeletons, have so far been developed to modify the Cu foil.

4.2.1 Metal-Cu scaffolds

Lithiophilic metal scaffolds can effectively improve the electrode wettability associated with reduced Li nucleation and plating overpotential, thus introducing uniform Li deposition. Xu et al. constructed a honeycomb-like 3D porous nickel scaffold on Cu foil (Ni@Cu) by electrodeposition [185]. The hierarchical Ni@Cu scaffold provides numerous conductive nickel tips to delocalize the charge distribution, resulting in uniform Li nucleation and deposition within the electrode. To decrease the nucleation barrier of Li metal, lithiophilic metals with

elaborately designed 3D nanostructures have been proposed to modify Cu current collectors [186]. For instance, Chen et al. fabricated a 3D porous Zn scaffold covered on a thin ZnO layer coated Cu foil (Zn/ZnO/Cu) by magnetron sputtering [187]. The Li-Zn alloy scaffold showing fast Li-ion diffusion rate enables reduced electrode polarization and homogeneous Li deposition. As a result, notable cycling stability was attained in both symmetric cells (500 h at 4 mA·cm^{-2}) and full cells (1,000 cycles with a capacity retention of 81%). Note that, when metal compounds were employed as the 3D skeletons, the *in-situ* generated 3D SEI layer would produce a uniformly distributed electric field to suppress Li dendrite growth [188]. Accordingly, Huang et al. reported a holey N-doped $TiNb_2O_7$ nanosheets coated Cu foil (N-TNO@Cu) through joint strategies of proton exchange, chemical exfoliation and annealing [189]. As a result of the well-guided Li nucleation and suppressed dendrites growth in the N-TNO@Cu electrode, the full cells assembled with LFP cathode exhibit excellent cycling stability in terms of a capacity retention of 95% after 1,000 cycles at 1,530 mA·g^{-1}.

Distinct from bare 3D scaffolds, the introduction of gradient structures including lithiophilicity, conductivity, porosity and their hybrids benefits bottom-up Li deposition, thus substantially improving the safety of LMBs [190, 191]. Zhang et al. prepared a CNF-based skeleton with a lithiophilic gradient on Cu foil, where the upper layer is sputtered Si particles and the lower layer is deposited ZnO particles. During Li plating, the ZnO particles with higher Li affinity induce favorable Li metal deposition on the bottom of the skeleton [192]. Excitingly, 3D skeletons, for example, glass fibers, with poor-conductivity or even insulating properties, could also be applied to form conductivity gradient structure on Cu substrates [193–195].

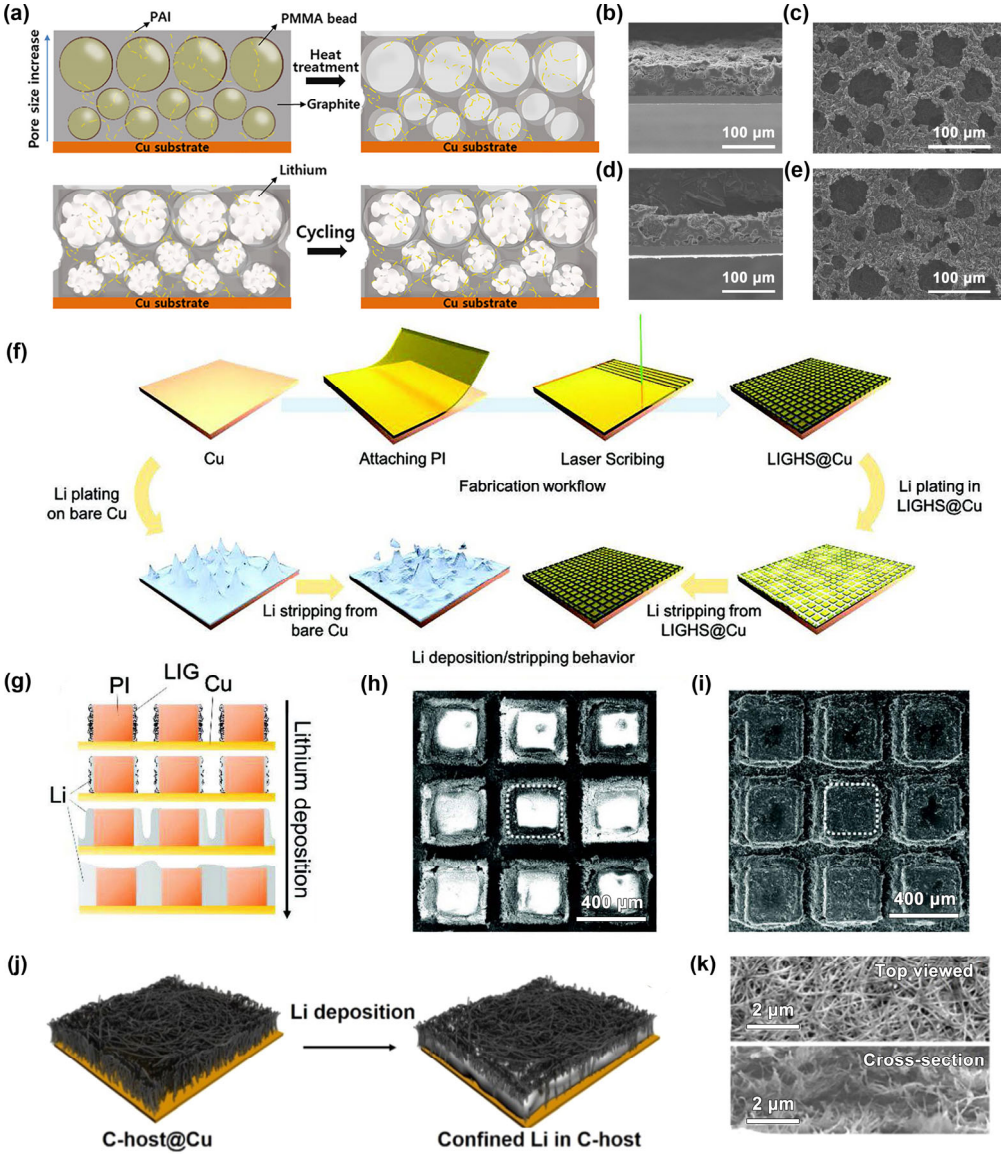

Figure 13 (a) Schematic illustration of the preparation of 3D-CPA and its Li cycling behaviors. SEM images of 3D-CPA (b, c) with 4 mAh·cm^{-2} Li plating and (d, e) after Li stripping. Reproduced with permission from Ref. [196], © American Chemical Society 2021. (f) Schematics of the preparation of LIGHS@Cu, and the Li deposition processes of bare Cu and LIGHS@Cu substrates. (g) Schematic of the Li nucleation and growth in LIGHS@Cu. SEM images of LIGHS@Cu (h) before and (i) after 0.5 mAh·cm^{-2} Li deposition at 1 mA·cm^{-2}. Reproduced with permission from Ref. [197], © WILEY-VCH Verlag GmbH & Co. KGaA, Weinheim 2019. (j) Schematic and (k) SEM images of Li deposition within the CNTs sponge. Reproduced with permission from Ref. [198], © Elsevier B.V. 2018.

However, in this respect, lithiophilic species decoration of the skeletons is necessary, so that to improve their interactions with Li ions.

4.2.2 *Carbon-Cu scaffolds*

Carbon-based materials, for example, hollow carbon nanocages [199], O,N co-doped porous carbon granules [200, 201], biomass-derived S,N co-doped porous carbon nanosheets [202], porous g-C_3N_4 microspheres [203], etc., have also been explored to construct composited Cu current collectors in view of their lightweight and good mechanical properties. Compared with Cu, carbon-based skeletons usually possess larger specific surface area and more internal space, which not only remarkably improve the wettability of electrolyte but also uniformize the distribution of Li-ion flux. Yu et al. prepared a porous 3D carbon/Cu framework by blade-casting the slurry containing vapor-grown carbon fiber, super P, and lithophilic $RbNO_3$ and $LiPF_6$ [204]. After optimizing the pore sizes and their distribution in the skeleton, Li deposition is well guided from bottom to top. Eventually, the composite electrode enables a volumetric specific capacity of 1,643 mAh·cm^{-3} and an ultrahigh CE of 99.36% at 1 mA·cm^{-2} and 1 mAh·cm^{-2} for over 860 cycles. Zhang et al. constructed a 3D micro-nano structured Cu skeleton coated by F-doped CNF network (MNCu/FC) through slurry-coating and carbonization [205]. The crosslinked lithiophilic carbon network effectively promotes the charge transfer for electrochemical reactions, leading to a dendrite-free Li deposition. Consequently, the MNCu/FC electrode delivers a CE of 97.9% after 150 cycles at 2 mA·cm^{-2} and 1 mAh·cm^{-2}. Noh et al. prepared a 3D carbon-based porous architecture covered Cu substrate (3D CPA) by blade casting, where graphite, polyamideimide, and PMMA were used the frame material, binder, and pore template agents, respectively [196]. As shown in Fig. 13(a), the pore-size gradient structure could induce Li deposition from bottom to top, which keeps the deposited Li metal away from the separator and hence drastically decreased risk of short-circuit or fire. The 3D CPA consistently presents smooth and dense morphologies regardless of with 4 mAh·cm^{-2} Li plating or after fully Li stripping (Figs. 13(b)–13(e)).

It is noted that the weak interaction between carbon and Cu may lead to a huge interfacial resistance or the exfoliation of carbon layer during long-term cycling. For that reason, the carbonization of pre-coated polymer layer on Cu substrates would be a valid route to build an efficient interface of the skeletons for better Li plating/stripping. Liu et al. prepared a 3D honeycomb-like hierarchical N-doped framework (HHNF) coated Cu by pre-oxidizing and carbonizing the PAN layer coated Cu foil [206]. The HHNF possesses plenty of ordered pores and interconnected skeletons, which not only homogenize the distributions of Li-ion and electric field, but also significantly improve the Li ions and electrons transport within the skeleton. In addition, the gradient distribution of electrical charges density from bottom Cu substrate to top HHNF leads to bottom-up deposition of Li metal. Therefore, the optimized Li deposition favors the long-term regulation of Li plating/stripping, resulting in greatly suppressed Li dendrite growth. Similarly, Chen et al. reported a vertically aligned CNFs (VACNF) array with conically stacked graphitic structure on Cu foil, which was synthesized through a direct current biased plasma enhanced chemical vapor deposition [207]. This *in-situ* composition model guarantees an intimate contact between carbon and Cu, affording a high electrical conductivity. While the graphitic edges of VACNF provide plentiful lithiophilic sites to facilitate even Li plating/stripping. Subsequently, Xu et al. prepared a N,O co-doped vertical carbon nanosheet arrays on Cu foil (NOCA@Cu) by self-assembly and the carbonization of PI [208]. The vertical channels in NOCA@Cu providing fast ions/electrons transport and spatially confined Li metal ensure a long-term cycling stability of up to 1,300 h at 0.5 mA·cm^{-2} and 1 mAh·cm^{-2}. Furthermore, Yi et al. employed a laser-scribing technique to etch Kapton tape (PI polymer), which attains a highly periodic pattern, namely, laser-induced graphene-based hierarchical structure on Cu foil (LIGHS@Cu) (Fig. 13(f)) [197]. The unusual structure is originated from the partial elimination and graphitization of PI film during laser processing, which greatly increase the electron conductivity for Li deposition following a "bottom-growth" model (Figs. 13(g)–13(i)). When coupling with LFP cathode, the full cells exhibit a long cyclic lifespan of 250 cycles with a capacity retention of over 90%.

The *in-situ* growth of CNTs or graphene on Cu foil is also an appealing route to address the poor interfacial contact between carbon skeletons and Cu substrates [209]. For example, Shen et al. proposed a 3D CNTs sponge with good alignment grown on Cu foil, which exhibits high flexibility and intimate interface contact with the substrate (Fig. 13(j)) [198]. They found that Li metal prefers to nucleate and grow into pillar-like shapes along the axial direction of CNTs (Fig. 13(k)). As a result, a stable cycling for over 250 cycles with ~99% CE (1 mA·cm^{-2}, 1 mAh·cm^{-2}) is achieved. Likewise, 3D CNTs can be deposited on graphene layer-coated Cu foil to reinforce the structural robustness and conductivity of the skeleton [210]. The resulting GCNT/Cu delivers a high electronic conductivity of 1.45 × 10^3 S·m^{-1} and accelerated Li-ion transport, thus promoting homogeneous Li deposition within the skeleton. Accordingly, the full cells assembled with sulfurized carbon cathode present an ultrahigh energy density of up to 750 Wh·kg^{-1}.

4.2.3 *MOFs-Cu scaffolds*

Owing to their huge potentials for regulating the morphology of deposited Li, MOFs have been considerably employed to construct 3D architectures on Cu substrates (Fig. 14(a)) [211]. In general, 3D MOFs coated Cu presents the advantages of providing 1) abundant lithiophilic sites to chelate with Li; 2) higher specific surface area to dissipate the Li-ion flux and homogenize electric field of the electrode; 3) excellent flexibility to accommodate the volume changes during Li

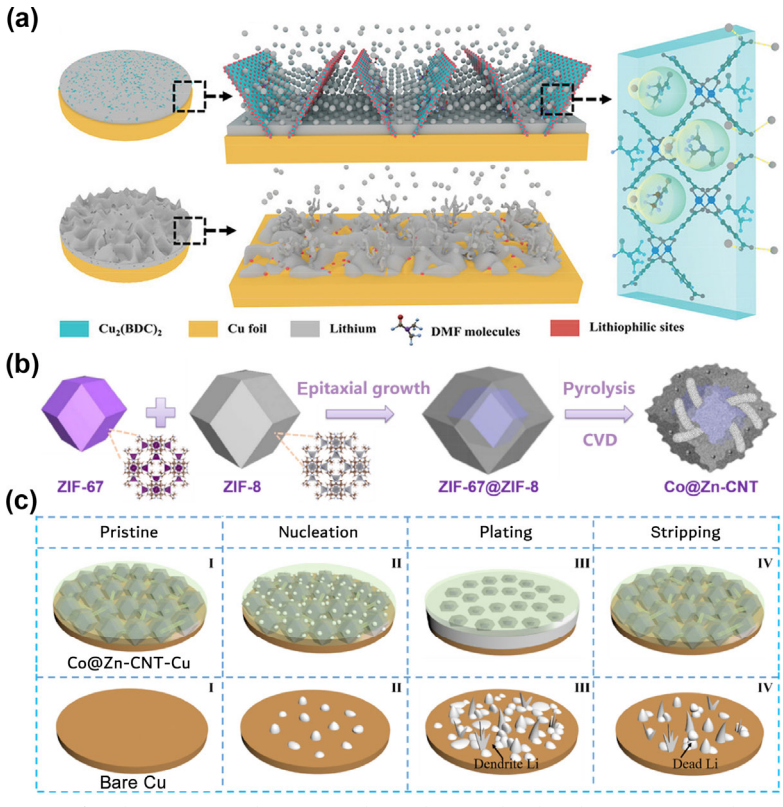

Figure 14 (a) Schematic illustration of Li deposition on planar Cu and (1, 4-benzenedicarboxylic cooper) nanosheets modified Cu. Reproduced with permission from Ref. [211], © Wiley-VCH GmbH 2021. (b) Schematic of the preparation of Co@Zn-CNT composite. (c) Schematic of the pristine state, Li nucleation, plating, and stripping processes on Co@Zn-CNT-Cu and bare Cu substrates. Reproduced with permission from Ref. [212], © Elsevier B.V. 2021.

plating/stripping [213–215]. After carbonization, the coordinated metals in MOFs are converted to be the active sites for Li deposition, while the organic linkers are carbonized into carbon skeletons. ZIF-8 is a kind of MOF materials with well-defined rhombic dodecahedron shape, which can be transformed into Zn encapsulated 3D mesoporous carbon scaffolds through annealing [216, 217]. Markedly, the electrode with ordered geometry affords a regular and stable interspace for uniformizing the deposition of Li. Following that, Shin et al. further embedded Ag nanoparticles into the ZIF-8-derived carbon host by the galvanic displacement reaction of Ag^+ with Zn, which was then coated on Cu substrate by blade casting [218]. The Ag nanoparticles induce the outward growth of Li metal starting from the internal pore of the skeleton, resulting in smooth Li deposition with good reversibility. Zhao et al. prepared a Co@Zn-CNT-Cu nanostructure through the pyrolysis of a core-shelled ZIF-67@ZIF-8, during which CNTs are *in-situ* growth on the scaffold (Fig. 14(b)) [212]. The crosslinked CNTs act as the support to reinforce the integrity of the electrode, whereas Zn serving as the lithiophilic sites for promoting Li nucleation (Fig. 14(c)). Besides, MOFs can also be integrated with Cu foil to form various gradient skeletons. Yun et al. coated a Ag layer underneath MOF-based skeleton to build a lithiophilicity gradient, which induces bottom-up Li deposition and hence improved cycling stability of LMAs [219]. Man et al. designed a conductivity gradient skeleton consisted by a fully carbonized conductive ZIF-67 upper layer and a partially carbonized insulating ZIF-67 bottom layer [220]. Benefitting from the high conductivity and massive lithiophilic sites, Li metal is preferentially deposited into the carbonized ZIF-67 skeleton. While the top insulating ZIF-67 not only acts as an ion-channel regulator to disperse the Li-ion flux, but also a flexible buffer layer to alleviate the electrode volume variations.

5 Nanostructured 3D Cu substrates

Planar modification and 3D structural design of Cu foils have been proven to be simple and efficient routes to regulate the Li deposition behavior of LMAs [31, 221], however, the obvious interfacial issue associated with large interface impedance remain unsolved [85]. To this end, nanostructured frameworks based on 3D Cu substrates have been proposed because of their 3D integrated skeleton providing higher specific surface area and faster ion/electron channels. In this chapter, the design principle and regulatory mechanism of nanostructured 3D Cu substrates for LMAs will be discussed in detail.

5.1 Modified Cu meshes

Cu mesh possessing rich porous structure and 3D patterned skeleton exhibits excellent ability to uniformize electric field distribution and accumulate Li metal deposition [222, 223]. Compared with planar Cu foil, Cu mesh substrates generally deliver faster charge transport due to their crosslinked 3D nanostructure and high specific surface area [21]. Nevertheless, the lithiophobic nature of bare Cu mesh causes a high Li nucleation barrier. Therefore, further structural modification of Cu mesh is necessary so that to better guide Li plating/stripping.

Tian et al. utilized the decomposition feature of lithium bis(fluorosulfonyl)imide (LiFSI) to generate a F, N, S doped interphase on the Cu mesh surface (Fig. 15(a)) [224]. The F-N-S active sites facilitate multi-components SEI with LiF, Li_3N and

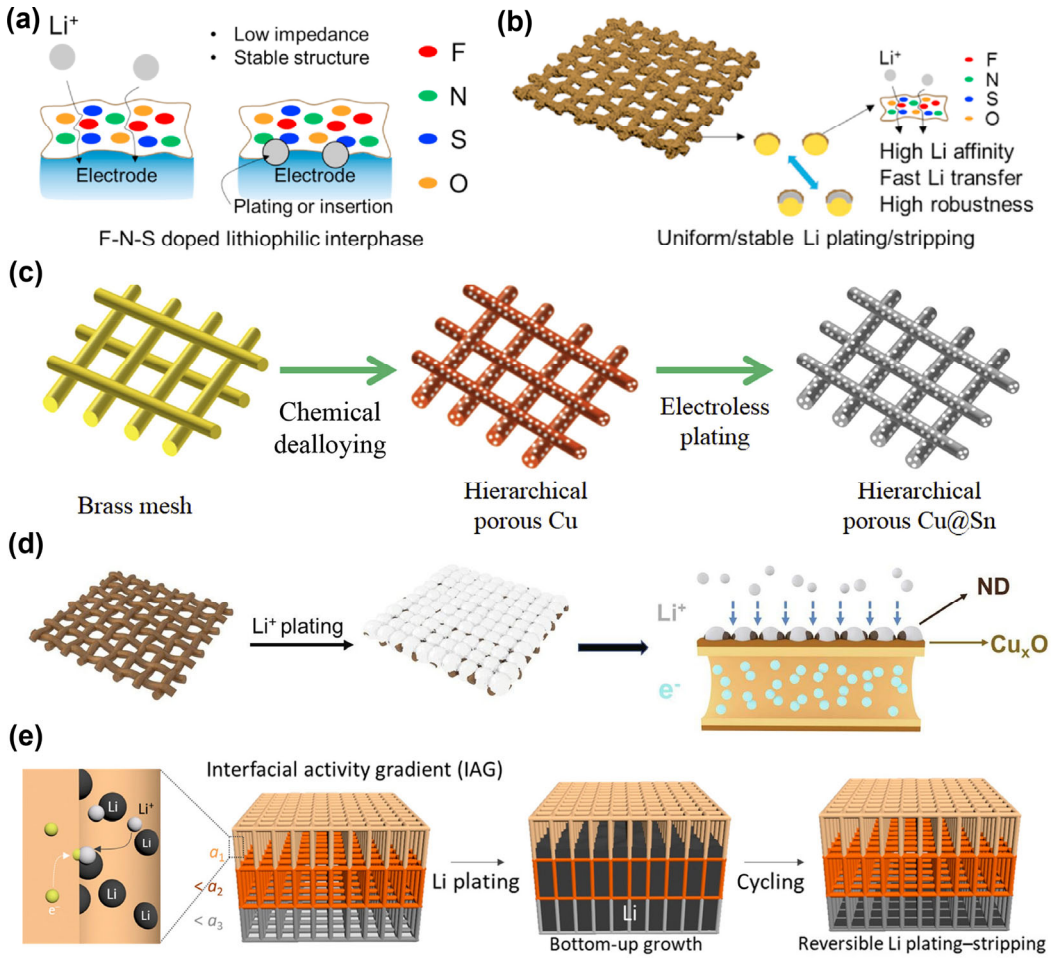

Figure 15 Schematic illustration of (a) the F-N-S doped lithiophilic interphase and (b) Li plating/stripping on the modified Cu mesh. Reproduced with permission from Ref. [224], © Elsevier B.V. 2021. (c) Schematic of the preparation of HP-Cu@Sn. Reproduced with permission from Ref. [225], © Elsevier B.V. 2020. (d) Schematic of Li deposition on the ND coated Cu_xO/Cu mesh. Reproduced with permission from Ref. [226], © Elsevier B.V. 2021. (e) Schematic of the Li deposition in a 3D porous framework with interfacial activity gradient. Reproduced with permission from Ref. [227], © American Chemical Society 2020.

Li_2S, thus providing a robust and fast Li-ion conducting interphase for homogenizing Li plating/stripping (Fig. 15(b)). Similarly, polyaniline was decorated on Cu mesh to promote dense and uniform SEI formation, and moreover, acted as the artificial lithiophilic interlayer for even Li deposition [228]. As a result, the electrode shows reversible Li plating/stripping processes even at a high current density of 10 mA·cm^{-2} and a large cycling capacity of 10 mAh·cm^{-2}. As a typical lithiophilic metals, Sn was applied to modify Cu mesh. For instance, Luan et al. constructed a dense Sn metal layer on the surface of Cu mesh by electrodeposition [222]. Luo et al. synthesized a Sn metal layer coated hierarchical porous Cu mesh (HP-Cu@Sn) by the combination of chemical dealloying and electroless plating (Fig. 15(c)) [225]. Benefiting from the enhanced lithiophilicity, the skeletons display fast infiltration of molten Li associated with low Li nucleation overpotential (<10 mV). It is worth mentioning that Cu mesh with high porosity intrinsically can accommodate the volume expansion of LMAs and ensure the uniform electric field and Li-ion flux distributions.

Similar to Cu foil, the surface of 3D Cu mesh could be easily converted to Cu-based compounds to improve its lithiophilicity. For example, Cu@CuO was obtained by the heat treatment of Cu mesh in air [229], Cu@Cu_3P was synthesized by the phosphidation of Cu mesh in the presence of NaH_2PO_2 [230], Cu@ZnO was prepared by the air annealing of brass mesh [231]. These modified Cu meshes with Cu-based compounds interface not only provide remarkable Li affinity for Li nucleation, but also exhibit hierarchical structure for Li accommodation. It is well-known that the structure of lithiophilic sites, i.e., morphology and distribution, plays a crucial role in influencing the uniformity of electron transport and Li migration. To avoid the local accumulation of electrons and ions caused by the non-normalized lithiophilic sites, Luo et al. prepared a composite skeleton comprising nanodiamond (ND) particle imbedded Cu_xO/Cu mesh (Fig. 15(d)) [226]. The insulating ND serving as an electric field shielding layer inhibits the accumulation of electron and the uneven conversion of lithiophilic sites effectively. As a result, smooth Li deposition and long-term cycling stability are achieved in the electrode.

It is widely known that Li nucleation associated with its initial deposition is more likely to occur at the top of the Cu mesh, resulting in the "top-growth" of Li metal. Accordingly, Li-ion transport toward the bottom of the skeletons is blocked,

which would trigger the fast growth of Li dendrites. To this end, Zhang et al. designed a hybrid lithiophilicity/conductivity gradient Cu mesh skeleton, where the top side was coated by a polymer blend of PAN/PVDF-HFP and the bottom side was sputtered with a layer of Au particles [232]. The selected polar polymer provides good Li affinity to homogenize Li-ion flux, while the Au layer facilitates Li nucleation/deposition at the bottom. Beyond that, lithiophilic gradient were constructed by stacking Cu mesh with different decorating layers. As reported by Yun et al., who prepared an intriguing multilayered Cu mesh skeleton consisting of Cu@PVDF mesh, Cu mesh, Cu@Ag mesh from top to bottom [227]. Their theoretical simulations and experimental results demonstrate that the as-formed interfacial activity gradient structure enables the effective regulation of the multiple reaction dynamics, resulting in preferential Li deposition at the bottom region (Fig. 15(e)). Consequently, the stable and ordered Li plating/stripping processes contribute to good reversibility and cycling stability of the electrode.

5.2 Modified Cu foams

Compared with Cu mesh, Cu foam exhibits a higher percentage of porosity and a higher degree of cross-linking. Therefore, Cu foam is expected to better uniformize the surface electric field and alleviate the volume changes of LMAs. Owing to the lithiophobic nature, bare Cu foam is unable to regulate Li plating/stripping, thus requiring further lithiophilic sites modification [233]. Typically, Sb layer was coated on Cu foam by the displacement reaction between $SbCl_3$ and Cu [234], Ag particles were introduced on Cu foam by electrodeposition [235], and Sn layer was decorated on Cu foam by physical vapor deposition [236]. These lithiophilic sites lower the Li nucleation overpotential of Cu foam and induce preferential Li deposition against dendrite formation, which significantly improve the cycling stability of LMAs. In particular, the metals that capable of alloying with Cu to form alloying interfaces, for example, Cu_6Sn_5, Cu_2Sb, and Cu_2Mg, could substantially decrease the Li nucleation barrier and facilitate electron/Li-ion transport [237–239]. Theoretical calculations suggest that the Cu-based alloy interphases show a stronger adsorption of Li atom, which is beneficial for durable LMAs.

Through delicate design, lithiophilic metal could be further applied as the secondary structure to construct modified Cu foam skeletons. For example, Sb metal was decorated on Cu nanowires by the displacement reaction between Cu and $SbCl_3$ [240], while Ag nanowires loaded Cu@CuO_x foam was constructed through a spray-coating process [241]. Other metal compounds with well-defined nanostructures have also been explored [242–244]. Impressively, $Ti_3C_2T_x$ with excellent electronic conductivity and abundant functional groups was utilized to modify Cu foam by electrophoretic deposition [245]. Thanks to the good lithiophilicity/conductivity and specific surface area, the as-obtained electrode shows a Li nucleation overpotential of 42 mV and improved molten Li infusion. Specially, a 3D porous Cu-Zn composite foam with interconnected and quasi-ordered pores was synthesized through electrochemical co-deposition technology [246]. The porous structure not only effectively reduces the local current density but also evenly distributes the electric field of the skeleton. Moreover, the lithiophilic surface improves the diffusivity of Li ions

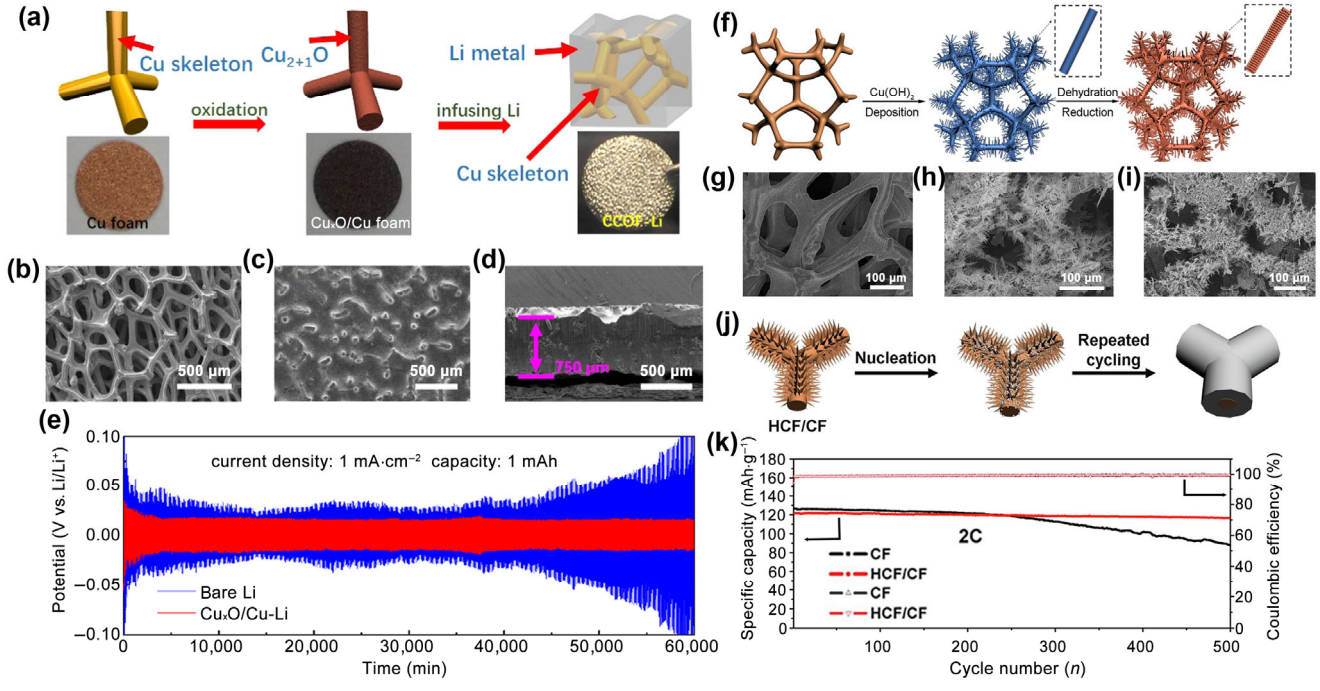

Figure 16 (a) Schematic illustration of the preparation of Cu_xO/Cu foam and the associated molten Li infusion. SEM images of (b) the pristine Cu_xO/Cu foam, and the (c) surface view and (d) cross-section view of Cu_xO/Cu-Li. (e) Cycling performance of the Cu_xO/Cu-Li and bare Li metal electrodes at 1 mA·cm^{-2} and 1 mAh·cm^{-2}. Reproduced with permission from Ref. [247], © Elsevier B.V. 2018. (f) Schematic illustration of the preparation of HCF/CF. SEM images of the Cu foam after (g) pre-treatment and (h) $Cu(OH)_2$ nanofibers arrays coating. (i) SEM image of HCF/CF. (j) Schematic of Li deposition on HCF/CF. (k) Cycling performance of the Cu-Li || LFP and HCF/CF-Li || LFP full cells at 340 mA·g^{-1}. Reproduced with permission from Ref. [248], © Elsevier B.V. 2019.

and induces uniform Li nucleation. As a consequence, the corresponding symmetric cells exhibit an extended cycling of up to 1,200 h for over 1,000 cycles.

Oxidation is a simple strategy to change the lithiophobicity nature of Cu foam [249]. Lin et al. prepared a rimous Cu foam with ant-nest porous structure through a combined sulfurization-oxidation-reduction process [250]. The re-constructing approach endows Cu foam with interconnected and hierarchical channels, leading to significantly increased specific surface area to uniformize the Li-ion flux and electric field. Moreover, the spontaneously formed Cu_xO layer lowers the Li nucleation barrier and induces uniform Li nucleation and deposition. Impressively, the well-designed electrode presents a high CE of 99% after 660 cycles at 1 mA·cm^{-2}, and an excellent cycling performance over 200 h at 3 mA·cm^{-2}. Direct calcination of Cu foam in air can also build a compact oxide layer on Cu foam (Cu_xO/Cu) (Fig. 16(a)). The Cu-based oxides layer possesses numerous pores with nano-micro sizes, which enhances the electrochemical specific surface area and the sites for Li nucleation. Therefore, molten Li can steadily and fleetly climb along the bottom of Cu_xO/Cu skeleton by the fast replacement reaction between Li metal and Cu_xO. The resultant Cu_xO/Cu-Li electrode with uniform Li plating/stripping processes consistently presents smooth Li metal morphology (Figs. 16(b)–16(d)) [247]. Meanwhile, the formed Li_2O-rich SEI layer regulates the nucleation/deposition of Li, enabling a long-cyclic electrode (Fig. 16(e)). Likewise, one-step O_2 plasma treatment was employed to construct lithiophilic Cu_xO layer on Cu foam, during which the Cu surface was fast oxidized by the negatively-charged oxygen ions (O^- or O^{2-}) [251]. The pre-generated Cu_xO layer contributes to the formation of a dense SEI layer for improving the cycling stability of LMAs [252].

Note that, Cu_xO/Cu foam can be modified by introducing additional functional species. For example, NH_4F was used as the fluorine source to *in-situ* generate a LiF-rich SEI on the Cu_xO/Cu foam, which results in a higher surface energy and a lower diffusion barrier to promote Li deposition [249]. Based on the chemical oxidation of Cu in alkaline solution, $Cu(OH)_2$ nanofibers arrays can also be self-assembled on Cu foam (Fig. 16(f)) [248, 253−255]. With this design, the Cu foam substrate provides massive interspace and enough mechanical strength to accommodate the volume changes during Li cycling. While the nanofibers arrays acting as a secondary protrusion structure guarantee more electrochemical centers to dissipate the local current density and induce uniform Li nucleation [256]. Recently, Zhao et al. developed a skeleton comprising hierarchical Cu nanofibers grown vertically on Cu foam (HCF/CF) (Figs. 16(g)–16(i)) [248]. The unique structure of HCF/CF enables uniform Li plating/stripping, leading to a long-term cycling life for 820 h at 1 mA·cm^{-2} (Fig. 16(j)). When coupling with LFP cathode, the full cells exhibit a stable cycling for over 500 cycles with 95.6% capacity retention (Fig. 16(k)). The $Cu(OH)_2$ nanofibers arrays could be converted to Cu_2S and Cu_3N through further sulfurization or nitrogenization [257, 258]. Owing to the higher ionic conductivity of Li_2S (~10^{-5} S·cm^{-1}) and Li_3N (~10^{-3} S·cm^{-1}), the resultant skeletons show faster electrochemical kinetics for Li deposition in a dendrite-free manner [259–261].

Carbon-based species are good candidates to modify Cu

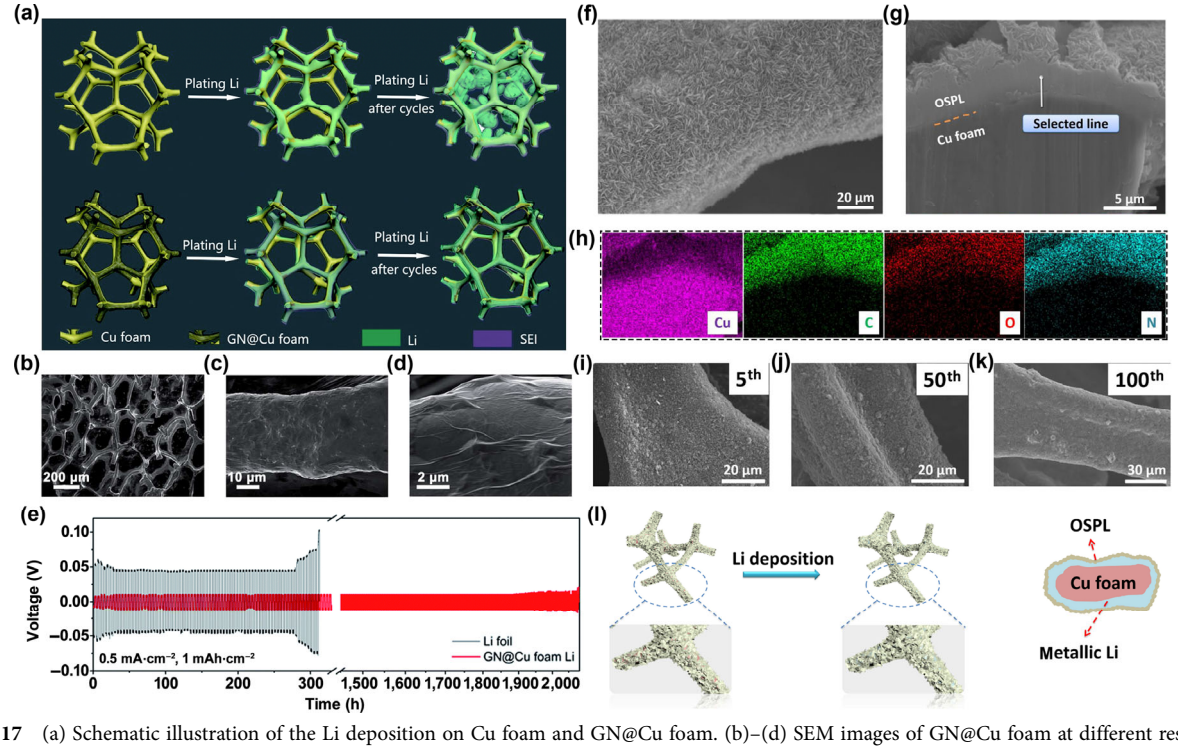

Figure 17 (a) Schematic illustration of the Li deposition on Cu foam and GN@Cu foam. (b)–(d) SEM images of GN@Cu foam at different resolution. (e) Cycling performance of the symmetric cells based on bare Li foil and GN@Cu foam Li electrode at 0.5 mA·cm^{-2} and 1 mAh·cm^{-2}. Reproduced with permission from Ref. [262], © The Royal Society of Chemistry 2018. SEM images of OSPL@Cu foam for the (f) surface view, (g) cross-section view and (h) corresponding element mapping. SEM images of OSPL@Cu electrodes after (i) 5, (j) 50 and (k) 100 cycles at 1 mA·cm^{-2}. (l) Schematic illustration of Li deposition on OSPL@Cu foam. Reproduced with permission from Ref. [263], © Elsevier B.V. 2020.

foam [264, 265]. As a notable example, N-rich graphene quantum dots (2–3 nm) were coated on Cu foam, which act as the nucleation seeds to induce uniform Li nucleation associated with the generation of a homogeneous and mechanically robust SEI layer [266]. Impressively, the electrode shows a stable cycling without Li dendrites formation even at an ultrahigh current density of 30 mA·cm^{-2}. Following that, graphene was employed to modify Cu foam (GN@Cu foam) because of its abundant active sites and conformal ability (Fig. 17(a)) [262, 267]. The secondary graphene network substantially promotes charge transport and enlarges the surface area to homogenize the distribution of Li-ion flux (Figs. 17(b)–17(d)). Consequently, the GN@Cu-Li electrode delivers a stable cycling performance of over 2,000 h at 0.5 mA·cm^{-2} and 1 mAh·cm^{-2} (Fig. 17(e)). Likewise, graphene oxide was used to support ZnO and then filled into Cu foam to form a composite electrode [268]. The micron-sized conductive network of graphene further splits the large pores of Cu foam into smaller ones, which significantly improves the storage capacity of Li metal and dissipates the local current density of the electrode. Accordingly, the modified Cu foam with molten Li shows an excellent cycling stability of 1,300 h and a low overpotential of ~30 mV. Liu et al. reported a cucumber-like lithiophilic composite skeleton (CLCS) by the annealing of PAN-coated Cu foams in H_2/Ar atmosphere [269]. PAN endows CLCS with abundant lithiophilic N-containing groups (i.e., pyridinic N, pyrrolic N, and Cu_xN sites), which render even Li nucleation and growth. Similarly, Zhou et al. developed a N-doped-carbon/ZnO modified Cu foam through the wet-coating of ZIF-8 solution associated with calcination [270]. In this composite skeleton, the N-rich sites and ZnO particles act as the lithiophilic nucleation seeds, which reduce the local current density and guide the Li-ion flux distribution for smooth Li deposition. Besides, a novel Cu_2O/C layer with moss-like morphology was also formed on Cu foam by the pyrolysis of MOF-199 embedded $Cu(OH)_2$@Cu [271]. The Cu_2O nanoparticles with highly exposed (100) and (110) surfaces impart the composite skeleton with a strong Li affinity for LMAs application.

Organics with functional groups can regulate the Li-ion migration within Cu foam because of their excellent adhesion and conformal ability [272, 273]. Liu et al. proposed a solid and dense organic supramolecular protective layer on Cu foam (OSPL@Cu) by the polycondensation of melamine and cyanuric acid (Figs. 17(f)–17(h)) [263]. First, OSPL exhibits lawn-like nanoarray morphology with numerous polar groups (e.g., amino group, carbonyl and triazine), which attracts Li ions and rearranges Li deposition (Figs. 17(i)–17(k)). Second, the insulating OSPL can shield the direct connection between Li metal and electrolyte to mitigate the corrosion of Li electrode. Third, the OSPL provides remarkable elasticity by virtue of the plentiful hydrogen bonds to adequately buffer the electrode volume expansion (Fig. 17(l)). Similarly, Yang et al. used poly (1,3,5-triethynylbenzene) (PTEB) to cover on a Cu nanowires integrated Cu foam [274]. The PTEB with lithiophilic acetylene bonds exhibits high reactivity with Li, thus effectively reducing the Li nucleation barrier and facilitating Li deposition.

5.3 3D self-built Cu skeletons

The inherent features of 3D Cu current collectors, such as pore size, tortuosity factor, volume of space, geometrical shape and surface chemistry, etc. may also affect the stability of LMAs and the model of Li deposition [275]. Specifically, the porosity and pores sizes, for one thing, can regulate Li plating/stripping within the 3D Cu skeletons. For another thing, they also directly determine the gravimetric/volumetric capacities of the LMAs [31, 276]. Therefore, the controllable fabrication of 3D Cu skeletons are crucial to achieve high-efficiency and long-lifespan LMAs. Along this line, the artificial construction

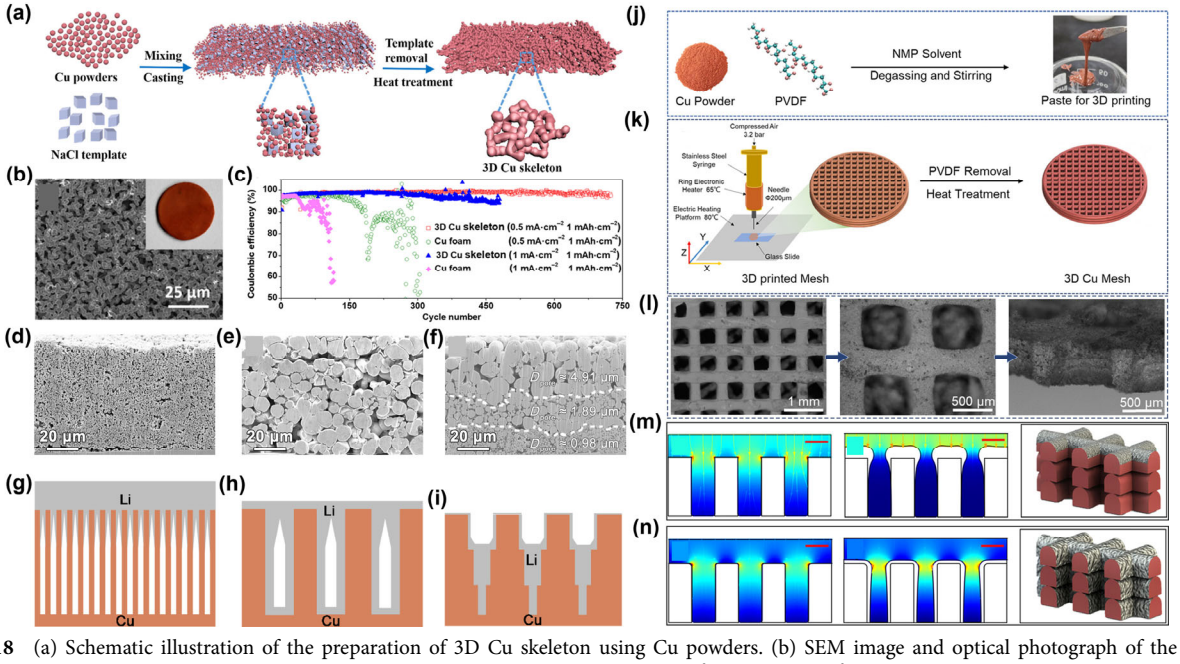

Figure 18 (a) Schematic illustration of the preparation of 3D Cu skeleton using Cu powders. (b) SEM image and optical photograph of the 3D Cu skeleton. (c) CE comparison of 3D Cu skeleton and Cu foam electrodes at 0.5 or 1 mA·cm^{-2} for 1 mAh·cm^{-2}. Reproduced with permission from Ref. [277], © American Chemical Society 2018. (d)–(f) SEM images and (g)–(i) the corresponding schematics of 3D porous Cu skeleton after Li metal plating: (d, g) small pores with a monodisperse pore size distribution, (e, h) large pores with a monodisperse pore size distribution, and (f, i) a gradient pore size distribution along the depth direction. Reproduced with permission from Ref. [278], © American Chemical Society 2021. Schematic illustrations of (j) the preparation of paste and (k) 3D printing-postprocessing processes of Cu mesh. (l) SEM images of 3D printing Cu mesh after heat treatment. Simulations of dendrite distributions at (m) high and (n) low current densities. Reproduced with permission from Ref. [279], © American Chemical Society 2021.

and structural customization of 3D Cu substrates have been positively proposed. At present, 3D self-built Cu skeletons constructed by 0D Cu particles and 1D Cu nanowires have been developed, which will be discussed in detail in this section.

5.3.1 *Cu particle-based skeletons*

The sintering of Cu powders has been extensively studied to construct 3D Cu skeletons, during which the neighboring Cu particles will form necks at contact points to build crosslinked networks. Wang et al. utilized NaCl-assisted powder sintering to prepare 3D porous Cu skeletons, which involves the balling of Cu powders and NaCl mixture prior to heat treatment (Figs. 18(a) and 18(b)) [277]. The well-distributed porous skeletons significantly dissipate the local current density on the electrode surface, resulting in the good reversibility of Li plating/stripping and stable cycling performance (Fig. 18(c)) [277]; Song et al. utilized Cu powders and SiO_2 nanoparticles to fabricate 3D porous Cu skeletons through a joint strategy of slurry mixing, calendaring, welding, and subsequent etching of SiO_2 in HF solution [280]. Owing to the high specific surface area, the distributions of Li-ion flux and electric field on the electrode are effectively optimized. Moreover, the interconnected framework and open pore structure facilitate the transfer of electrons and the diffusion of Li ions. After pore structure optimization, Li metal can uniformly deposit into the internal pores of the 3D Cu skeleton, which renders an impressive cycling of 1,200 h at 1 mA·cm^{-2}.

Aiming to quantitatively reveal the influence of Cu skeletons on Li deposition, Meng et al. synthesized four types of porous Cu skeletons with different sizes and well-structured microchannels. The fabrication involves the mechanical pressing of Cu and Fe powders associated with the etching of Fe from Cu-Fe ingots [281]. It is suggested that high porosity is beneficial for reducing the local current density of the skeleton, whilst excessive pores will induce the fast consumptions of electrolyte and active Li. Lee et al. also explored the role of pore size distribution of Cu skeletons in affecting their Li deposition [278]. As shown in Figs. 18(d)–18(f), three kinds of porous Cu skeletons were synthesized through the stacking and sintering of Cu powders and PVDF. The results indicate that an unsatisfied "top-growth" model of Li metal will occur in the cases of small pores and large pores with a monodisperse pore size distribution, which is due to the clogging of the outermost pores. By contrast, the pore size gradient framework achieves a superconformal electrodeposition of Li metal, which is ascribed to its larger surface areas in the middle and bottom regions that provide lower local current density (Figs. 18(g)–18(i)). Following that, Zhang et al. prepared a N-doped graphene modified 3D porous Cu skeleton through the chemical dealloying and CVD process [282]; while Qiang et al. prepared a 3D porous Cu-Zn alloy by the powder metallurgy of Cu and Zn powders [283]. In particular, Lin et al. adopted a template-sacrificial hot fusion construction method to build a 3D Cu skeleton, where atomized Cu and polyurethane powders are used as the raw material and template agent, respectively. Furthermore, Au was decorated on porous Cu skeleton through thermal evaporation in view of its guidance for Li deposition. Benefitting from the structural merits and the lithiophilicity of Au, the Au/Cu composite skeleton exhibits a stable cycling performance for more than 1,300 h at 1 mA·cm^{-2} in carbonate-based electrolyte [284].

3D printing of Cu-based slurry (i.e., Cu powders) is an emerging strategy to produce 3D integrated Cu skeletons. Owing to the flexible controllability of size and shape, 3D printed Cu skeletons normally exhibit orderly and periodically geometrical structure, which is favorable for the uniform distribution of Li-ion flux [285]. For instance, Chen et al. constructed a 3D grid Cu mesh by the layer-by-layer process

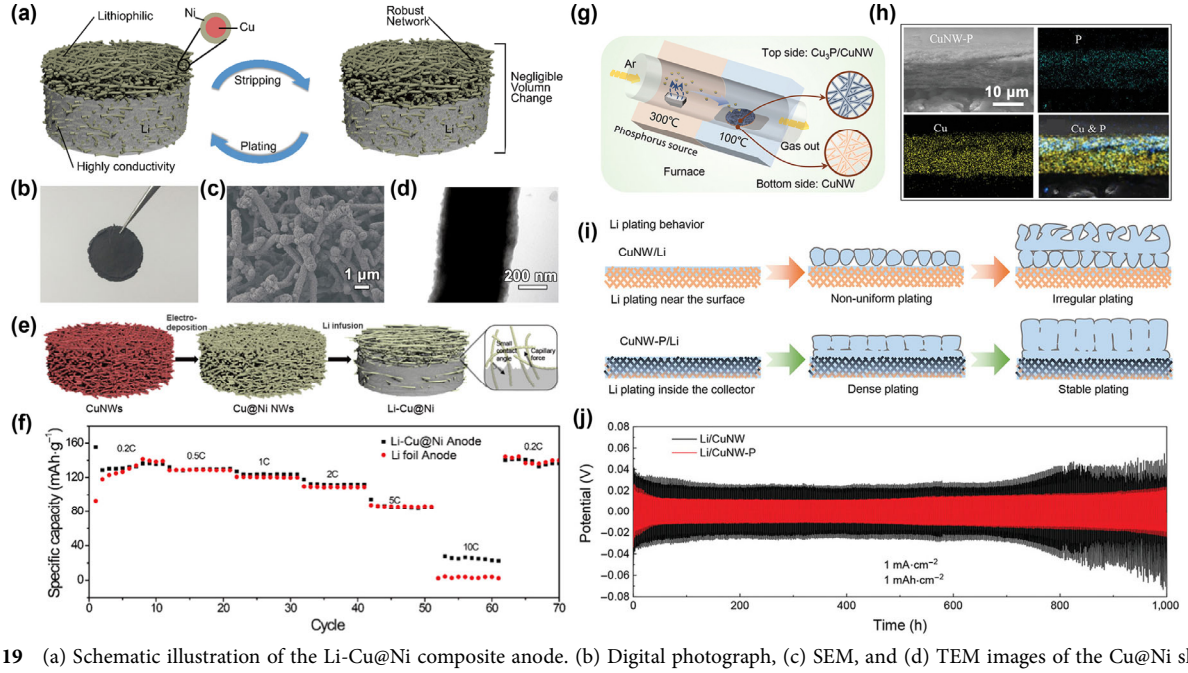

Figure 19 (a) Schematic illustration of the Li-Cu@Ni composite anode. (b) Digital photograph, (c) SEM, and (d) TEM images of the Cu@Ni skeleton. (e) Schematic of the preparation of Li-Cu@Ni composite anode. (f) Time-lapse images of Li melt-infusion process for the Cu@Ni skeleton. Reproduced with permission from Ref. [286], © Elsevier B.V. 2017. (g) Schematic of the setup for phosphidation. (h) Cross-section SEM image and the corresponding element mapping of CuNW-P. (i) Schematics of Li deposition on the Cu nanowires and CuNW-P current collectors. (j) Cycling performance of the symmetrical cells based on the Cu nanowires and CuNW-P current collectors at 1 mA·cm^{-2} and 1 mAh·cm^{-2}. Reproduced with permission from Ref. [287], © WILEY-VCH Verlag GmbH & Co. KGaA, Weinheim 2019.

based on 3D printing technique, where the slurry was consisted by Cu powders and PVDF binder (Figs. 18(j) and 18(k)) [279]. After solidification and calcination, the Cu powders were well fused and bridged both horizontally and vertically (Fig. 18(l)). COMSOL simulations and *in-situ* optical observations indicate that the Cu mesh scaffold provides even Li-ion flux distribution, which promotes homogeneous Li deposition without dendrite formation (Figs. 18(m) and 18(n)). Impressively, the well-designed Cu skeletons achieve a deep plating and stripping capacity of up to 50 mAh·cm^{-2} at 5 mA·cm^{-2}, and a superb cycling of 1,000 cycles at 10 mA·cm^{-2} and 1 mAh·cm^{-2}.

5.3.2 *Cu nanowire-based skeletons*

3D integrated Cu nanowires skeletons can be synthesized by the vacuum suction filtration or self-evaporation of solvents process. Lu et al. wrapped a layer of metal Ni on 3D Cu nanowires skeleton by electrochemical deposition (Cu@Ni) (Figs. 19(a) and 19(b)) [286]. The self-supporting Cu@Ni nanowires skeleton provides abundant opened porous structure and robust structural stability, which not only lower the Li nucleation overpotential, but also facilitate electron transfer and Li-ion migration (Figs. 19(c) and 19(d)). Consequently, the Cu@Ni nanowires skeleton achieves fast infusing of molten Li (Figs. 19(e) and 19(f)). After coupling with $LiCoO_2$ cathode, the full cells deliver stable cycling and rate performance. Similarly, many lithiophilic species, such as Cu_xO, N-doped carbon, graphdiyne, etc., have also been explored to improve the Li affinity of self-built Cu nanowires skeletons [288−290].

3D Cu nanowires skeletons with lithiophilicity or conductivity gradient were constructed due to the excellent processability and flexible self-assembly features of the nanowires. As shown Fig. 19(g), Zhang et al. prepared a Cu_3P nanowires gradient skeleton by regulating the phosphidation parameters of Cu nanowires (CuNW-P) [287]. In this gradient structure, Cu_3P exhibits gradually decreased distribution from top to bottom, where the less phosphidized bottom side maintains lower lithiophilicity and higher electronic conductivity as compared to the top side (Fig. 19(h)). Benefiting from the "bottom-growth" model of Li metal, a flat and smooth deposition is noted at the bottom of the skeleton (Fig. 19(i)). By contrast, in the case of Cu nanowires skeleton, a loose and disordered Li deposition was observed, which is not conducive to the reversible Li plating/stripping processes. Therefore, the Cu_3P nanowires electrode delivers a long-term cycling of 1,000 h at a current density of 1 mA·cm^{-2} (Fig. 19(j)). Recently, Hong et al. constructed a stable Cu nanowires-based skeleton with conductivity gradient by a simple layer-by-layer vacuum infiltration. The skeleton is comprised of a top insulating cellulose nanofibers/SiO_2 layer, a low conductivity Cu nanowires/CNFs middle layer, and a highly conductive Cu nanowires bottom layer [291]. With this design, the polar functional groups in the top layer reserves Li ions and uniformizes Li-ion flux, the middle layer provides effective dead-Li capturing, while the bottom layer induces preferential Li deposition. Consequently, the full cells assembled with NCM811 cathode exhibit a stable cycling with a CE of up to 99.8% after 100 cycles (200 mA·g^{-1}).

6 Conclusion and perspective

LMAs have gained burgeoning interests as next-generation high-energy-density batteries due to the lowest redox overpotential, ultrahigh theoretical specific capacity and light weight of Li. However, the parasitic issues of LMAs, including hyperactivity, unstable SEI, dendrite growth and huge volume expansion, severely inhibit their practical applications. Thus far, functionalized Cu current collectors have been intensively developed to overcome these stubborn challenges. Based on the design principle and associated mechanisms, functionalized Cu current collectors are divided into planar modified Cu foil, 3D architectured Cu foil and nanostructured 3D Cu substrates. The related advances are summarized as follows:

(1) *Planar modified Cu foils:* The lithophilization of Cu foil has been proposed to improve its ability for regulating Li plating/striping. First, atom-scale modification reveals the influence of crystal orientation and defects of Cu substrates on Li deposition. Second, patterned Cu foils with regular and periodic morphology render uniform electric field and Li-ion flux distribution for Li deposition. Third, lithiophilic species decorated Cu foils lower the Li nucleation overpotential, which facilitates Li deposition in a dendrite-free manner. Finally, functional protective layers attached Cu foils homogenize Li-ion migration and relieve the stress concentrations during cycling. All in all, the planar modified Cu foils have achieved remarkably improved Li plating/stripping processes.

(2) *3D architectured Cu foils:* 3D architecture design not only enables large surface specific area to dissipate the local current density of electrode, but also provides abundant interspace to accommodate the associated volume expansion. On one hand, Cu foils are employed as the substrates to *in-situ* construct 3D integrated Cu-based scaffolds, which drastically promote electronic conductivity for large-capacity Li deposition. On the other hand, Cu foils are treated as the scaffolds to build 3D composite frameworks, in which the introduced lithiophilic sites suppress the growth of Li dendrites. As a consequence, 3D architectured Cu foils have made great progress for stabilizing Li nucleation and deposition, especially under the conditions of high current density and cycling capacity.

(3) *Nanostructured 3D Cu substrates*: Owing to the lightweight and integration characteristics, 3D Cu substrates can substantially reduce the weight of inactive components and effectively regulate the Li plating/stripping behaviors of LMAs. In this regard, nanostructuring of 3D Cu substrates in terms of the lithophilization of commercial 3D Cu skeletons (i.e., Cu mesh and Cu foam) and the development of 3D self-built Cu skeletons have been intensively studied. The nanostructured 3D Cu skeletons with well-defined architectures and excellent structural stability show powerful regulatory effects for Li electrochemistry and commercial application foreground. Accordingly, dendrite-free LMAs with long-term stability and high-rate capability are obtained.

Thanks to the development of functionalized Cu current collectors, the electrochemical performances of LMAs have so far achieved significant improvements. Nonetheless, obstacles that hinder the practical applications of LMAs for long-lifespan and high-energy-density LMBs still remain to be solved. Several directions for future studies are suggested as follows:

(1) *Dynamic monitoring of Li plating/stripping processes within Cu-based current collectors.* At present, the evaluations of Li plating/stripping behaviors on Cu current collectors mainly depend on *ex-situ* techniques, which may destroy the original electrode surface and cannot analyze the in-real time electrochemical state of Li. Adopting or exploiting advanced monitoring techniques to *in-situ* observe the Li plating/stripping processes within the Cu-based current collectors will provide more clear fundamental understanding and instructions for the research and development of LMAs.

(2) *Evaluation of Li plating/stripping behaviors under extreme conditions.* The structure-performance relationship between Cu current collectors and LMAs was normally evaluated under laboratory conditions. However, extreme conditions, such as high/low temperatures, high pressure, large deformation, etc., may cause structural collapse of the Cu current collectors, thereby provoking fast battery failure and even safety hazards. Therefore, exploring functionalized Cu current collectors that capable of affording smooth Li plating/stripping under extreme conditions is crucial for the specific application of LMBs.

(3) *Extension and exploration from the coin cells to pouch cells.* Currently, the investigation of LMAs is normally carried out by using coin cells, which can't compete with pouch cells for real application. Given that the sizes and stress states of coin cells and pouch cells are complete difference, their electrochemical performances might be distinct from each other. Therefore, evaluating the Li plating/stripping behaviors of functionalized Cu current collectors at the pouch cells are an essential to obtain in-depth insights into their practical applications.

(4) *Anode-free LMBs based on the functionalized Cu-based current collectors.* In anode-free LMBs, the Li ions extracted from cathode are directly plated on Cu current collector, which are expected to show higher energy density since no excess of Li is involved. To date, the development of long-life anode-free LMBs remains a challenge because of their poor cycling efficiencies, one of which is attributed to the lack of ideal current collectors for reversible Li plating/stripping. Accordingly, functionalized Cu current collectors that capable of guiding uniform and stable Li cycling are highly imperative for realizing anode-free LMBs.

Declaration of conflicting interest

The authors declare no conflicting interests regarding the content of this article.

Acknowledgements

This work was supported by the National Natural Science Foundation of China (Nos. 22279104, 51902261 and 61935017), the National Key Research and Development Program of China (No. 2020YFA0709900), the Singapore Ministry of Education AcRF Tier 1: 2020-T1-001-031, RG4/20, the 111 project (D18023) from Zhengzhou University.

References

[1] Schmuch, R.; Wagner, R.; Hörpel, G.; Placke, T.; Winter, M. Performance and cost of materials for lithium-based rechargeable automotive batteries. *Nat. Energy* **2018**, *3*, 267–278.

[2] Chi, X. W.; Li, M. L.; Di, J. C.; Bai, P.; Song, L. N.; Wang, X. X.; Li, F.; Liang, S.; Xu, J. J.; Yu, J. H. A highly stable and flexible zeolite electrolyte solid-state Li-air battery. *Nature* **2021**, *592*, 551–557.

[3] Ma, X. T.; Azhari, L.; Wang, Y. Li-ion battery recycling challenges. *Chem* **2021**, *7*, 2843–2847.

[4] Yuan, S. Y.; Kong, T. Y.; Zhang, Y. Y.; Dong, P.; Zhang, Y. J.; Dong, X. L.; Wang, Y. G.; Xia, Y. Y. Advanced electrolyte design for high-energy-density Li-metal batteries under practical conditions. *Angew. Chem., Int. Ed.* **2021**, *60*, 25624–25638.

[5] Ai, W.; Huang, Z. N.; Wu, L. S.; Du, Z. Z.; Zou, C. J.; He, Z. Y.; Shahbazian-Yassar, R.; Huang, W.; Yu, T. High-rate, long cycle-life Li-ion battery anodes enabled by ultrasmall tin-based nanoparticles encapsulation. *Energy Storage Mater.* **2018**, *14*, 169–178.

[6] Ai, W.; Luo, Z. M.; Jiang, J.; Zhu, J. H.; Du, Z. Z.; Fan, Z. X.; Xie, L. H.; Zhang, H.; Huang, W.; Yu, T. Nitrogen and sulfur codoped graphene: Multifunctional electrode materials for high-performance Li-Ion batteries and oxygen reduction reaction. *Adv. Mater.* **2014**, *26*, 6186–6192.

[7] Yoon, K.; Lee, S.; Oh, K.; Kang, K. Challenges and strategies towards practically feasible solid-state lithium metal batteries. *Adv. Mater.* **2022**, *34*, 2104666.

[8] Li, L. P.; Liu, W. Y.; Dong, H. Y.; Gui, Q. Y.; Hu, Z. Q.; Li, Y. Y.; Liu, J. P. Surface and interface engineering of nanoarrays toward advanced electrodes and electrochemical energy storage devices. *Adv. Mater.* **2021**, *33*, 2004959.

[9] Zhang, Y. J.; Wu, Y.; Li, H. Y.; Chen, J. H.; Lei, D. N.; Wang, C. X. A dual-function liquid electrolyte additive for high-energy non-aqueous lithium metal batteries. *Nat. Commun.* **2022**, *13*, 1297.

[10] Sun, J. M.; Du, Z. Z.; Liu, Y. H.; Ai, W.; Wang, K.; Wang, T.; Du, H. F.; Liu, L.; Huang, W. State-of-the-art and future challenges in high energy lithium-selenium batteries. *Adv. Mater.* **2021**, *33*, 2003845.

[11] Xia, C.; Kwok, C. Y.; Nazar, L. F. A high-energy-density lithium-oxygen battery based on a reversible four-electron conversion to lithium oxide. *Science* **2018**, *361*, 777–781.

[12] Sun, J. M.; Liu, Y. H.; Liu, L.; He, S.; Du, Z. Z.; Wang, K.; Xie, L. H.; Du, H. F.; Ai, W. Expediting sulfur reduction/evolution reactions with integrated electrocatalytic network: A comprehensive kinetic map. *Nano Lett.* **2022**, *22*, 3728–3736.

[13] Whittingham, M. S. Chalcogenide battery. [Li/$LiClO_4$ in tetrahydrofuran + dimethoxyethane/TiS_2/ is preferred embodiment]. U.S. Patent US 4009052, February 22, 1977.

[14] Whittingham, M. S. Lithium titanium disulfide cathodes. *Nat. Energy* **2021**, *6*, 214.

[15] Niu, C. J.; Lee, H.; Chen, S. R.; Li, Q. Y.; Du, J.; Xu, W.; Zhang, J. G.; Whittingham, M. S.; Xiao, J.; Liu, J. High-energy lithium metal pouch cells with limited anode swelling and long stable cycles. *Nat. Energy* **2019**, *4*, 551–559.

[16] Cheng, X. B.; Zhang, R.; Zhao, C. Z.; Zhang, Q. Toward safe lithium metal anode in rechargeable batteries: A review. *Chem. Rev.* **2017**, *117*, 10403–10473.

[17] Zhang, X.; Yang, Y. A.; Zhou, Z. Towards practical lithium-metal anodes. *Chem. Soc. Rev.* **2020**, *49*, 3040–3071.

[18] Wang, Q. Y.; Liu, B.; Shen, Y. H.; Wu, J. K.; Zhao, Z. Q.; Zhong, C.; Hu, W. B. Confronting the challenges in lithium anodes for lithium metal batteries. *Adv. Sci.* **2021**, *8*, 2101111.

[19] Li, J. W.; Kong, Z.; Liu, X. X.; Zheng, B. C.; Fan, Q. H.; Garratt, E.; Schuelke, T.; Wang, K. L.; Xu, H.; Jin, H. Strategies to anode protection in lithium metal battery: A review. *InfoMat* **2021**, *3*, 1333–1363.

[20] Wei, C. L.; Zhang, Y. C.; Tian, Y.; Tan, L. W.; An, Y. L.; Qian, Y.; Xi, B. J.; Xiong, S. L.; Feng, J. K.; Qian, Y. T. Design of safe, long-cycling and high-energy lithium metal anodes in all working conditions: Progress, challenges and perspectives. *Energy Storage Mater.* **2021**, *38*, 157–189.

[21] Liu, Y. C.; Gao, D.; Xiang, H. F.; Feng, X. Y.; Yu, Y. Research progress on copper-based current collector for lithium metal batteries. *Energy Fuels* **2021**, *35*, 12921–12937.

[22] Choudhury, R.; Wild, J.; Yang, Y. Engineering current collectors for batteries with high specific energy. *Joule* **2021**, *5*, 1301–1305.

[23] Wang, S. H.; Yue, J. P.; Dong, W.; Zuo, T. T.; Li, J. Y.; Liu, X. L.; Zhang, X. D.; Liu, L.; Shi, J. L.; Yin, Y. X. et al. Tuning wettability of molten lithium via a chemical strategy for lithium metal anodes. *Nat. Commun.* **2019**, *10*, 4930.

[24] Yan, K.; Lu, Z. D.; Lee, H. W.; Xiong, F.; Hsu, P. C.; Li, Y. Z.; Zhao, J.; Chu, S.; Cui, Y. Selective deposition and stable encapsulation of lithium through heterogeneous seeded growth. *Nat. Energy* **2016**, *1*, 16010.

[25] Guan, X. Z.; Wang, A. X.; Liu, S.; Li, G. J.; Liang, F.; Yang, Y. W.; Liu, X. L.; Luo, J. Y. Controlling nucleation in lithium metal anodes. *Small* **2018**, *14*, 1801423.

[26] Jäckle, M.; Groß, A. Microscopic properties of lithium, sodium, and magnesium battery anode materials related to possible dendrite growth. *J. Chem. Phys.* **2014**, *141*, 174710.

[27] Chazalviel, J. N. Electrochemical aspects of the generation of ramified metallic electrodeposits. *Phys*. *Rev*. *A* **1990**, *42*, 7355–7367.
[28] Ely, D. R.; García, R. E. Heterogeneous nucleation and growth of lithium electrodeposits on negative electrodes. *J*. *Electrochem*. *Soc*. **2013**, *160*, A662–A668.
[29] Pei, A.; Zheng, G. Y.; Shi, F. F.; Li, Y. Z.; Cui, Y. Nanoscale nucleation and growth of electrodeposited lithium metal. *Nano Lett*. **2017**, *17*, 1132–1139.
[30] Lin, D. C.; Liu, Y. Y.; Cui, Y. Reviving the lithium metal anode for high-energy batteries. *Nat*. *Nanotechnol*. **2017**, *12*, 194–206.
[31] Liu, Y. H.; Sun, J. M.; Hu, X. Q.; Li, Y. F.; Du, H. F.; Wang, K.; Du, Z. Z.; Gong, X.; Ai, W.; Huang, W. Lithiophilic sites dependency of lithium deposition in Li metal host anodes. *Nano Energy* **2022**, *94*, 106883.
[32] Deng, Y. L.; Gao, J.; Wang, M.; Luo, C. S.; Zhou, C. J. Y.; Wu, M. Q. Homogenizing the Li-ion flux by multi-element alloying modified for 3D dendrite-free lithium anode. *Energy Storage Mater*. **2022**, *48*, 114–122.
[33] Peled, E.; Golodnitsky, D.; Ardel, G. Advanced model for solid electrolyte interphase electrodes in liquid and polymer electrolytes. *J*. *Electrochem*. *Soc*. **1997**, *144*, L208–L210.
[34] Shi, S. Q.; Lu, P.; Liu, Z. Y.; Qi, Y.; Hector, L. G. Jr.; Li, H.; Harris, S. J. Direct calculation of Li-ion transport in the solid electrolyte interphase. *J*. *Am*. *Chem*. *Soc*. **2012**, *134*, 15476–15487.
[35] Kushima, A.; So, K. P.; Su, C.; Bai, P.; Kuriyama, N.; Maebashi, T.; Fujiwara, Y.; Bazant, M. Z.; Li, J. Liquid cell transmission electron microscopy observation of lithium metal growth and dissolution: Root growth, dead lithium and lithium flotsams. *Nano Energy* **2017**, *32*, 271–279.
[36] Zeng, Z. Y.; Liang, W. I.; Liao, H. G.; Xin, H. L.; Chu, Y. H.; Zheng, H. M. Visualization of electrode-electrolyte interfaces in $LiPF_6$/EC/DEC electrolyte for lithium ion batteries via *in situ* TEM. *Nano Lett*. **2014**, *14*, 1745–1750.
[37] Shen, X.; Zhang, R.; Shi, P.; Chen, X.; Zhang, Q. How does external pressure shape Li dendrites in Li metal batteries? *Adv*. *Energy Mater*. **2021**, *11*, 2003416.
[38] Fang, C. C.; Li, J. X.; Zhang, M. H.; Zhang, Y. H.; Yang, F.; Lee, J. Z.; Lee, M. H.; Alvarado, J.; Schroeder, M. A.; Yang, Y. Y. C. et al. Quantifying inactive lithium in lithium metal batteries. *Nature* **2019**, *572*, 511–515.
[39] Jin, C. B.; Liu, T. F.; Sheng, O. W.; Li, M.; Liu, T. C.; Yuan, Y. F.; Nai, J. W.; Ju, Z. J.; Zhang, W. K.; Liu, Y. J. et al. Rejuvenating dead lithium supply in lithium metal anodes by iodine redox. *Nat*. *Energy* **2021**, *6*, 378–387.
[40] Yuan, H. D.; Ding, X. F.; Liu, T. F.; Nai, J. W.; Wang, Y.; Liu, Y. J.; Liu, C. T.; Tao, X. Y. A review of concepts and contributions in lithium metal anode development. *Mater*. *Today* **2022**, *53*, 173–196.
[41] Boyle, D. T.; Huang, W.; Wang, H. S.; Li, Y. Z.; Chen, H.; Yu, Z. A.; Zhang, W. B.; Bao, Z. N.; Cui, Y. Corrosion of lithium metal anodes during calendar ageing and its microscopic origins. *Nat*. *Energy* **2021**, *6*, 487–494.
[42] Liu, F.; Xu, R.; Wu, Y. C.; Boyle, D. T.; Yang, A. K.; Xu, J. W.; Zhu, Y. Y.; Ye, Y. S.; Yu, Z. A.; Zhang, Z. W. et al. Dynamic spatial progression of isolated lithium during battery operations. *Nature* **2021**, *600*, 659–663.
[43] Gao, R. M.; Yang, H.; Wang, C. Y.; Ye, H.; Cao, F. F.; Guo, Z. P. Fatigue-resistant interfacial layer for safe lithium metal batteries. *Angew*. *Chem*., *Int*. *Ed*. **2021**, *60*, 25508–25513.
[44] Huang, L.; Lu, T.; Xu, G. J.; Zhang, X. H.; Jiang, Z. X.; Zhang, Z. Q.; Wang, Y. T.; Han, P. X.; Cui, G. L.; Chen, L. Q. Thermal runaway routes of large-format lithium-sulfur pouch cell batteries. *Joule* **2022**, *6*, 906–922.
[45] Johnson, B. A.; White, R. E. Characterization of commercially available lithium-ion batteries. *J*. *Power Sources* **1998**, *70*, 48–54.
[46] Zhu, P. C.; Gastol, D.; Marshall, J.; Sommerville, R.; Goodship, V.; Kendrick, E. A review of current collectors for lithium-ion batteries. *J*. *Power Sources* **2021**, *485*, 229321.
[47] Lain, M. J.; Brandon, J.; Kendrick, E. Design strategies for high power vs. High energy lithium ion cells. *Batteries* **2019**, *5*, 64.
[48] Li, Y. Z.; Li, Y. B.; Pei, A.; Yan, K.; Sun, Y. M.; Wu, C. L.; Joubert, L. M.; Chin, R.; Koh, A. L.; Yu, Y. et al. Atomic structure of sensitive battery materials and interfaces revealed by cryo-electron microscopy. *Science* **2017**, *358*, 506–510.
[49] Gu, Y.; Xu, H. Y.; Zhang, X. G.; Wang, W. W.; He, J. W.; Tang, S.; Yan, J. W.; Wu, D. Y.; Zheng, M. S.; Dong, Q. F. et al. Lithiophilic faceted Cu(100) surfaces: High utilization of host surface and cavities for lithium metal anodes. *Angew*. *Chem*., *Int*. *Ed*. **2019**, *58*, 3092–3096.
[50] Kim, Y. J.; Kwon, S. H.; Noh, H.; Yuk, S.; Lee, H.; Jin, H. S.; Lee, J.; Zhang, J. G.; Lee, S. G.; Guim, H. et al. Facet selectivity of Cu current collector for Li electrodeposition. *Energy Storage Mater*. **2019**, *19*, 154–162.
[51] Ishikawa, K.; Harada, S.; Tagawa, M.; Ujihara, T. Effect of crystal orientation of Cu current collectors on cycling stability of Li metal anodes. *ACS Appl*. *Mater*. *Interfaces* **2020**, *12*, 9341–9346.
[52] Zhao, Q.; Deng, Y.; Utomo, N. W.; Zheng, J. X.; Biswal, P.; Yin, J. F.; Archer, L. A. On the crystallography and reversibility of lithium electrodeposits at ultrahigh capacity. *Nat*. *Commun*. **2021**, *12*, 6034.
[53] Kim, J. Y.; Chae, O. B.; Wu, M.; Lim, E.; Kim, G.; Hong, Y. J.; Jung, W. B.; Choi, S.; Kim, D. Y.; Gereige, I. et al. Extraordinary dendrite-free Li deposition on highly uniform facet wrinkled Cu substrates in carbonate electrolytes. *Nano Energy* **2021**, *82*, 105736.
[54] Røe, I. T.; Schnell, S. K. Slow surface diffusion on Cu substrates in Li metal batteries. *J*. *Mater*. *Chem*. *A* **2021**, *9*, 11042–11048.
[55] Qin, L. G.; Wu, Y. C.; Shen, M. Y.; Song, B. R.; Li, Y. H.; Sun, S. Q.; Zhang, H. Y.; Liu, C. F.; Chen, J. Straining copper foils to regulate the nucleation of lithium for stable lithium metal anode. *Energy Storage Mater*. **2022**, *44*, 278–284.
[56] Zou, P. C.; Wang, Y.; Chiang, S. W.; Wang, X. Y.; Kang, F. Y.; Yang, C. Directing lateral growth of lithium dendrites in micro-compartmented anode arrays for safe lithium metal batteries. *Nat*. *Commun*. **2018**, *9*, 464.
[57] Park, S.; Ahn, K.; Lim, H. K.; Jin, H. J.; Han, S.; Yun, Y. S. Intagliated Cu substrate containing multifunctional lithiophilic trenches for Li metal anodes. *Chem*. *Eng*. *J*. **2022**, *428*, 130939.
[58] Lim, G. J. H.; Lyu, Z.; Zhang, X.; Koh, J. J.; Zhang, Y.; He, C. B.; Adams, S.; Wang, J.; Ding, J. Robust pure copper framework by extrusion 3D printing for advanced lithium metal anodes. *J*. *Mater*. *Chem*. *A* **2020**, *8*, 9058–9067.
[59] Wang, S. H.; Yin, Y. X.; Zuo, T. T.; Dong, W.; Li, J. Y.; Shi, J. L.; Zhang, C. H.; Li, N. W.; Li, C. J.; Guo, Y. G. Stable Li metal anodes via regulating lithium plating/stripping in vertically aligned microchannels. *Adv*. *Mater*. **2017**, *29*, 1703729.
[60] Jiang, J. M.; Pan, Z. H.; Kou, Z. K.; Nie, P.; Chen, C. L.; Li, Z. W.; Li, S. P.; Zhu, Q.; Dou, H.; Zhang, X. G. et al. Lithiophilic polymer interphase anchored on laser-punched 3D holey Cu matrix enables uniform lithium nucleation leading to super-stable lithium metal anodes. *Energy Storage Mater*. **2020**, *29*, 84–91.
[61] Liu, Y. M.; Yin, X. G.; Shen, X.; Zou, P. C.; Qin, X. Y.; Yang, C.; Zhang, Q.; Kang, F. Y.; Chen, G. H.; Li, B. H. Horizontal stress release for protuberance-free Li metal anode. *Adv*. *Funct*. *Mater*. **2020**, *30*, 2002522.
[62] Dong, W.; Wang, K.; Han, J. L.; Yu, Y.; Liu, G. H.; Li, C.; Tong, P. F.; Li, W. J.; Yang, C. L.; Lu, Z. H. Regulating lithium electrodeposition with laser-structured current collectors for stable lithium metal batteries. *ACS Appl*. *Mater*. *Interfaces* **2021**, *13*, 8417–8425.
[63] Wang, Y. Y.; Zhao, Z. X.; Zeng, W.; Liu, X. B.; Wang, L.; Zhu, J.; Lu, B. A. Hierarchically porous Cu current collector with lithiophilic Cu_xO interphase towards high-performance lithium metal batteries. *J*. *Energy Chem*. **2021**, *58*, 292–299.
[64] Jang, T.; Kang, J. H.; Kim, S.; Shim, M.; Lee, J.; Song, J.; Kim, W.; Ryu, K.; Byon, H. R. Nanometer-scale surface roughness of a 3-D Cu substrate promoting Li nucleation in Li-metal batteries. *ACS Appl*. *Energy Mater*. **2021**, *4*, 2644–2651.
[65] Li, Z. Q.; Huang, X. L.; Kong, L.; Qin, N.; Wang, Z. Y.; Yin, L. H.; Li, Y. Z.; Gan, Q. M.; Liao, K. M.; Gu, S. et al. Gradient nano-recipes to guide lithium deposition in a tunable reservoir for anode-free batteries. *Energy Storage Mater*. **2022**, *45*, 40–47.
[66] Cipollone, D.; Yang, H.; Yang, F.; Bright, J.; Liu, B.T.; Winch, N.;

Wu, N. Q.; Sierros, K. A. 3D printing of an anode scaffold for lithium batteries guided by mixture design-based sequential learning. *J. Mater. Process. Technol.* **2021**, *295*, 117159.
[67] Wang, Y.; Tan, J.; Li, Z. H.; Ma, L. L.; Liu, Z.; Ye, M. X.; Shen, J. F. Recent progress on enhancing the Lithiophilicity of hosts for dendrite-free lithium metal batteries. *Energy Storage Mater.* **2022**, *53*, 156–182.
[68] Heine, J.; Krüger, S.; Hartnig, C.; Wietelmann, U.; Winter, M.; Bieker, P. Coated lithium powder (CLiP) electrodes for lithium-metal batteries. *Adv. Energy Mater.* **2014**, *4*, 1300815.
[69] Cao, Z. J.; Li, B.; Yang, S. B. Dendrite-free lithium anodes with ultra-deep stripping and plating properties based on vertically oriented lithium-copper-lithium arrays. *Adv. Mater.* **2019**, *31*, 1901310.
[70] Zhu, M. G.; Xu, K. L.; Li, D. Y.; Xu, T.; Sun, W.; Zhu, Y. C.; Qian, Y. T. Guiding smooth Li plating and stripping by a spherical island model for lithium metal anodes. *ACS Appl. Mater. Interfaces* **2020**, *12*, 38098–38105.
[71] Du, J. M.; Wang, W. Y.; Wan, M. T.; Wang, X. C.; Li, G. C.; Tan, Y. C.; Li, C. H.; Tu, S. B.; Sun, Y. M. Doctor-blade casting fabrication of ultrathin Li metal electrode for high-energy-density batteries. *Adv. Energy Mater.* **2021**, *11*, 2102259.
[72] Jung, W. B.; Chae, O. B.; Kim, M.; Kim, Y.; Hong, Y. J.; Kim, J. Y.; Choi, S.; Kim, D. Y.; Moon, S.; Suk, J. et al. Effect of highly periodic Au nanopatterns on dendrite suppression in lithium metal batteries. *ACS Appl. Mater. Interfaces* **2021**, *13*, 60978–60986.
[73] Cui, S. Q.; Zhai, P. B.; Yang, W. W.; Wei, Y.; Xiao, J.; Deng, L. B.; Gong, Y. J. Large-scale modification of commercial copper foil with lithiophilic metal layer for Li metal battery. *Small* **2020**, *16*, 1905620.
[74] Hou, Z.; Yu, Y. K.; Wang, W. H.; Zhao, X. X.; Di, Q.; Chen, Q. W.; Chen, W.; Liu, Y. L.; Quan, Z. W. Lithiophilic Ag nanoparticle layer on Cu current collector toward stable Li metal anode. *ACS Appl. Mater. Interfaces* **2019**, *11*, 8148–8154.
[75] Cho, K. Y.; Hong, S. H.; Kwon, J.; Song, H. Y.; Kim, S.; Jo, S.; Eom, K. Effects of a nanometrically formed lithiophilic silver@copper current collector on the electrochemical nucleation and growth behaviors of lithium metal anodes. *Appl. Surf. Sci.* **2021**, *554*, 149578.
[76] Fan, M.; Chen, B.; Wang, K.; Yu, Q.; Ding, Y.; Lei, Z.; Liu, F.; Shen, Y.; He, G. Robust silver nanowire membrane with high porosity to construct stable Li metal anodes. *Mater. Today Energy* **2021**, *21*, 100751.
[77] Zhang, N.; Yu, S. H.; Abruña, H. D. Regulating lithium nucleation and growth by zinc modified current collectors. *Nano Res.* **2020**, *13*, 45–51.
[78] He, D. Q.; Cui, W. J.; Liao, X. B.; Xie, X. F.; Mao, M. H.; Sang, X. H.; Zhai, P. C.; Zhao, Y.; Huang, Y. H.; Zhao, W. Y. Electronic localization derived excellent stability of Li metal anode with ultrathin alloy. *Adv. Sci.* **2022**, *9*, 2105656.
[79] Zhang, S. M.; Yang, G. J.; Liu, Z. P.; Weng, S. T.; Li, X. Y.; Wang, X. F.; Gao, Y. R.; Wang, Z. X.; Chen, L. Q. Phase diagram determined lithium plating/stripping behaviors on lithiophilic substrates. *ACS Energy Lett.* **2021**, *6*, 4118–4126.
[80] Zhang, Q.; Luan, J. Y.; Tang, Y. G.; Ji, X. B.; Wang, S. Y.; Wang, H. Y. A facile annealing strategy for achieving *in situ* controllable Cu_2O nanoparticle decorated copper foil as a current collector for stable lithium metal anodes. *J. Mater. Chem. A* **2018**, *6*, 18444–18448.
[81] Li, Q.; Pan, H. Y.; Li, W. J.; Wang, Y.; Wang, J. Y.; Zheng, J. Y.; Yu, X. Q.; Li, H.; Chen, L. Q. Homogeneous interface conductivity for lithium dendrite-free anode. *ACS Energy Lett.* **2018**, *3*, 2259–2266.
[82] Jin, D.; Roh, Y.; Jo, T.; Shin, D. O.; Song, J.; Kim, J. Y.; Lee, Y. G.; Lee, H.; Ryou, M. H.; Lee, Y. M. Submicron interlayer for stabilizing thin Li metal powder electrode. *Chem. Eng. J.* **2021**, *406*, 126834.
[83] Yin, D. M.; Wang, Z. M.; Li, Q.; Xue, H. J.; Cheng, Y.; Wang, L. M.; Huang, G. *In situ* growth of lithiophilic MOF layer enabling dendrite-free lithium deposition. *iScience* **2020**, *23*, 101869.
[84] Um, J. H.; Kim, K.; Park, J.; Sung, Y.; Yu, S. H. Revisiting the strategies for stabilizing lithium metal anodes. *J. Mater. Chem. A* **2020**, *8*, 13874–13895.
[85] Ghazi, Z. A.; Sun, Z. H.; Sun, C. G.; Qi, F. L.; An, B. G.; Li, F.; Cheng, H. M. Key aspects of lithium metal anodes for lithium metal batteries. *Small* **2019**, *15*, 1900687.
[86] Chen, Y. Q.; Xu, X. Y.; Gao, L. W.; Yu, G. Y.; Kapitanova, O. O.; Xiong, S. Z.; Volkov, V. S.; Song, Z.X.; Liu, Y. Y. Two birds with one stone: Using indium oxide surficial modification to tune inner helmholtz plane and regulate nucleation for dendrite-free lithium anode. *Small Methods* **2022**, *6*, 2200113.
[87] Oyakhire, S. T.; Zhang, W. B.; Shin, A.; Xu, R.; Boyle, D. T.; Yu, Z. A.; Ye, Y. S.; Yang, Y. F.; Raiford, J. A.; Huang, W. et al. Electrical resistance of the current collector controls lithium morphology. *Nat. Commun.* **2022**, *13*, 3986.
[88] Zhuang, D. M.; Huang, X. L.; Chen, Z. H.; Gong, H.; Sheng, L.; Song, L.; Wang, T.; He, J. P. The synergistic effect of Cu_2O and boric acid forming solid electrolyte interphase layer to restrain the dendritic growth. *J. Power Sources* **2020**, *458*, 228055.
[89] Schönherr, K.; Schumm, B.; Hippauf, F.; Lissy, R.; Althues, H.; Leyens, C.; Kaskel, S. Liquid lithium metal processing into ultrathin metal anodes for solid state batteries. *Chem. Eng. J. Adv.* **2022**, *9*, 100218.
[90] Hu, M. F.; Yuan, Y.; Guo, M.; Pan, Y. K.; Long, D. H. A substrate-influenced three-dimensional unoriented dispersion pathway for dendrite-free lithium metal anodes. *J. Mater. Chem. A* **2018**, *6*, 14910–14918.
[91] Oyakhire, S. T.; Huang, W.; Wang, H. S.; Boyle, D. T.; Schneider, J. R.; de Paula, C.; Wu, Y. C.; Cui, Y.; Bent, S. F. Revealing and elucidating ALD-derived control of lithium plating microstructure. *Adv. Energy Mater.* **2020**, *10*, 2002736.
[92] Tan, L.; Li, X. L.; Liu, T. C.; Li, X. H. Atomic layer deposition-strengthened lithiophilicity of ultrathin TiO_2 film decorated Cu foil for stable lithium metal anode. *J. Power Sources* **2020**, *463*, 228157.
[93] Zhu, Y.; Meng, F. P.; Sun, N. N.; Huai, L. Y.; Wang, M. Q.; Ren, F. H.; Li, Z. D.; Peng, Z.; Huang, F.; Gu, H. et al. Suppressing sponge-like Li deposition via AlN-modified substrate for stable Li metal anode. *ACS Appl. Mater. Interfaces* **2019**, *11*, 42261–42270.
[94] Ma, Y. T.; Li, L.; Wang, L. L.; Qian, J.; Hu, X.; Qu, W. J.; Wang, Z. H.; Luo, R.; Fu, S. Y.; Wu, F. et al. A mixed modified layer formed *in situ* to protect and guide lithium plating/stripping behavior. *ACS Appl. Mater. Interfaces* **2020**, *12*, 31411–31418.
[95] Ye, H.; Xin, S.; Yin, Y. X.; Guo, Y. G. Advanced porous carbon materials for high-efficient lithium metal anodes. *Adv. Energy Mater.* **2017**, *7*, 1700530.
[96] Zhang, S. S.; Fan, X. L.; Wang, C. S. Efficient and stable cycling of lithium metal enabled by a conductive carbon primer layer. *Sustainable Energy Fuels* **2018**, *2*, 163–168.
[97] Sun, J. M.; Liu, Y. H.; Du, H. F.; He, S.; Liu, L.; Fu, Z. Q.; Xie, L. H.; Ai, W.; Huang, W. Molecularly designed N, S co-doped carbon nanowalls decorated on graphene as a highly efficient sulfur reservoir for Li-S batteries: A supramolecular strategy. *J. Mater. Chem. A* **2020**, *8*, 5449–5457.
[98] Chen, M. X.; Cheng, L. W.; Chen, J. C.; Zhou, Y.; Liang, J. D.; Dong, S.; Chen, M.; Wang, X. T.; Wang, H. Facile and scalable modification of a Cu current collector toward uniform li deposition of the Li metal anode. *ACS Appl. Mater. Interfaces* **2020**, *12*, 3681–3687.
[99] Luan, X. Y.; Wang, C. G.; Wang, C. S.; Gu, X.; Yang, J.; Qian, Y. T. Stable lithium deposition enabled by an acid-treated g-C_3N_4 interface layer for a lithium metal anode. *ACS Appl. Mater. Interfaces* **2020**, *12*, 11265–11272.
[100] Wang, K.; Li, X. D.; Wang, N.; Yang, Z.; Gao, J.; He, J. J.; Zhang, Y. L.; Huang, C. S. Lithiophilicity acetylene bonds induced nucleation and deposition of dendrite-free lithium metal anode. *ACS Appl. Energy Mater.* **2020**, *3*, 2623–2633.
[101] Fan, Y. C.; Zhao, Y.; Li, S.; Liu, Y.; Lv, Y.; Zhu, Y.; Xiang, R.; Maruyama, S.; Zhang, H.; Zhang, Q. F. Altering polythiophene derivative substrates to explore the mechanism of heterogeneous lithium nucleation for dendrite-free lithium metal anodes. *J. Energy Chem.* **2021**, *59*, 63–68.
[102] Wen, Z. X.; Fang, W. Q.; Chen, L.; Guo, Z. W.; Zhang, N.; Liu,

X. H.; Chen, G. Anticorrosive copper current collector passivated by self-assembled porous membrane for highly stable lithium metal batteries. *Adv. Funct. Mater.* **2021**, *31*, 2104930.
[103] Ni, X. Y.; Liu, J.; Ji, H. Q.; Chen, L. B.; Qian, T.; Yan, C. L. Ordered lithium ion channels of covalent organic frameworks with lithiophilic groups enable uniform and efficient Li plating/stripping. *J. Energy Chem.* **2021**, *61*, 135–140.
[104] Jiang, Z. G.; Liu, T. F.; Yan, L. J.; Liu, J.; Dong, F. F.; Ling, M.; Liang, C. D.; Lin, Z. Metal-organic framework nanosheets-guided uniform lithium deposition for metallic lithium batteries. *Energy Storage Mater.* **2018**, *11*, 267–273.
[105] Chen, H.; Yang, Y. F.; Boyle, D. T.; Jeong, Y. K.; Xu, R.; de Vasconcelos, L. S.; Huang, Z. J.; Wang, H. S.; Wang, H. X.; Huang, W. X. et al. Free-standing ultrathin lithium metal-graphene oxide host foils with controllable thickness for lithium batteries. *Nat. Energy* **2021**, *6*, 790–798.
[106] Park, S. H.; Jun, D.; Lee, G. H.; Lee, S. G.; Lee, Y. J. Toward high-performance anodeless batteries based on controlled lithium metal deposition: A review. *J. Mater. Chem. A* **2021**, *9*, 14656–14681.
[107] Li, X. C.; Jiang, H. L.; Liu, Y.; Guo, X. L.; He, G. H.; Chu, Z.; Yu, G. H. Hierarchically porous membranes for lithium rechargeable batteries: Recent progress and opportunities. *EcoMat* **2022**, *4*, e12162.
[108] Su, T. T.; Le, J. B.; Ren, W. F.; Zhang, S. J.; Yuan, J. M.; Wang, K.; Shao, C. Y.; Li, J. T.; Sun, S. G.; Sun, R. C. Heteroatom-rich polymers as a protective film to control lithium growth for high-performance lithium-metal batteries. *J. Power Sources* **2022**, *521*, 230949.
[109] Han, Z. Y.; Zhang, C.; Lin, Q. W.; Zhang, Y. B.; Deng, Y. Q.; Han, J. W.; Wu, D. C.; Kang, F. Y.; Yang, Q. H.; Lv, W. A protective layer for lithium metal anode: Why and how. *Small Methods* **2021**, *5*, 2001035.
[110] Zheng, G. Y.; Lee, S. W.; Liang, Z.; Lee, H. W.; Yan, K.; Yao, H. B.; Wang, H. T.; Li, W. Y.; Chu, S.; Cui, Y. Interconnected hollow carbon nanospheres for stable lithium metal anodes. *Nat. Nanotechnol.* **2014**, *9*, 618–623.
[111] Yan, K.; Lee, H. W.; Gao, T.; Zheng, G. Y.; Yao, H. B.; Wang, H. T.; Lu, Z. D.; Zhou, Y.; Liang, Z.; Liu, Z. F. et al. Ultrathin two-dimensional atomic crystals as stable interfacial layer for improvement of lithium metal anode. *Nano Lett.* **2014**, *14*, 6016–6022.
[112] Liu, X. Y.; Liu, Z. J.; Yang, H.; Qing, P.; Wei, W. F.; Ji, X. B.; Chen, Y. J.; Chen, L. B. Uniform lithium deposition induced by double lithiophobic sandwich structure for stable lithium metal anode. *Adv. Mater. Interfaces* **2022**, *9*, 2200011.
[113] Xie, J.; Liao, L.; Gong, Y. J.; Li, Y. B.; Shi, F. F.; Pei, A.; Sun, J.; Zhang, R. F.; Kong, B.; Subbaraman, R. et al. Stitching h-BN by atomic layer deposition of LiF as a stable interface for lithium metal anode. *Sci. Adv.* **2017**, *3*, eaao3170.
[114] Zhu, B.; Jin, Y.; Hu, X. Z.; Zheng, Q. H.; Zhang, S.; Wang, Q. J.; Zhu, J. Poly(dimethylsiloxane) thin film as a stable interfacial layer for high-performance lithium-metal battery anodes. *Adv. Mater.* **2017**, *29*, 1603755.
[115] Tamwattana, O.; Park, H.; Kim, J.; Hwang, I.; Yoon, G.; Hwang, T. H.; Kang, Y. S.; Park, J.; Meethong, N.; Kang, K. High-dielectric polymer coating for uniform lithium deposition in anode-free lithium batteries. *ACS Energy Lett.* **2021**, *6*, 4416–4425.
[116] Li, J. H.; Cai, Y. F.; Wu, H. M.; Yu, Z. A.; Yan, X. Z.; Zhang, Q. H.; Gao, T. Z.; Liu, K.; Jia, X. D.; Bao, Z. A. Polymers in lithium-ion and lithium metal batteries. *Adv. Energy Mater.* **2021**, *11*, 2003239.
[117] Zheng, G. Y.; Wang, C.; Pei, A.; Lopez, J.; Shi, F. F.; Chen, Z.; Sendek, A. D.; Lee, H. W.; Lu, Z. D.; Schneider, H. et al. High-performance lithium metal negative electrode with a soft and flowable polymer coating. *ACS Energy Lett.* **2016**, *1*, 1247–1255.
[118] Zhou, H. Y.; Yu, S. C.; Liu, H. D.; Liu, P. Protective coatings for lithium metal anodes: Recent progress and future perspectives. *J. Power Sources* **2020**, *450*, 227632.
[119] Luo, J.; Fang, C. C.; Wu, N. L. High polarity poly(vinylidene difluoride) thin coating for dendrite-free and high-performance lithium metal anodes. *Adv. Energy Mater.* **2018**, *8*, 1701482.
[120] Xu, B. Q.; Zhai, H. W.; Liao, X. B.; Qie, B. Y.; Mandal, J.; Gong, T. Y.; Tan, L. Y.; Yang, X. J.; Sun, K. R.; Cheng, Q. et al. Porous insulating matrix for lithium metal anode with long cycling stability and high power. *Energy Storage Mater.* **2019**, *17*, 31–37.
[121] Yan, Y.; Shu, C. Z.; Zheng, R. X.; Li, M. L.; Ran, Z. Q.; He, M.; Hu, A. J.; Zeng, T.; Xu, H. Y.; Zeng, Y. Modulating Sand's time by ion-transport-enhancement toward dendrite-free lithium metal anode. *Nano Res.* **2022**, *15*, 3150–3160.
[122] Chen, A. L.; Shang, N.; Ouyang, Y.; Mo, L. L.; Zhou, C. Y.; Tjiu, W. W.; Lai, F. L.; Miao, Y. E.; Liu, T. X. Electroactive polymeric nanofibrous composite to drive *in situ* construction of lithiophilic SEI for stable lithium metal anodes. *eScience* **2022**, *2*, 192–200.
[123] Jeon, Y.; Kang, S. J.; Joo, S. H.; Cho, M.; Park, S. O.; Liu, N.; Kwak, S. K.; Lee, H. W.; Song, H. K. Pyridinic-to-graphitic conformational change of nitrogen in graphitic carbon nitride by lithium coordination during lithium plating. *Energy Storage Mater.* **2020**, *31*, 505–514.
[124] Xiong, X. S.; Yan, W. Q.; Zhu, Y. S.; Liu, L. L.; Fu, L. J.; Chen, Y. H.; Yu, N. F.; Wu, Y. P.; Wang, B.; Xiao, R. $Li_4Ti_5O_{12}$ coating on copper foil as ion redistributor layer for stable lithium metal anode. *Adv. Energy Mater.* **2022**, *12*, 2103112.
[125] Yang, D.; Li, J.; Yang, F.; Li, J.; He, L.; Zhao, H. N.; Wei, L. Y.; Wang, Y. Z.; Wang, X. D.; Wei, Y. J. A rigid-flexible protecting film with surface pits structure for dendrite-free and high-performance lithium metal anode. *Nano Lett.* **2021**, *21*, 7063–7069.
[126] Huang, M. S.; Yao, Z. G.; Wu, Q. P.; Zheng, Y. J.; Liu, J. J.; Li, C. L. Robustness-heterogeneity-induced ultrathin 2D structure in Li plating for highly reversible Li-metal batteries. *ACS Appl. Mater. Interfaces* **2020**, *12*, 46132–46145.
[127] Liang, Z.; Zheng, G. Y.; Liu, C.; Liu, N.; Li, W. Y.; Yan, K.; Yao, H. B.; Hsu, P. C.; Chu, S.; Cui, Y. Polymer nanofiber-guided uniform lithium deposition for battery electrodes. *Nano Lett.* **2015**, *15*, 2910–2916.
[128] Zhou, S.; Zhang, Y. F.; Chai, S. M.; Usman, I.; Qiao, Y.; Luo, S. Z.; Xie, X. F.; Chen, J.; Liang, S. Q.; Pan, A. Q. et al. Incorporation of LiF into functionalized polymer fiber networks enabling high capacity and high rate cycling of lithium metal composite anodes. *Chem. Eng. J.* **2021**, *404*, 126508.
[129] He, Y.; Xu, H. W.; Shi, J. L.; Liu, P. Y.; Tian, Z. Q.; Dong, N.; Luo, K.; Zhou, X. F.; Liu, Z. P. Polydopamine coating layer modified current collector for dendrite-free Li metal anode. *Energy Storage Mater.* **2019**, *23*, 418–426.
[130] Sun, X.R.; Yang, S. H.; Zhang, T.; Shi, Y. B.; Dong, L.; Ai, G.; Li, D. J.; Mao, W. F. Regulating Li-ion flux with a high-dielectric hybrid artificial SEI for stable Li metal anodes. *Nanoscale* **2022**, *14*, 5033–5043.
[131] Lang, J. L.; Song, J. A.; Qi, L. H.; Luo, Y. Z.; Luo, X. Y.; Wu, H. Uniform lithium deposition induced by polyacrylonitrile submicron fiber array for stable lithium metal anode. *ACS Appl. Mater. Interfaces* **2017**, *9*, 10360–10365.
[132] Shen, F.; Wang, K. M.; Yin, Y. T.; Shi, L.; Zeng, D. Y.; Han, X. G. PAN/PI functional double-layer coating for dendrite-free lithium metal anodes. *J. Mater. Chem. A* **2020**, *8*, 6183–6189.
[133] Sahalie, N. A.; Wondimkun, Z. T.; Su, W. N.; Weret, M. A.; Fenta, F. W.; Berhe, G. B.; Huang, C. J.; Hsu, Y. C.; Hwang, B. J. Multifunctional properties of Al_2O_3/polyacrylonitrile composite coating on Cu to suppress dendritic growth in anode-free Li-metal battery. *ACS Appl. Energy Mater.* **2020**, *3*, 7666–7679.
[134] Weng, Y. T.; Liu, H. W.; Pei, A.; Shi, F. F.; Wang, H. S.; Lin, C. Y.; Huang, S. S.; Su, L. Y.; Hsu, J. P.; Fang, C. C. et al. An ultrathin ionomer interphase for high efficiency lithium anode in carbonate based electrolyte. *Nat. Commun.* **2019**, *10*, 5824.
[135] Nan, Y.; Li, S. M.; Han, C.; Yan, H. B.; Ma, Y. X.; Liu, J. H.; Yang, S. B.; Li, B. Interlamellar lithium-ion conductor reformed interface for high performance lithium metal anode. *Adv. Funct. Mater.* **2021**, *31*, 2102336.
[136] Dong, Q. Y.; Hong, B.; Fan, H. L.; Gao, C. H.; Huang, X. J.; Bai, M. H.; Zhou, Y. G.; Lai, Y. Q. A self-adapting artificial SEI layer enables superdense lithium deposition for high performance lithium anode. *Energy Storage Mater.* **2022**, *45*, 1220–1228.

[137] Fan, L. S.; Guo, Z. K.; Zhang, Y.; Wu, X.; Zhao, C. Y.; Sun, X.; Yang, G. Y.; Feng, Y. J.; Zhang, N. Q. Stable artificial solid electrolyte interphase films for lithium metal anode via metal-organic frameworks cemented by polyvinyl alcohol. *J. Mater. Chem. A* **2020**, *8*, 251–258.
[138] Cui, X. M.; Chu, Y.; Wang, X. H.; Zhang, X. Z.; Li, Y. X.; Pan, Q. M. Stabilizing lithium metal anodes by a self-healable and Li-regulating interlayer. *ACS Appl. Mater. Interfaces* **2021**, *13*, 44983–44990.
[139] Wang, W. B.; Yang, Z. H.; Zhang, Y. T.; Wang, A. P.; Zhang, Y. R.; Chen, L. L.; Li, Q.; Qiao, S. L. Highly stable lithium metal anode enabled by lithiophilic and spatial-confined spherical-covalent organic framework. *Energy Storage Mater.* **2022**, *46*, 374–383.
[140] Li, Z. H.; Ji, W. Y.; Wang, T. X.; Zhang, Y. R.; Li, Z.; Ding, X. S.; Han, B. H.; Feng, W. Guiding uniformly distributed Li-ion flux by lithiophilic covalent organic framework interlayers for high-performance lithium metal anodes. *ACS Appl. Mater. Interfaces* **2021**, *13*, 22586–22596.
[141] Bai, S. Y.; Liu, X. Z.; Zhu, K.; Wu, S. C.; Zhou, H. S. Metal-organic framework-based separator for lithium-sulfur batteries. *Nat. Energy* **2016**, *1*, 16094.
[142] Li, C. F.; Lu, R. C.; Amin, K.; Zhang, B. B.; Liu, H.; Zheng, W.; Guo, J. Z.; Du, P. Y.; Mao, L. J.; Lu, X. Q. et al. Robust anion-shielding metal-organic frameworks based composite interlayers to achieve uniform Li deposition for stable Li-metal anode. *ChemElectroChem* **2022**, *9*, e202101596.
[143] Qian, J.; Li, Y.; Zhang, M. L.; Luo, R.; Wang, F. J.; Ye, Y. S.; Xing, Y.; Li, W. L.; Qu, W. J.; Wang, L. L. et al. Protecting lithium/sodium metal anode with metal-organic framework based compact and robust shield. *Nano Energy* **2019**, *60*, 866–874.
[144] Zeng, T.; Yan, Y.; He, M.; Zheng, R. X.; Du, D. Y.; Ren, L. F.; Zhou, B.; Shu, C. Z. Boosted Li^+ transference number enabled via interfacial engineering for dendrite-free lithium metal anodes. *Chem. Commun.* **2021**, *57*, 12687–12690.
[145] Wu, J. Y.; Rao, Z. X.; Liu, X. T.; Shen, Y.; Fang, C.; Yuan, L. X.; Li, Z.; Zhang, W. X.; Xie, X. L.; Huang, Y. H. Polycationic polymer layer for air-stable and dendrite-free Li metal anodes in carbonate electrolytes. *Adv. Mater.* **2021**, *33*, 2007428.
[146] Zhang, K.; Liu, W.; Gao, Y. L.; Wang, X. W.; Chen, Z. X.; Ning, R. Q.; Yu, W.; Li, R. L.; Li, L.; Li, X. et al. A high-performance lithium metal battery with ion-selective nanofluidic transport in a conjugated microporous polymer protective layer. *Adv. Mater.* **2021**, *33*, 2006323.
[147] Stalin, S.; Chen, P. Y.; Li, G. J.; Deng, Y.; Rouse, Z.; Cheng, Y. F.; Zhang, Z. Y.; Biswal, P.; Jin, S.; Baker, S. P. et al. Ultrathin zwitterionic polymeric interphases for stable lithium metal anodes. *Matter* **2021**, *4*, 3753–3773.
[148] Jin, T.; Liu, M.; Su, K.; Lu, Y.; Cheng, G.; Liu, Y.; Li, N. W.; Yu, L. Polymer zwitterion-based artificial interphase layers for stable lithium metal anodes. *ACS Appl. Mater. Interfaces* **2021**, *13*, 57489–57496.
[149] Park, S.; Jin, H. J.; Yun, Y. S. Advances in the design of 3D-structured electrode materials for lithium-metal anodes. *Adv. Mater.* **2020**, *32*, 2002193.
[150] Cheng, Y. F.; Chen, J. B.; Chen, Y. M.; Ke, X.; Li, J.; Yang, Y.; Shi, Z. C. Lithium host: Advanced architecture components for lithium metal anode. *Energy Storage Mater.* **2021**, *38*, 276–298.
[151] Yang, C. P.; Yin, Y. X.; Zhang, S. F.; Li, N. W.; Guo, Y. G. Accommodating lithium into 3D current collectors with a submicron skeleton towards long-life lithium metal anodes. *Nat. Commun.* **2015**, *6*, 8058.
[152] Qiu, H. L.; Tang, T. Y.; Asif, M.; Huang, X. X.; Hou, Y. L. 3D porous Cu current collectors derived by hydrogen bubble dynamic template for enhanced Li metal anode performance. *Adv. Funct. Mater.* **2019**, *29*, 1808468.
[153] Zhang, Z. G.; Xu, X. Y.; Wang, S. W.; Peng, Z.; Liu, M.; Zhou, J. J.; Shen, C.; Wang, D. Y. Li_2O-reinforced Cu nanoclusters as porous structure for dendrite-free and long-lifespan lithium metal anode. *ACS Appl. Mater. Interfaces* **2016**, *8*, 26801–26808.
[154] Li, S. B.; He, Q. Q.; Chen, K.; Huang, S. S.; Wu, F.; Wang, G. Q.; Sun, W. F.; Fu, S. Q.; Feng, X. X.; Zhou, Y. et al. Facile chemical fabrication of a three-dimensional copper current collector for stable lithium metal anodes. *J. Electrochem. Soc.* **2021**, *168*, 070502.
[155] Guan, R. Z.; Liu, S.; Wang, C.; Yang, Y. H.; Lu, D. J.; Bian, X. F. Lithiophilic Sn sites on 3D Cu current collector induced uniform lithium plating/stripping. *Chem. Eng. J.* **2021**, *425*, 130177.
[156] Yin, D. M.; Huang, G.; Wang, S. H.; Yuan, D. X.; Wang, X. X.; Li, Q.; Sun, Q. J.; Xue, H. J.; Wang, L. M.; Ming, J. Free-standing 3D nitrogen-carbon anchored Cu nanorod arrays: *In situ* derivation from a metal-organic framework and strategy to stabilize lithium metal anodes. *J. Mater. Chem. A* **2020**, *8*, 1425–1431.
[157] Ma, X. T.; Liu, Z. T.; Chen, H. L. Facile and scalable electrodeposition of copper current collectors for high-performance Li-metal batteries. *Nano Energy* **2019**, *59*, 500–507.
[158] Kim, Y.; Jeong, S.; Bae, H. E.; Tron, A.; Sung, Y. E.; Mun, J.; Kwon, O. J. Electrochemical behavior of residual salts and an effective method to remove impurities in the formation of porous copper electrode for lithium metal batteries. *Int. J. Energy Res.* **2021**, *45*, 10738–10745.
[159] Choi, B. N.; Seo, J. Y.; Kim, B.; Kim, Y. S.; Chung, C. H. Electro-deposition of the lithium metal anode on dendritic copper current collectors for lithium battery application. *Appl. Surf. Sci.* **2020**, *506*, 144884.
[160] Wang, R.; Shi, F. X.; He, X.; Shi, J. Q.; Ma, T.; Jin, S.; Tao, Z. L. Three-dimensional lithiophilic Cu@Sn nanocones for dendrite-free lithium metal anodes. *Sci. China Mater.* **2021**, *64*, 1087–1094.
[161] Tang, Y. P.; Shen, K.; Lv, Z. Y.; Xu, X.; Hou, G. Y.; Cao, H. Z.; Wu, L. K.; Zheng, G. Q.; Deng, Y. D. Three-dimensional ordered macroporous Cu current collector for lithium metal anode: Uniform nucleation by seed crystal. *J. Power Sources* **2018**, *403*, 82–89.
[162] Chen, K. H.; Sanchez, A. J.; Kazyak, E.; Davis, A. L.; Dasgupta, N. P. Synergistic effect of 3D current collectors and ALD surface modification for high Coulombic efficiency lithium metal anodes. *Adv. Energy Mater.* **2019**, *9*, 1802534.
[163] Shi, Y. J.; Wang, Z. B.; Gao, H.; Niu, J. Z.; Ma, W. S.; Qin, J. Y.; Peng, Z. Q.; Zhang, Z. H. A self-supported, three-dimensional porous copper film as a current collector for advanced lithium metal batteries. *J. Mater. Chem. A* **2019**, *7*, 1092–1098.
[164] Zhang, D.; Dai, A.; Wu, M.; Shen, K.; Xiao, T.; Hou, G. Y.; Lu, J.; Tang, Y. P. Lithiophilic 3D porous CuZn current collector for stable lithium metal batteries. *ACS Energy Lett.* **2020**, *5*, 180–186.
[165] Wu, X.; He, G.; Ding, Y. Dealloyed nanoporous materials for rechargeable lithium batteries. *Electrochem. Energy Rev.* **2020**, *3*, 541–580.
[166] Zhang, W. Y.; Jin, H. X.; Xu, C.; Zhao, S. M.; Du, Y. Q.; Zhang, J. X. Diffusion couples Cu-X (X=Sn, Zn, Al) derived 3D porous current collector for dendrite-free lithium metal battery. *J. Power Sources* **2019**, *440*, 227142.
[167] Chi, S. S.; Wang, Q. R.; Han, B.; Luo, C.; Jiang, Y. D.; Wang, J.; Wang, C. Y.; Yu, Y.; Deng, Y. H. Lithiophilic Zn sites in porous CuZn alloy induced uniform li nucleation and dendrite-free Li metal deposition. *Nano Lett.* **2020**, *20*, 2724–2732.
[168] Yun, Q. B.; He, Y. B.; Lv, W.; Zhao, Y.; Li, B. H.; Kang, F. Y.; Yang, Q. H. Chemical dealloying derived 3D porous current collector for Li metal anodes. *Adv. Mater.* **2016**, *28*, 6932–6939.
[169] An, Y. L.; Fei, H. F.; Zeng, G. F.; Xu, X. Y.; Ci, L. J.; Xi, B. J.; Xiong, S. L.; Feng, J. K.; Qian, Y. T. Vacuum distillation derived 3D porous current collector for stable lithium-metal batteries. *Nano Energy* **2018**, *47*, 503–511.
[170] Liu, H.; Wang, E. R.; Zhang, Q.; Ren, Y. B.; Guo, X. W.; Wang, L.; Li, G. Y.; Yu, H. J. Unique 3D nanoporous/macroporous structure Cu current collector for dendrite-free lithium deposition. *Energy Storage Mater.* **2019**, *17*, 253–259.
[171] Zhao, H.; Lei, D. N.; He, Y. B.; Yuan, Y. F.; Yun, Q. B.; Ni, B.; Lv, W.; Li, B. H.; Yang, Q. H.; Kang, F. Y. et al. Compact 3D copper with uniform porous structure derived by electrochemical dealloying as dendrite-free lithium metal anode current collector. *Adv. Energy Mater.* **2018**, *8*, 1800266.
[172] Chang, X. S.; Liu, H.; Yang, H.; Di, J.; Tang, W. H.; Fu, H. D.;

Li, M. Y.; Liu, R. P. Co-guiding the dendrite-free plating of lithium on lithiophilic ZnO and fluoride modified 3D porous copper for stable Li metal anode. *J. Materiomics* **2020**, *6*, 54–61.
[173] Luo, Y.; He, G. Q. Clusters of CuO nanorods arrays for stable lithium metal anode. *J. Mater. Sci.* **2020**, *55*, 9048–9056.
[174] Qiu, X. G.; Yu, M.; Fan, G. L.; Liu, J. D.; Wang, Y. L.; Zhao, K.; Ding, J. Y.; Cheng, F. Y. Growing nanostructured CuO on copper foil via chemical etching to upgrade metallic lithium anode. *ACS Appl. Mater. Interfaces* **2021**, *13*, 6367–6374.
[175] Gong, Z.; Lian, C.; Wang, P. D.; Huang, K.; Zhu, K.; Ye, K.; Yan, J.; Wang, G. L.; Cao, D. X. Lithiophilic Cu-Li_2O matrix on a Cu collector to stabilize lithium deposition for lithium metal batteries. *Energy Environ. Mater.* **2022**, *5*, 1270–1277.
[176] Zhang, C.; Lv, W.; Zhou, G. M.; Huang, Z. J.; Zhang, Y. B.; Lyu, R.; Wu, H. L.; Yun, Q. B.; Kang, F. Y.; Yang, Q. H. Vertically aligned lithiophilic CuO nanosheets on a Cu collector to stabilize lithium deposition for lithium metal batteries. *Adv. Energy Mater.* **2018**, *8*, 1703404.
[177] Luan, J. Y.; Zhang, Q.; Yuan, H. Y.; Sun, D.; Peng, Z. G.; Tang, Y. G.; Ji, X. B.; Wang, H. Y. Plasma-strengthened lithiophilicity of copper oxide nanosheet-decorated Cu foil for stable lithium metal anode. *Adv. Sci.* **2019**, *6*, 1901433.
[178] Wang, X. Y.; Xu, K.; Ke, L. W.; Zhang, Q.; Jin, D. Q.; Shang, H.; Rui, K.; Yan, Y.; Lin, H. J.; Zhu, J. X. Ultrafast microwave polarizing electrons to form vertically aligned metal hybrids as lithiophilic buffer for lithium-metal batteries. *ACS Appl. Mater. Interfaces* **2021**, *13*, 16594–16601.
[179] Sun, C. Y.; Yang, Y. H.; Bian, X. F.; Guan, R. Z.; Wang, C.; Lu, D. J.; Gao, L.; Zhang, D. M. Uniform deposition of Li-metal anodes guided by 3D current collectors with *in situ* modification of the lithiophilic matrix. *ACS Appl. Mater. Interfaces* **2021**, *13*, 48691–48699.
[180] Wei, L.; Li, L.; Zhao, T.; Zhang, N. X.; Zhao, Y. Y.; Wu, F.; Chen, R. J. MOF-derived lithiophilic CuO nanorod arrays for stable lithium metal anodes. *Nanoscale* **2020**, *12*, 9416–9422.
[181] Shen, H. R.; Qi, F. L.; Li, H. C.; Tang, P.; Gao, X. N.; Yang, S.; Hu, Z. C.; Li, Z. B.; Tan, J.; Bai, S. et al. Ultrafast electrochemical growth of lithiophilic nano-flake arrays for stable lithium metal anode. *Adv. Funct. Mater.* **2021**, *31*, 2103309.
[182] Zhao, M. M.; Huang, X. L.; Zhuang, D. M.; Sheng, L.; Xie, X.; Cao, M.; Pan, J. J.; Fan, H. Y.; He, J. P. Constructing porous nanosphere structure current collector by nitriding for lithium metal batteries. *J. Energy Storage* **2022**, *47*, 103665.
[183] Sun, C. Z.; Lin, A. M.; Li, W. W.; Jin, J.; Sun, Y. Y.; Yang, J. H.; Wen, Z. Y. *In situ* conversion of Cu_3P nanowires to mixed ion/electron-conducting skeleton for homogeneous lithium deposition. *Adv. Energy Mater.* **2020**, *10*, 1902989.
[184] Luo, Z.; Li, S.; Yang, L.; Tian, Y.; Xu, L. Q.; Zou, G. Q.; Hou, H. S.; Wei, W. F.; Chen, L. B.; Ji, X. B. Interfacially redistributed charge for robust lithium metal anode. *Nano Energy* **2021**, *87*, 106212.
[185] Xu, Y. L.; Menon, A. S.; Harks, P. P. R. M. L.; Hermes, D. C.; Haverkate, L. A.; Unnikrishnan, S.; Mulder, F. M. Honeycomb-like porous 3D nickel electrodeposition for stable Li and Na metal anodes. *Energy Storage Mater.* **2018**, *12*, 69–78.
[186] Li, S. W.; Ma, Y.; Ren, J.; Liu, H. Y.; Zhang, K.; Zhang, Y. Y.; Tang, X. Y.; Wu, W. W.; Sun, C. C.; Wei, B. Q. Integrated, flexible lithium metal battery with improved mechanical and electrochemical cycling stability. *ACS Appl. Energy Mater.* **2019**, *2*, 3642–3650.
[187] Chen, Q. L.; Yang, Y. F.; Zheng, H. F.; Xie, Q. S.; Yan, X. L.; Ma, Y. T.; Wang, L. S.; Peng, D. L. Electrochemically induced highly ion conductive porous scaffolds to stabilize lithium deposition for lithium metal anodes. *J. Mater. Chem. A* **2019**, *7*, 11683–11689.
[188] Gan, R. Y.; Liu, Y. L.; Yang, N.; Tong, C.; Deng, M. M.; Dong, Q.; Tang, X. Y.; Fu, N.; Li, C. P.; Wei, Z. D. Lithium electrodeposited on lithiophilic LTO/Ti_3C_2 substrate as a dendrite-free lithium metal anode. *J. Mater. Chem. A* **2020**, *8*, 20650–20657.
[189] Huang, Z. Y.; Li, Z.; Zhu, M.; Wang, G. Y.; Yu, F. F.; Wu, M. H.; Xu, G.; Dou, S. X.; Liu, H. K.; Wu, C. Highly stable lithium/sodium metal batteries with high utilization enabled by a holey two-dimensional N-doped $TiNb_2O_7$ host. *Nano Lett.* **2021**, *21*, 10453–10461.
[190] Guan, W. Q.; Hu, X. Q.; Liu, Y. H.; Sun, J. M.; He, C.; Du, Z. Z.; Bi, J. X.; Wang, K.; Ai, W. Advances in the emerging gradient designs of Li metal hosts. *Research* **2022**, *2022*, 9846537.
[191] Wu, J. Y.; Ju, Z. Y.; Zhang, X.; Marschilok, A. C.; Takeuchi, K. J.; Wang, H. L.; Takeuchi, E. S.; Yu, G. H. Gradient design for high-energy and high-power batteries. *Adv. Mater.* **2022**, *34*, 2202780.
[192] Zhang, L.; Zheng, H. F.; Liu, B.; Xie, Q. S.; Chen, Q. L.; Lin, L.; Lin, J.; Qu, B. H.; Wang, L. S.; Peng, D. L. Homogeneous bottom-growth of lithium metal anode enabled by double-gradient lithiophilic skeleton. *J. Energy Chem.* **2021**, *57*, 392–400.
[193] Cheng, X. B.; Hou, T. Z.; Zhang, R.; Peng, H. J.; Zhao, C. Z.; Huang, J. Q.; Zhang, Q. Dendrite-free lithium deposition induced by uniformly distributed lithium ions for efficient lithium metal batteries. *Adv. Mater.* **2016**, *28*, 2888–2895.
[194] Ran, Q. W.; Wang, L. P.; Li, L.; Zhao, Y. L.; Lu, Z. G.; Chen, S. Y.; Zou, J.; Chen, P. Y.; Gao, J.; Niu, X. B. 3D oxidized polyacrylonitrile/Ag framework guided bottom-up lithium deposition for dendrite-free lithium metal batteries. *Chem. Eng. J.* **2021**, *426*, 130780.
[195] Fan, L.; Zhuang, H. L.; Zhang, W. D.; Fu, Y.; Liao, Z. H.; Lu, Y. Y. Stable lithium electrodeposition at ultra-high current densities enabled by 3D PMF/Li composite anode. *Adv. Energy Mater.* **2018**, *8*, 1703360.
[196] Noh, H. J.; Lee, M. H.; Kim, B. G.; Park, J. H.; Lee, S. M.; Choi, J. H. 3D carbon-based porous anode with a pore-size gradient for high-performance lithium metal batteries. *ACS Appl. Mater. Interfaces* **2021**, *13*, 55227–55234.
[197] Yi, J. S.; Chen, J. H.; Yang, Z.; Dai, Y.; Li, W. M.; Cui, J.; Ciucci, F.; Lu, Z. H.; Yang, C. L. Facile patterning of laser-induced graphene with tailored Li nucleation kinetics for stable lithium-metal batteries. *Adv. Energy Mater.* **2019**, *9*, 1901796.
[198] Shen, F.; Zhang, F.; Zheng, Y. J.; Fan, Z. Y.; Li, Z. H.; Sun, Z. T.; Xuan, Y. Y.; Zhao, B.; Lin, Z. Q.; Gui, X. C. et al. Direct growth of 3D host on Cu foil for stable lithium metal anode. *Energy Storage Mater.* **2018**, *13*, 323–328.
[199] Fan, H. L.; Dong, Q. Y.; Gao, C. H.; Hong, B.; Zhang, Z. A.; Zhang, K.; Lai, Y. Q. Encapsulating metallic lithium into carbon nanocages which enables a low-volume effect and a dendrite-free lithium metal anode. *ACS Appl. Mater. Interfaces* **2019**, *11*, 30902–30910.
[200] Liu, Y. M.; Qin, X. Y.; Zhang, S. Q.; Huang, Y. L.; Kang, F. Y.; Chen, G. H.; Li, B. H. Oxygen and nitrogen co-doped porous carbon granules enabling dendrite-free lithium metal anode. *Energy Storage Mater.* **2019**, *18*, 320–327.
[201] Liu, Y. M.; Qin, X. Y.; Zhang, S. Q.; Zhang, L. H.; Kang, F. Y.; Chen, G. H.; Duan, X. F.; Li, B. H. A scalable slurry process to fabricate a 3D lithiophilic and conductive framework for a high performance lithium metal anode. *J. Mater. Chem. A* **2019**, *7*, 13225–13233.
[202] Chen, M.; Zheng, J. H.; Sheng, O. W.; Jin, C. B.; Yuan, H. D.; Liu, T. F.; Liu, Y. J.; Wang, Y.; Nai, J. W.; Tao, X. Y. Sulfur-nitrogen co-doped porous carbon nanosheets to control lithium growth for a stable lithium metal anode. *J. Mater. Chem. A* **2019**, *7*, 18267–18274.
[203] Guo, Q.; Deng, W.; Xia, S. J.; Zhang, Z. B.; Zhao, F.; Hu, B. J.; Zhang, S. S.; Zhou, X. F.; Chen, G. Z.; Liu, Z. P. Nano-channel-based physical and chemical synergic regulation for dendrite-free lithium plating. *Nano Res.* **2021**, *14*, 3585–3597.
[204] Yu, S. C.; Wu, Z. H.; Holoubek, J.; Liu, H. D.; Hopkins, E.; Xiao, Y. X.; Xing, X.; Lee, M. H.; Liu, P. A fiber-based 3D lithium host for lean electrolyte lithium metal batteries. *Adv. Sci.* **2022**, *9*, 2104829.
[205] Zhang, J. M.; Sun, D.; Tang, Z.; Xie, C. L.; Yang, J.; Tang, J. J.; Zhou, X. Y.; Tang, Y. G.; Wang, H. Y. Scalable slurry-coating induced integrated 3D lithiophilic architecture for stable lithium metal anodes. *J. Power Sources* **2021**, *485*, 229334.
[206] Liu, T. C.; Ge, J. X.; Wang, H. C.; Zhang, Y. F.; Wang, Y. Unusual inside-outside Li deposition within three-dimensional honeycomb-like

hierarchical nitrogen-doped framework for a dendrite-free lithium metal anode. *ACS Appl. Energy Mater*. **2021**, *4*, 2838–2846.
[207] Chen, Y. Z.; Elangovan, A.; Zeng, D. L.; Zhang, Y. F.; Ke, H. Z.; Li, J.; Sun, Y. B.; Cheng, H. S. Vertically aligned carbon nanofibers on Cu foil as a 3D current collector for reversible Li plating/stripping toward high-performance Li-S batteries. *Adv. Funct. Mater*. **2020**, *30*, 1906444.
[208] Xu, Z. X.; Xu, L. Y.; Xu, Z. X.; Deng, Z. P.; Wang, X. L. N, O-codoped carbon nanosheet array enabling stable lithium metal anode. *Adv. Funct. Mater*. **2021**, *31*, 2102354.
[209] Lin, K.; Xu, X. F.; Qin, X. Y.; Wang, S. W.; Han, C. P.; Geng, H. R.; Li, X. J.; Kang, F. Y.; Chen, G. H.; Li, B. H. Dendrite-free lithium deposition enabled by a vertically aligned graphene pillar architecture. *Carbon* **2021**, *185*, 152–160.
[210] Raji, A. R. O.; Villegas Salvatierra, R.; Kim, N. D.; Fan, X. J.; Li, Y. L.; Silva, G. A. L.; Sha, J. W.; Tour, J. M. Lithium batteries with nearly maximum metal storage. *ACS Nano* **2017**, *11*, 6362–6369.
[211] Wu, Q. P.; Zheng, Y. J.; Guan, X.; Xu, J.; Cao, F. H.; Li, C. L. Dynamical SEI reinforced by open-architecture MOF film with stereoscopic lithiophilic sites for high-performance lithium-metal batteries. *Adv. Funct. Mater*. **2021**, *31*, 2101034.
[212] Zhao, T.; Li, S. W.; Liu, F.; Wang, Z. Q.; Wang, H. L.; Liu, Y. J.; Tang, X. Y.; Bai, M.; Zhang, M.; Ma, Y. Molten-Li infusion of ultra-thin interfacial modification layer towards the highly-reversible, energy-dense metallic batteries. *Energy Storage Mater*. **2022**, *45*, 796–804.
[213] Sim, W. H.; Jeong, H. M. Efficient lithium growth control from ordered nitrogen-chelated lithium-ion for high performance lithium metal batteries. *Adv. Sci*. **2021**, *8*, 2002144.
[214] Zhao, J.; Yuan, H. Y.; Wang, G. L.; Lim, X. F.; Ye, H. L.; Wee, V.; Fang, Y. Z.; Lee, J. Y.; Zhao, D. Stabilization of lithium metal anodes by conductive metal-organic framework architectures. *J. Mater. Chem. A* **2021**, *9*, 12099–12108.
[215] Ma, Y.; Wei, L.; He, Y.; Yuan, X. Z.; Su, Y. H.; Gu, Y. T.; Li, X. J.; Zhao, X. H.; Qin, Y. Z.; Mu, Q. Q. et al. A "blockchain" synergy in conductive polymer-filled metal-organic frameworks for dendrite-free Li plating/stripping with high coulombic efficiency. *Angew. Chem., Int. Ed*. **2022**, *61*, e202116291.
[216] Wang, L. Y.; Zhu, X. Y.; Guan, Y. P.; Zhang, J. L.; Ai, F.; Zhang, W. F.; Xiang, Y.; Vijayan, S.; Li, G. D.; Huang, Y. Q. et al. ZnO/carbon framework derived from metal-organic frameworks as a stable host for lithium metal anodes. *Energy Storage Mater*. **2018**, *11*, 191–196.
[217] Lei, Z. W.; Shen, J. L.; Zhang, W. D.; Wang, Q. R.; Wang, J.; Deng, Y. H.; Wang, C. Y. Exploring porous zeolitic imidazolate frame work-8 (ZIF-8) as an efficient filler for high-performance poly(ethyleneoxide)-based solid polymer electrolytes. *Nano Res.* **2020**, *13*, 2259–2267.
[218] Shin, H. R.; Yun, J.; Eom, G. H.; Moon, J.; Kim, J. H.; Park, M. S.; Lee, J. W.; Dou, S. X. Mechanistic and nanoarchitectonics insight into Li-host interactions in carbon hosts for reversible Li metal storage. *Nano Energy* **2022**, *95*, 106999.
[219] Yun, J.; Shin, H. R.; Won, E. S.; Kang, H. C.; Lee, J. W. Confined Li metal storage in porous carbon frameworks promoted by strong Li-substrate interaction. *Chem. Eng. J*. **2022**, *430*, 132897.
[220] Man, J. Z.; Liu, W. L.; Zhang, H. B.; Liu, K.; Cui, Y. F.; Yin, J. P.; Wang, X. Y.; Sun, J. C. A metal-organic framework derived electrical insulating-conductive double-layer configuration for stable lithium metal anodes. *J. Mater. Chem. A* **2021**, *9*, 13661–13669.
[221] Sun, B.; Zhang, Q.; Xu, W. L.; Zhao, R.; Zhu, H.; Lv, W.; Li, X. K.; Yang, N. J. A gradient topology host for a dendrite-free lithium metal anode. *Nano Energy* **2022**, *94*, 106937.
[222] Luan, J. Y.; Zhang, Q.; Yuan, H. Y.; Peng, Z. G.; Tang, Y. G.; Wu, S. A.; Wang, H. Y. Sn layer decorated copper mesh with superior lithiophilicity for stable lithium metal anode. *Chem. Eng. J*. **2020**, *395*, 124922.
[223] Li, Q.; Zhu, S. P.; Lu, Y. Y. 3D porous Cu current collector/Li-metal composite anode for stable lithium-metal batteries. *Adv. Funct. Mater*. **2017**, *27*, 1606422.
[224] Tian, A. L.; Luo, K. L.; Li, Z. D.; Ma, M. M.; Li, S.; Wang, X. Y.; Wang, D. Y.; Peng, Z. F-N-S doped lithiophilic interphases for stable Li metal and alloy anodes. *J. Power Sources* **2021**, *508*, 230334.
[225] Luo, Z.; Liu, C.; Tian, Y.; Zhang, Y.; Jiang, Y. L.; Hu, J. H.; Hou, H. S.; Zou, G. Q.; Ji, X. B. Dendrite-free lithium metal anode with lithiophilic interphase from hierarchical frameworks by tuned nucleation. *Energy Storage Mater*. **2020**, *27*, 124–132.
[226] Luo, K. L.; Leng, Z. Y.; Li, Z. D.; Ma, M. M.; Li, S.; Xie, W. P.; Wang, D. Y.; Cao, X. L.; Peng, Z. Shielded electric field-boosted lithiophilic Sites: A Janus interface toward stable lithium metal anodes. *Chem. Eng. J*. **2021**, *416*, 129142.
[227] Yun, J.; Park, B. K.; Won, E. S.; Choi, S. H.; Kang, H. C.; Kim, J. H.; Park, M. S.; Lee, J. W. Bottom-up lithium growth triggered by interfacial activity gradient on porous framework for lithium-metal anode. *ACS Energy Lett*. **2020**, *5*, 3108–3114.
[228] Hu, X. Y.; Xu, P.; Deng, S. W.; Lei, J.; Lin, X. D.; Wu, Q. H.; Zheng, M. S.; Dong, Q. F. Inducing ordered Li deposition on a PANI-decorated Cu mesh for an advanced Li anode. *J. Mater. Chem. A* **2020**, *8*, 17056–17064.
[229] Huang, S. B.; Chen, L.; Wang, T. S.; Hu, J. K.; Zhang, Q. F.; Zhang, H.; Nan, C. W.; Fan, L. Z. Self-propagating enabling high lithium metal utilization ratio composite anodes for lithium metal batteries. *Nano Lett*. **2021**, *21*, 791–797.
[230] Xu, P.; Hu, X. Y.; Liu, X. Y.; Lin, X. D.; Fan, X. X.; Cui, X. Y.; Sun, C.; Wu, Q. H.; Lian, X. B.; Yuan, R. M. et al. A lithium-metal anode with ultra-high areal capacity (50 $mAh{\cdot}cm^{-2}$) by gridding lithium plating/stripping. *Energy Storage Mater*. **2021**, *38*, 190–199.
[231] Huang, S. B.; Zhang, W. F.; Ming, H.; Cao, G. P.; Fan, L. Z.; Zhang, H. Chemical energy release driven lithiophilic layer on 1 m^2 commercial brass mesh toward highly stable lithium metal batteries. *Nano Lett*. **2019**, *19*, 1832–1837.
[232] Zhang, S.; Deng, W.; Zhou, X.; He, B.; Liang, J.; Zhao, F.; Guo, Q.; Liu, Z. Controlled lithium plating in three-dimensional hosts through nucleation overpotential regulation toward high-areal-capacity lithium metal anode. *Mater. Today Energy* **2021**, *21*, 100770.
[233] Chen, W. Y.; Li, S. P.; Wang, C. H.; Dou, H.; Zhang, X. G. Targeted deposition in a lithiophilic silver-modified 3D Cu host for lithium-metal anodes. *Energy Environ. Mater*., in press, DOI: 10.1002/eem2.12412.
[234] Wang, J. R.; Wang, M. M.; He, X. D.; Wang, S.; Dong, J. M.; Chen, F.; Yasmin, A.; Chen, C. H. A lithiophilic 3D conductive skeleton for high performance Li metal battery. *ACS Appl. Energy Mater*. **2020**, *3*, 7265–7271.
[235] Fan, H. L.; Gao, C. H.; Dong, Q. Y.; Hong, B.; Fang, Z.; Hu, M. Y.; Lai, Y. Q. Silver sites guide spatially homogeneous plating of lithium metal in 3D host. *J. Electroanal. Chem*. **2018**, *824*, 175–180.
[236] Liu, T. C.; Chen, X. D.; Zhan, C. C.; Cao, X. H.; Wang, Y. W.; Liu, J. H. Selective lithium deposition on 3D porous heterogeneous lithiophilic skeleton for ultrastable lithium metal anodes. *ChemNanoMat* **2020**, *6*, 1200–1207.
[237] Ni, Z. C.; Zhang, Y. Y.; Zhu, B. W.; Wang, Y. J.; Wang, Y.; Li, X.; Zhang, Y. J.; Sun, S. G. A multifunctional Cu_6Sn_5 interface layer for dendritic-free lithium metal anode. *J. Colloid Interf. Sci*. **2022**, *605*, 223–230.
[238] Wang, J. R.; Wang, M. M.; Chen, F.; Li, Y. X.; Zhang, L. M.; Zhao, Y.; Chen, C. H. *In-situ* construction of lithiophilic interphase in vertical micro-channels of 3D copper current collector for high performance lithium-metal batteries. *Energy Storage Mater*. **2021**, *34*, 22–27.
[239] Chen, T.; Shi, J. J.; Xing, J. X.; Liu, Y. C.; Wang, Z. H.; Xiao, J. L.; Liu, H. L.; Chen, Y.; Sun, X. L.; Li, J. Z. Self-formed lithiophilic alloy buffer layer on copper foam framework for advanced lithium metal anodes. *ACS Appl. Energy Mater*. **2021**, *4*, 4879–4886.
[240] Fu, X. L.; Shang, C. Q.; Zhou, G. F.; Wang, X. Lithiophilic Sb surface modified Cu nanowires grown on Cu foam: A synergistic 1D@3D hierarchical structure for stable lithium metal anodes. *J. Mater. Chem. A* **2021**, *9*, 24963–24970.
[241] Wang, C.; Mu, X. W.; Yu, J. M.; Lu, Z. D.; Han, J. Scalable hierarchical lithiophilic engineering of metal foam enables stable

lithium metal batteries. *Chem. Eng. J.* **2022**, *435*, 134643.
[242] Zhang, R. H.; Li, Y.; Qiao, L.; Li, D. W.; Deng, J. L.; Zhou, J. J.; Xie, L.; Hou, Y.; Wang, T.; Tian, W. et al. Atomic layer deposition assisted superassembly of ultrathin ZnO layer decorated hierarchical Cu foam for stable lithium metal anode. *Energy Storage Mater.* **2021**, *37*, 123–134.
[243] Zhang, R. H.; Li, Y.; Wang, M.; Li, D. W.; Zhou, J. J.; Xie, L.; Wang, T.; Tian, W.; Zhai, Y. J.; Gong, H. Y. et al. Super-assembled hierarchical CoO nanosheets-cu foam composites as multi-level hosts for high-performance lithium metal anodes. *Small* **2021**, *17*, 2101301.
[244] Liu, T. C.; Chen, S. Q.; Sun, W. W.; Lv, L. P.; Du, F. H.; Liu, H.; Wang, Y. Lithiophilic vertical cactus-like framework derived from Cu/Zn-based coordination polymer through *in situ* chemical etching for stable lithium metal batteries. *Adv. Funct. Mater.* **2021**, *31*, 2008514.
[245] Zhang, L. Y.; Jin, Q.; Zhao, K. X.; Zhang, X. T.; Wu, L. L. Lithiophilic $Ti_3C_2T_x$-modified Cu foam by electrophoretic deposition for dendrite-free lithium metal anodes. *ACS Appl. Energy Mater.* **2022**, *5*, 2514–2521.
[246] Cheng, Y. F.; Ke, X.; Chen, Y. M.; Huang, X. Y.; Shi, Z. C.; Guo, Z. P. Lithiophobic-lithiophilic composite architecture through co-deposition technology toward high-performance lithium metal batteries. *Nano Energy* **2019**, *63*, 103854.
[247] Yue, X. Y.; Wang, W. W.; Wang, Q. C.; Meng, J. K.; Wang, X. X.; Song, Y.; Fu, Z. W.; Wu, X. J.; Zhou, Y. N. Cuprite-coated Cu foam skeleton host enabling lateral growth of lithium dendrites for advanced Li metal batteries. *Energy Storage Mater.* **2019**, *21*, 180–189.
[248] Zhao, Y.; Hao, S. G.; Su, L.; Ma, Z. P.; Shao, G. J. Hierarchical Cu fibers induced Li uniform nucleation for dendrite-free lithium metal anode. *Chem. Eng. J.* **2020**, *392*, 123691.
[249] Feng, Y. Y.; Zhang, C. F.; Li, B.; Xiong, S. Z.; Song, J. X. Low-volume-change, dendrite-free lithium metal anodes enabled by lithophilic 3D matrix with LiF-enriched surface. *J. Mater. Chem. A* **2019**, *7*, 6090–6098.
[250] Lin, K.; Xu, X. F.; Qin, X. Y.; Zhang, G. Q.; Liu, M.; Lv, F. Z.; Xia, Y.; Kang, F. Y.; Chen, G. H.; Li, B. H. Restructured rimous copper foam as robust lithium host. *Energy Storage Mater.* **2020**, *26*, 250–259.
[251] Cai, Y. F.; Qin, B.; Li, C.; Si, X. Q.; Cao, J.; Zheng, X. H.; Qi, J. L. Stable lithium metal anode achieved by shortening diffusion path on solid electrolyte interface derived from Cu_2O lithiophilic layer. *Chem. Eng. J.* **2022**, *433*, 133689.
[252] Jeong, M. G.; Kwak, W. J.; Kim, J. Y.; Lee, J. K.; Sun, Y. K.; Jung, H. G. Uniformly distributed reaction by 3D host-lithium composite anode for high rate capability and reversibility of Li-O_2 batteries. *Chem. Eng. J.* **2022**, *427*, 130914.
[253] Li, R.; Wang, J. X.; Lin, L. D.; Wang, H.; Wang, C. M.; Zhang, C. H.; Song, C. H.; Tian, F.; Yang, J.; Qian, Y. T. Pressure-tuned and surface-oxidized copper foams for dendrite-free Li metal anodes. *Mater. Today Energy* **2020**, *15*, 100367.
[254] Tan, L.; Li, X. H.; Cheng, M.; Liu, T. C.; Wang, Z. X.; Guo, H. J.; Yan, G. C.; Li, L. J.; Liu, Y.; Wang, J. X. *In-situ* tailored 3D Li_2O@Cu nanowires array enabling stable lithium metal anode with ultra-high coulombic efficiency. *J. Power Sources* **2020**, *463*, 228178.
[255] Lu, R. C.; Zhang, B. B.; Cheng, Y. L.; Amin, K.; Yang, C.; Zhou, Q. Y.; Mao, L. J.; Wei, Z. X. Dual-regulation of ions/electrons in a 3D Cu-Cu_xO host to guide uniform lithium growth for high-performance lithium metal anodes. *J. Mater. Chem. A* **2021**, *9*, 10393–10403.
[256] Lu, Z. Y.; Tai, Z. X.; Yu, Z. P.; LaGrow, A. P.; Bondarchuk, O.; Sousa, J. P. S.; Meng, L. J.; Peng, Z. J.; Liu, L. F. Lithium-copper alloy embedded in 3D porous copper foam with enhanced electrochemical performance toward lithium metal batteries. *Mater. Today Energy* **2021**, *22*, 100871.
[257] Zhai, P. B.; Wei, Y.; Xiao, J.; Liu, W.; Zuo, J. H.; Gu, X. K.; Yang, W. W.; Cui, S. Q.; Li, B.; Yang, S. B. et al. *In situ* generation of artificial solid-electrolyte interphases on 3D conducting scaffolds for high-performance lithium-metal anodes. *Adv. Energy Mater.* **2020**, *10*, 1903339.
[258] Park, H.; Kwon, J.; Song, T.; Paik, U. Lithiophilic surface treatment of metal- and metallic compound-based frameworks by gas nitriding for lithium metal batteries. *J. Power Sources* **2020**, *477*, 228776.
[259] Li, Z. H.; He, Q.; Zhou, C.; Li, Y.; Liu, Z. H.; Hong, X. F.; Xu, X.; Zhao, Y.; Mai, L. Q. Rationally design lithiophilic surfaces toward high-energy Lithium metal battery. *Energy Storage Mater.* **2021**, *37*, 40–46.
[260] Huang, Z. J.; Zhang, C.; Lv, W.; Zhou, G. M.; Zhang, Y. B.; Deng, Y. Q.; Wu, H. L.; Kang, F. Y.; Yang, Q. H. Realizing stable lithium deposition by *in situ* grown Cu_2S nanowires inside commercial Cu foam for lithium metal anodes. *J. Mater. Chem. A* **2019**, *7*, 727–732.
[261] Lei, M. N.; You, Z. Y.; Ren, L. B.; Liu, X. R.; Wang, J. G. Construction of copper oxynitride nanoarrays with enhanced lithiophilicity toward stable lithium metal anodes. *J. Power Sources* **2020**, *463*, 228191.
[262] Yang, G. H.; Chen, J. D.; Xiao, P. T.; Agboola, P. O.; Shakir, I.; Xu, Y. X. Graphene anchored on Cu foam as a lithiophilic 3D current collector for a stable and dendrite-free lithium metal anode. *J. Mater. Chem. A* **2018**, *6*, 9899–9905.
[263] Liu, T. C.; Ge, J. X.; Xu, Y.; Lv, L. P.; Sun, W. W.; Wang, Y. Organic supramolecular protective layer with rearranged and defensive Li deposition for stable and dendrite-free lithium metal anode. *Energy Storage Mater.* **2020**, *32*, 261–271.
[264] Jiang, X. M.; Chen, Y. J.; Meng, X. K.; Cao, W. G.; Liu, C. C.; Huang, Q.; Naik, N.; Murugadoss, V.; Huang, M. N.; Guo, Z. H. The impact of electrode with carbon materials on safety performance of lithium-ion batteries: A review. *Carbon* **2022**, *191*, 448–470.
[265] Pathak, R.; Chen, K.; Wu, F.; Mane, A. U.; Bugga, R. V.; Elam, J. W.; Qiao, Q.; Zhou, Y. Advanced strategies for the development of porous carbon as a Li host/current collector for lithium metal batteries. *Energy Storage Mater.* **2021**, *41*, 448–465.
[266] Ponraj, R.; Yun, J. H.; Wang, J. E.; Chen, X. J.; Kim, D. J.; Kim, D. K. Regulating lithium metal interface using seed-coating layer for high-power batteries. *Chem. Eng. J.* **2022**, *433*, 134380.
[267] Pei, F.; Fu, A.; Ye, W. B.; Peng, J.; Fang, X. L.; Wang, M. S.; Zheng, N. F. Robust lithium metal anodes realized by lithiophilic 3D porous current collectors for constructing high-energy lithium-sulfur batteries. *ACS Nano* **2019**, *13*, 8337–8346.
[268] Zhu, W. H.; Deng, W.; Zhao, F.; Liang, S. S.; Zhou, X. F.; Liu, Z. P. Graphene network nested Cu foam for reducing size of lithium metal towards stable metallic lithium anode. *Energy Storage Mater.* **2019**, *21*, 107–114.
[269] Liu, T. C.; Wang, J. L.; Xu, Y.; Zhang, Y. F.; Wang, Y. Dendrite-free and stable lithium metal battery achieved by a model of stepwise lithium deposition and stripping. *Nano-Micro Lett.* **2021**, *13*, 170.
[270] Zhou, Y.; Zhao, K.; Han, Y.; Sun, Z. H.; Zhang, H. T.; Xu, L. Q.; Ma, Y. F.; Chen, Y. S. A nitrogen-doped-carbon/ZnO modified Cu foam current collector for high-performance Li metal batteries. *J. Mater. Chem. A* **2019**, *7*, 5712–5718.
[271] Qian, J.; Wang, S.; Li, Y.; Zhang, M. L.; Wang, F. J.; Zhao, Y. Y.; Sun, Q.; Li, L.; Wu, F.; Chen, R. J. Lithium induced nano-sized copper with exposed lithiophilic surfaces to achieve dense lithium deposition for lithium metal anode. *Adv. Funct. Mater.* **2021**, *31*, 2006950.
[272] Park, J.; Joo, S. H.; Kim, Y. J.; Park, J. H.; Kwak, S. K.; Ahn, S.; Kang, S. J. Organic semiconductor cocrystal for highly conductive lithium host electrode. *Adv. Funct. Mater.* **2019**, *29*, 1902888.
[273] Wang, H. S.; Liu, Y. Y.; Li, Y. Z.; Cui, Y. Lithium metal anode materials design: Interphase and host. *Electrochem. Energy Rev.* **2019**, *2*, 509–517.
[274] Yang, S.; Xiao, R.; Zhang, T. W.; Li, Y.; Zhong, B. H.; Wu, Z. G.; Guo, X. D. Cu nanowires modified with carbon-rich conjugated framework PTEB for stabilizing lithium metal anodes. *Chem. Commun.* **2021**, *57*, 13606–13609.

[275] Yue, Y.; Liang, H. 3D current collectors for lithium-ion batteries: A topical review. *Small Methods* **2018**, *2*, 1800056.
[276] Nanda, S.; Gupta, A.; Manthiram, A. Anode-free full cells: A pathway to high-energy density lithium-metal batteries. *Adv. Energy Mater.* **2021**, *11*, 2000804.
[277] Wang, Y. Y.; Wang, Z. J.; Lei, D. N.; Lv, W.; Zhao, Q.; Ni, B.; Liu, Y.; Li, B. H.; Kang, F. Y.; He, Y. B. Spherical Li deposited inside 3D Cu skeleton as anode with ultrastable performance. *ACS Appl. Mater. Interfaces* **2018**, *10*, 20244–20249.
[278] Lee, J.; Won, E. S.; Kim, D. M.; Kim, H.; Kwon, B.; Park, K.; Jo, S.; Lee, S.; Lee, J. W.; Lee, K. T. Three-dimensional porous frameworks for Li metal batteries: Superconformal versus conformal Li growth. *ACS Appl. Mater. Interfaces* **2021**, *13*, 33056–33065.
[279] Chen, C. L.; Li, S. P.; Notten, P. H. L.; Zhang, Y. H.; Hao, Q. L.; Zhang, X. G.; Lei, W. 3D printed lithium-metal full batteries based on a high-performance three-dimensional anode current collector. *ACS Appl. Mater. Interfaces* **2021**, *13*, 24785–24794.
[280] Song, H. Y.; Eom, K. Realizing superior energy in a full-cell LIB employing a Li-metal anode via the rational design of a Cu-scaffold host structure with an extremely high porosity. *Energy Storage Mater.* **2021**, *36*, 326–332.
[281] Lu, B. Y.; Olivera, E.; Scharf, J.; Chouchane, M.; Fang, C. C.; Ceja, M.; Pangilinan, L. E.; Zheng, S. Q.; Dawson, A.; Cheng, D. Y. et al. Quantitatively designing porous copper current collectors for lithium metal anodes. *ACS Appl. Energy Mater.* **2021**, *4*, 6454–6465.
[282] Zhang, R.; Wen, S. W.; Wang, N.; Qin, K. Q.; Liu, E. Z.; Shi, C. S.; Zhao, N. Q. N-doped graphene modified 3D porous Cu current collector toward microscale homogeneous Li deposition for Li metal anodes. *Adv. Energy Mater.* **2018**, *8*, 1800914.
[283] Qiang, Z.; Liu, B.; Yang, B. J.; Ma, P. J.; Yan, X. B.; Wang, B. X. Preparation of three-dimensional copper-zinc alloy current collector by powder metallurgy for lithium metal battery anode. *ChemElectroChem* **2021**, *8*, 2479–2487.
[284] Lin, H. N.; Zhang, Z. W.; Wang, Y. D.; Zhang, X. L.; Tie, Z. X.; Jin, Z. Template-sacrificed hot fusion construction and nanoseed modification of 3D porous copper nanoscaffold host for stable-cycling lithium metal anodes. *Adv. Funct. Mater.* **2021**, *31*, 2102735.
[285] Zhou, S.; Usman, I.; Wang, Y. J.; Pan, A. Q. 3D printing for rechargeable lithium metal batteries. *Energy Storage Mater.* **2021**, *38*, 141–156.
[286] Lu, L. L.; Zhang, Y.; Pan, Z.; Yao, H. B.; Zhou, F.; Yu, S. H. Lithiophilic Cu-Ni core-shell nanowire network as a stable host for improving lithium anode performance. *Energy Storage Mater.* **2017**, *9*, 31–38.
[287] Zhang, C.; Lyu, R.; Lv, W.; Li, H.; Jiang, W.; Li, J.; Gu, S. C.; Zhou, G. M.; Huang, Z. J.; Zhang, Y. B. et al. A lightweight 3D Cu nanowire network with phosphidation gradient as current collector for high-density nucleation and stable deposition of lithium. *Adv. Mater.* **2019**, *31*, 1904991.
[288] Zhang, L. H.; Yin, X. G.; Shen, S. B.; Liu, Y.; Li, T.; Wang, H.; Lv, X. H.; Qin, X. Y.; Chiang, S. W.; Fu, Y. Z. et al. Simultaneously homogenized electric field and ionic flux for reversible ultrahigh-areal-capacity Li deposition. *Nano Lett.* **2020**, *20*, 5662–5669.
[289] Shang, H.; Gu, Y.; Wang, Y. B.; Zuo, Z. C. N-doped graphdiyne coating for dendrite-free lithium metal batteries. *Chem. -Eur. J.* **2020**, *26*, 5434–5440.
[290] Shang, H.; Zuo, Z. C.; Li, Y. L. Highly lithiophilic graphdiyne nanofilm on 3D free-standing Cu nanowires for high-energy-density electrodes. *ACS Appl. Mater. Interfaces* **2019**, *11*, 17678–17685.
[291] Hong, S. H.; Jung, D. H.; Kim, J. H.; Lee, Y. H.; Cho, S. J.; Joo, S. H.; Lee, H. W.; Lee, K. S.; Lee, S. Y. Electrical conductivity gradient based on heterofibrous scaffolds for stable lithium-metal batteries. *Adv. Funct. Mater.* **2020**, *30*, 1908868.

Yuhang Liu is currently a Ph.D. candidate in the Institute of Flexible Electronics at Northwestern Polytechnical University under the supervision of Prof. Wei Huang and Prof. Wei Ai. His research interests are focused on high-capacity nanofibers-based electrodes and flexbile Li metal batteries.

Yifan Li received his master's degree from the Northwestern Polytechnical University under the supervision of Prof. Wei Ai. His research interests are focused on new energy devices and flexible energy storage.

Wei Ai is a professor of the Institute of Flexible Electronics at Northwestern Polytechnical University. He received his Ph.D. and M.S. degrees from Nanyang Technological University and Nanjing University of Posts and Telecommunications, respectively. His research interests include electrochemical materials and technologies, new energy devices and flexible intelligence technologies.

Qingyu Yan is currently a professor in Nanyang Technology University. He finished his Ph.D. degree from State University of New York at Stony Brook. After that, he joined Rensselaer Polytechnic Institute as a research fellow. He joined Nanyang Technological University as an assistant professor in early 2008 and became a professor in 2018. Yan's research interests mainly include thermoelectric materials and energy storage materials.